

Short-Hard Gamma-Ray Bursts

Ehud Nakar

*Theoretical Astrophysics, California Institute of Technology, MC 130-33,
Pasadena, CA 91125, USA*

Abstract

Two types of Gamma-ray bursts (GRBs) are observed: short duration hard spectrum GRBs and long duration soft spectrum GRBs. For many years long GRBs were the focus of intense research while the lack of observational data limited the study of short-hard GRBs (SHBs). In 2005 a breakthrough occurred following the first detections of SHB afterglows, longer wavelength emission that follows the burst of gamma-rays. Similarly to long GRBs, afterglow detections led to the identification of SHB host galaxies and measurement of their redshifts. These observations established that SHBs are cosmological relativistic sources that, unlike long GRBs, do not originate from the collapse of massive stars, and therefore constitute a distinct physical phenomenon. One viable model for SHB origin is the coalescence of compact binary systems (double neutron stars or a neutron star and a black hole), in which case SHBs are the electromagnetic counterparts of strong gravitational-wave sources. The theoretical and observational study of SHBs following the recent pivotal discoveries is reviewed, along with new theoretical results that are presented here for the first time.

Contents

1	Introduction	3
2	Observations	6
2.1	Prompt emission	8
2.2	Afterglow	15
2.3	Observed redshift distribution	22
2.4	Host galaxies and cluster associations	26
2.5	Limits on a supernova component	29

Email address: udini@tapir.caltech.edu (Ehud Nakar).

2.6	Observed rate	29
2.7	Identifying an SHB	29
2.8	Additional putative SHBs	32
2.9	SHB interlopers	33
3	Relativistic outflows and the prompt emission	35
3.1	Relativistic effects	36
3.2	The Lorentz factor of the outflow	39
3.3	The composition of the relativistic outflow	43
3.4	The prompt emission	46
3.5	High energy Cosmic-rays and neutrinos	52
4	The afterglow - Theory	54
4.1	Standard model - synchrotron radiation from a spherically symmetric adiabatic blast wave	54
4.2	Synchrotron self-Compton	58
4.3	Early afterglow and the reverse shock	60
4.4	“Naked” afterglow	63
4.5	X-ray dark afterglows and γ -ray efficiency	63
4.6	Angular structure of the outflow	65
4.7	Afterglow variability	68
4.8	The early X-ray “tail”	71
4.9	Macronova	72
4.10	Relativistic collisionless shocks	73
5	Progenitors and the central engine	76
5.1	Progenitors lifetime and intrinsic rate	77
5.2	Coalescence of a compact binary	84
5.3	Other progenitor models	99

6	Gravitational waves from SHBs	103
6.1	NS-NS or NS-BH coalescence	103
6.2	Other processes that radiate gravitational waves	105

List of Tables

1	Short vs. Long GRBs	7
2	Prompt emission and afterglow properties	16
3	Putative host galaxy properties	28
4	GRBs with $T_{90} \geq 2$ s that were proposed to be SHBs	32

1 Introduction

Gamma-ray bursts (GRBs) are short intense flashes of soft (\sim MeV) γ -rays that are detectable once or twice a day. The observed bursts arrive from apparently random directions in the sky and they last between tens of milliseconds and thousands of seconds. Their physical origin remains a focal point of research and debate ever since they were first detected, more than three decades ago.

More than twenty years ago hints that the GRB duration distribution is bimodal have emerged (Mazets *et al.* , 1981; Norris *et al.* , 1984) , suggesting that the GRB population might not be monolithic. The idea that GRBs are most likely composed out of two major distinctive sub-populations became the common view following the influential work of Kouveliotou *et al.* (1993). Based on 222 GRBs detected by the Burst And Transient Source Experiment (*BATSE*¹) on board the Compton Gamma-Ray Observatory, Kouveliotou *et al.* (1993) confirmed that the GRB duration distribution is indeed bimodal, with a minimum around 2 s. They have further shown that bursts with durations shorter than 2 s are composed, on average, of higher energy (harder) photons than longer bursts. It took a dozen additional years before recent observations confirmed that the two sub-populations, defined in duration-hardness space, indeed represent two distinctive physical phenomena. Throughout this review I use the term short-hard GRBs (SHBs), or simply short GRBs, for bursts that share the physical properties of the population that constitutes

¹ <http://www.batse.msfc.nasa.gov/batse/>

the majority of the short-hard events in the duration-hardness space². Bursts with physical properties common to the population that constitutes the majority of long-soft events are denoted simply as long GRBs. The term GRBs is used to describe the whole population of the busters, short and long.

A major revolution in GRB research came with the launch of *BATSE* in 1991. *BATSE* detected bursts at a rate of one per day, a quarter of which were short. The isotropic distribution of bursts on the sky (both long and short) and the paucity of weak bursts indicated that the origin of GRBs is extra-Galactic and most likely cosmological. However, because of the inability to identify the distance of any specific burst based on the observed gamma-rays alone, the final confirmation of the cosmological origin of GRBs had to wait (for a review of *BATSE* results see [Fishman & Meegan, 1995](#)). The final validation that long GRBs arrive from remote locations in the Universe came following the discovery by the Dutch-Italian satellite BeppoSAX that the prompt γ -ray emission of long GRBs, lasting minutes or less, is followed by X-ray emission that can be detected for hours and days ([Costa et al. , 1997](#)). Observations of this X-ray emission enabled accurate localizations of bursts and led to the detection of associated optical ([van Paradijs et al. , 1997](#)) and radio ([Frail et al. , 1997](#)) emission, that can be observed, in some cases, for weeks and years, respectively. Longer wave-length emission that follows the prompt GRB is called the “afterglow” and it provides a wealth of information about the physics of the burst. Most importantly, sub-arcsecond localization of optical afterglows enabled secure identification of galaxies that host long GRBs, leading to the measurement of their redshifts, and finally establishing an unambiguous distance scale for these events (e.g., [Kulkarni et al. , 1998](#)). In some cases, the burst redshift was measured directly by detection of absorption lines in the spectra of optical afterglows (e.g., [Metzger et al. , 1997](#)).

These observations revolutionized the study of long GRBs. The confirmation of their cosmological origin and the detailed observations of a growing sample of afterglows supported a physical picture according to which long GRBs are produced by a catastrophic event involving a stellar-mass object or system that releases a vast amount of energy ($\gtrsim 0.001M_{\odot}c^2$) in a compact region (< 100 km) on time scales of seconds to minutes. This energy source, referred to as the “central engine”, accelerates an ultra-relativistic outflow to Lorentz factor $\gtrsim 100$ and it is this outflow that generates the observed γ -ray prompt emission, and later the afterglow, at large distances from the source. This model is now generally accepted.

² Note that it is not necessary that the duration of a specific burst corresponds one-to-one to its physical properties (e.g., the nature of the progenitor). It is possible for example that there is a small fraction of bursts that are associated physically with long GRBs but their duration is short and vice versa.

The nature of the stellar progenitor of long GRBs remained a matter of debate for many years. Until 2003, when a detection of a long GRB at a relatively low redshift ($z=0.168$) by *HETE-2*³ led to the identification of a type Ic supernova (SN) spectrum superposed on the afterglow of this burst (Stanek *et al.*, 2003; Hjorth *et al.*, 2003). This observation confirmed previous suggestions that at least some long GRBs are associated with SNe (e.g. Galama *et al.*, 1998; Bloom *et al.*, 1999). Following this association and several additional evidence (e.g., Fruchter *et al.*, 2006) the consensus today is that most, and probably all, long GRBs are produced by the collapse of very massive stars (e.g., Woosley, 1993; Paczynski, 1998; MacFadyen & Woosley, 1999).

Comparable studies of SHBs were not conducted during this time. Being shorter and harder they eluded accurate localization and no SHB afterglow was detected despite the effort. The breakthrough in the study of SHBs occurred, finally, during the spring-summer of 2005 when *Swift* and *HETE-2* succeeded in localizing several SHBs, leading to afterglow detections and to the determination of their redshifts. Following these discoveries, and fueled by a continuous flow of SHB detections by *Swift*, the study of SHBs progressed rapidly. The first conclusions from these observations were that SHBs are cosmological, but unlike long GRBs, their progenitors are not massive stars, thereby confirming that these two observationally defined classes are distinctive physical phenomena. On the other hand, the comparable luminosities and roughly similar afterglows of long and short GRBs, suggested that similar physical processes are involved in both types of explosions.

The aim of this paper is to review and summarize the theoretical study of SHBs following the recent observations. These observations are described in §2 and aspects that have direct implications for the current theoretical understanding of SHBs are emphasized. Special attention is given to the observational challenge of identifying a burst as a SHB.

Relativistic effects and the prompt emission theory model are discussed in §3 while the afterglow theory is discussed in §4. The theory of both the prompt and the afterglow emission is discussed in the framework of models in which the emission is produced by a relativistic outflow that first expands quasi-spherically (see definition in §3.1.2) and that later its interaction with the ambient medium leads to the formation of a blast wave that propagates into this medium. These models include the “classic” fireball model of radiation accelerated baryonic plasma as well as other types of relativistic outflows (e.g., Poynting-flux-dominated). The physics of GRB emission (prompt and afterglow) was intensively studied in the context of long GRBs, while there is little work specific to SHBs. As both the prompt emission and the afterglows of long and short GRBs are quite similar, long GRB models are typically ap-

³ The High Energy Transient Explorer; <http://heasarc.gsfc.nasa.gov/docs/hete2/hete2.html>

plied to SHBs as well. The fireball and related models were comprehensively covered by several excellent reviews, and I refer the reader to these reviews for a detailed description of these models (Piran, 1999, 2000; Zhang & Mészáros, 2004; Piran, 2005b; Mészáros, 2006; Lyutikov, 2006). In order for this review to be self contained, I include a brief overview of the basics of the fireball and related models, emphasizing aspects that are relevant to SHBs. I focus on the interpretation of SHB observations in the framework of these models. In several cases I extend existing models and re-derive predictions and constraints that are relevant to SHB parameter space. These derivations and some novel conclusions that follow appear for the first time in this review (see highlighted sections in Table 1).

I go on to review proposed SHB progenitor models and the formation of the central engine §5 (for an excellent comprehensive review of the topic see Lee & Ramirez-Ruiz, 2006). The leading progenitor candidate is the coalescence of a neutron star (NS) with another neutron star or with a black hole (BH). This idea was commented upon some twenty years ago (Paczynski, 1986; Goodman, 1986; Goodman, Dar & Nussinov, 1987) and was first explored in detail by Eichler *et al.* (1989). It successfully survived twenty years of observations and got some support from the properties of SHB afterglows and of the identified host galaxies. I therefore dedicate most of the discussion on SHB progenitors to the aspects of these mergers that are relevant to SHBs. Nevertheless, a merger origin for SHBs is not confirmed, and other progenitor models are still viable, and are discussed here as well.

Mergers of NS-NS or NS-BH binaries are also the most promising sources of gravitational-waves that may be detected by ground-based observatories. This of course makes SHBs very interesting, as the possible electromagnetic counterparts of gravitational-wave signals that are expected to be detected within a decade. The prospects of gravitational wave detection from SHBs are discussed in §6.

For convenience, Table 1 summarizes and compares observational properties of short and long GRBs, and their theoretical interpretations in the fireball model framework. This table can also serve as a quick reference guide for the different topics covered in this review. Through the review $\Omega_m = 0.3$, $\Omega_\Lambda = 0.7$ and $H_0 = 70 \text{ kms}^{-1} \text{ Mpc}^{-1}$ cosmology is used.

2 Observations

Gamma-Ray burst observations are grossly divided into two main phases - the prompt gamma-ray emission and the afterglow. The prompt gamma-rays are intense bursts of $\sim \text{MeV}$ γ -rays that are detected by gamma-ray space

Table 1
Short vs. Long GRBs

	Short GRBs	Long GRBs	Section*
General			
<i>BATSE</i> observed all sky rate	$\approx 170\text{yr}^{-1}$	$\approx 500\text{ yr}^{-1}$	§2.6
<i>BATSE</i> observed local rate density	$\sim 10\text{ Gpc}^{-3}\text{ yr}^{-1}$	$\sim 0.5\text{ Gpc}^{-3}\text{ yr}^{-1}$	§2.6
Host Galaxy types	Early & Late	Late	§2.4
Host specific SFR	$\lesssim 1\text{ M}_{\odot}/\text{yr}/(L/L_{*})$	$\sim 10\text{ M}_{\odot}/\text{yr}/(L/L_{*})$	§2.4
Median observed redshift	≈ 0.25	≈ 2.5	§2.3
Supernovae association	No	Yes (at least some)	§2.5
Progenitor	NS-BH/NS-NS/?	Massive star	§5
Prompt emission			
Typical <i>BATSE</i> duration	$\approx 0.8\text{ s}$	$\approx 30\text{ s}$	§2.1.1
Best fit spectral model ^a	Power-law + exp cutoff	Band function	§2.1.3
$E_{\gamma,iso}^b$	$10^{49} - 10^{51}\text{ erg}$	$10^{52} - 10^{54}\text{ erg}$	§2.1.4
$L_{\gamma,iso}^b$	$10^{50} - 10^{52}\text{ erg/s}$	$10^{50} - 10^{52}\text{ erg/s}$	§2.1.4
Average observed flux ^c	$\sim 5 \cdot 10^{-10}\text{ GeV/cm}^2/\text{s/sr}$	$\sim 10^{-8}\text{ GeV/cm}^2/\text{s/sr}$	
Local energy output rate ^d	$\sim 10^{51}\text{ erg Gpc}^{-3}\text{ yr}^{-1}$	$\sim 10^{53}\text{ erg Gpc}^{-3}\text{ yr}^{-1}$	
Total energy output ^e	$\sim 10^{63}\text{ erg}$	$\sim 10^{66}\text{ erg}$	
X-Ray afterglow			
X-ray dark	Some bursts	None	§2.2.1 & §4.5
Typical decay phase ($\sim t^{-1}$)	Yes	Yes	§2.2.1 & §4.1
Shallow decay phase ($\sim t^{-0.25}$)	Not observed yet	Yes	§2.2.1
X-ray flares	Yes	Yes	§2.2.1 & §4.7
Fireball model^f			
Lorentz factor	$\gtrsim 30$	$\gtrsim 100$	§3.2
Prompt emission energy source	Internal processes ^g	Internal processes ^g	§3.4.1
Afterglow energy source	External shock	External shock	§4.1
Synchrotron self-Compton	$Y \ll 1$	$Y \gtrsim 1$	§4.2
Early afterglow & prompt emission	Well separated	May overlap	§4.3
Early afterglow (baryonic flow)	Optically faint	Optically bright	§4.3
Gamma-ray efficiency	$\sim 10\%$	$\gtrsim 10\%$	§4.5
X-ray dark afterglows ^h	$n \lesssim 10^{-5}\text{ cm}^{-3}$	-	§4.5
Average beaming	$1 < f_b^{-1} \lesssim 100$	$f_b^{-1} \sim 75$	§4.6

* The section in which the SHB table entry is discussed. Highlighted sections present new results that appear in this review for the first time.

^a The spectral model that provides the best fit to most of the bursts (may be affected by observational selection effects).

^b Isotropic equivalent quantities per burst.

^c The total observed $\sim\text{MeV}$ γ -ray flux from GRBs, averaged over long time ($\gg 1$ day).

^d The energy output density rate in $\sim\text{MeV}$ γ -rays of the entire local GRB population.

^e The total energy output in $\sim\text{MeV}$ γ -rays of the entire GRB population in the observed universe.

^f Theoretical interpretations in a framework of models where outflow of any type (e.g., baryonic, Poynting-flux-dominated) expands quasi-spherically and interacts with the ambient medium by driving a blast wave into it.

^g In Poynting-flux-dominated outflow models the dissipation of the internal magnetic field that leads to the prompt emission may be induced by interaction with the external medium.

^h The most likely, but not the only, explanation of X-ray dark afterglows (see §4.5 for details).

observatories and are localized by current instruments to within several arcminutes. Afterglows are X-ray, optical and radio emission that follow the prompt gamma-rays and can be observed in some cases weeks, months and years after the bursts, respectively.

BATSE detected the prompt emission from ~ 3000 GRBs, about 1/4 of which are SHBs. Additionally, prompt emission from more than a hundred SHBs were observed by *Konus-Wind*⁴ and other spacecraft that were, or still are, part of the Interplanetary Network⁵ (IPN). This is compared to a handful of SHB afterglows that were observed following accurate localization of the prompt emission by *Swift* and *HETE-2*. In some of these cases the sub-arcsecond localization of the afterglow led to an unambiguous identification of the burst redshift and host galaxy. These observations are briefly reviewed below.

2.1 Prompt emission

Most of the prompt emission properties are derived using *BATSE* bursts. Typically, the SHB sample is drawn out of the complete *BATSE* GRB sample using the criterion $T_{90} < 2$ s (defined below). This is clearly a rough cut (see §2.7), but it is sufficient for the purpose of statistical studies which are weakly affected by a small contamination of the sample.

2.1.1 Duration

The true (intrinsic) duration distribution of SHBs is unknown. At the short end, the observed distribution is affected by the minimal *BATSE* trigger time (64 ms) while the long end the distribution blends into that of long GRBs. Figure 1 depicts the T_{90} distribution of the entire *BATSE* GRB sample, where T_{90} is the duration encompassing the 5'th to the 95'th percentiles of the total counts in the energy range 20–2000 keV. The duration distribution is bimodal with a minimum around 2 s (Kouveliotou *et al.*, 1993). For this reason the dividing line between short and long GRBs is usually drawn at $T_{90} = 2$ s. This distinction suffices for the purpose of statistical population analysis, but one should bear in mind that there are short GRBs with $T_{90} > 2$ s, and long GRBs with $T_{90} < 2$ s. Horváth (2002) finds that this bimodal distribution can be decomposed into two lognormal distributions, as presented in figure 1. The SHB distribution peaks at $T_{90} \approx 0.8$ s, and the full-width-half-maximum of the distribution is 1.4 dex. If this decomposition represents the physical one then 25%[3.5%] of *BATSE* SHBs last longer than 2[10] s.

⁴ <http://lheawww.gsfc.nasa.gov/docs/gamcosray/legr/konus/>

⁵ <http://www.ssl.berkeley.edu/ipn3/>

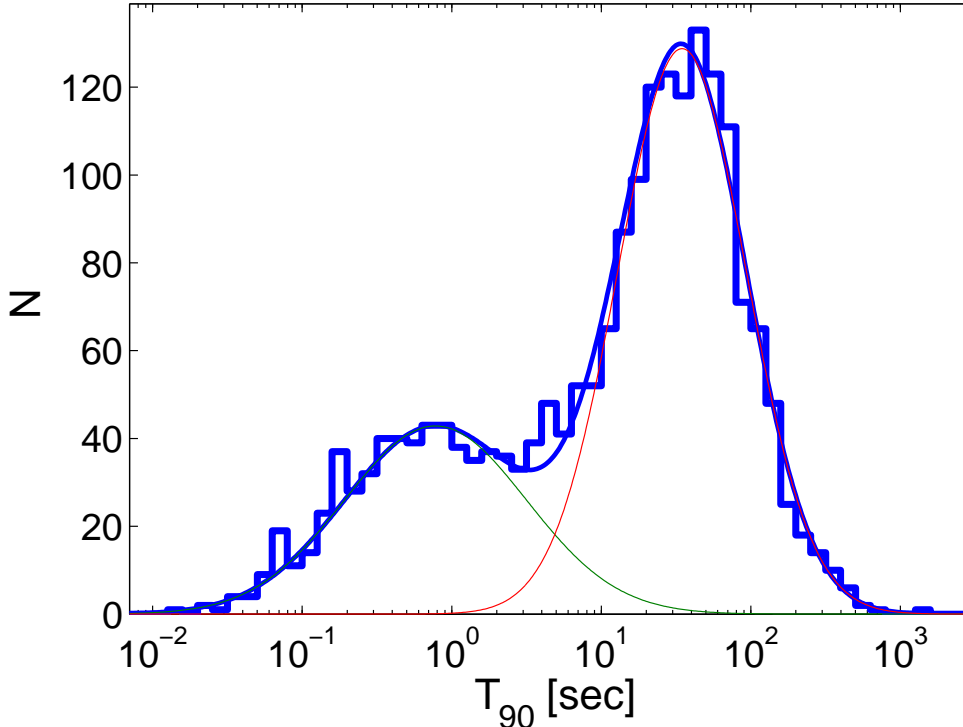


Fig. 1. The bimodal duration distribution of GRBs. The observations (2041 bursts in the current *BATSE* catalog) are marked by the thick stairs. The decomposition of the distribution into two lognormal distributions, as determined by Horváth (2002), (*thin solid lines*) and the sum of these components (*thick solid line*) are superposed.

It was recently realized that at least in some SHBs the initial short and hard γ -ray prompt emission is followed by a much longer X-ray “tail” that lasts tens to hundreds of seconds. Typically, this tail is too faint to affect *BATSE* T_{90} , although in some cases it probably does (Norris & Bonnell, 2006). The properties of this soft tail and its implications for the identification of SHBs are discussed later (§2.2.2 and §2.7).

2.1.2 Temporal structure

Only a small fraction of the *BATSE* SHB sample have sufficient signal to noise ratio (S/N) to conduct analysis of the fine temporal structure. Nakar & Piran (2002b) analyze a sample of 33 bright SHBs at a resolution of 2 ms, looking for variability (separate pulses) within the bursts. The low S/N and the limited time resolution imply that the observed variability is only a lower limit of the true one. Yet, they find that most of the bursts in the sample exhibit variability on time scales that are shorter than the bursts’ durations (see Fig. 2 for a typical SHB light curve). More than half of the bursts in their sample show at least two well-separated pulses and more than a third show rapid variability in the sense that the shortest pulse is shorter by more than an order of magnitude than the burst duration. No correlation is found between

the duration of a burst and the duration of its sub-pulses (given that the burst is not single pulsed). The duration distribution of single pulses ranges from 5 ms to 300 ms with a broad peak around 50 ms. Thus, the lower limit on the shortest time scale observed in these SHBs is of the order of 10 ms, and is set by the resolution limit. Shorter time scales are probably present, as evident from a single case in which a very bright < 1 ms pulse is observed in a SHB (Scargle, Norris & Bonnell, 1998, fainter pulses than this one cannot be resolved on ms time scale). McBreen et al. (2001) analyzed the distribution of various temporal properties of pulses in 100 bright *BATSE* SHBs. They find that the rise times, fall times, FWHM, pulse amplitudes and areas are all consistent with lognormal distributions and that time intervals between pulses and pulse amplitudes are highly correlated with each other.

A comparison of the temporal structure of bright SHBs to the initial 2 s of a sample of long GRBs⁶ shows similar time scales and similar distributions of pulse durations (Nakar & Piran, 2002b). This similarity is demonstrated in figure 2. Similarly, McBreen et al. (2001) find a great similarity between the lognormal distributions and correlations in the temporal structure of short and long GRBs. On the other hand, an examination of the temporal evolution of pulses as a function of frequency shows a different behavior in long and short bursts. Norris, Scargle & Bonnell (2001) compare the spectral lags of short and long GRBs. Spectral lag is a measurement of the spectral evolution timescale of the pulse structure, where a positive value indicates a hard-to-soft evolution (see Norris, Marani & Bonnell, 2000, for an exact definition). They find that long bursts show positive spectral lags that extend up to ~ 2 s with a core around 50 ms. SHBs, however, show a symmetric distribution of lags that ranges between ± 30 ms.

Thus the temporal structure of SHBs shows both similarities and dissimilarities to that of long GRBs. Unfortunately additional comparisons of the temporal structure of short and long bursts were not carried out so far, mostly because of the difficulty in the analysis of SHB light curves. While the temporal structure of long GRBs was explored in detail (e.g., Norris et al., 1996), only the general properties of the temporal structure of SHBs are known.

2.1.3 Spectrum

Comparison of the hardness ratio of SHBs to that of long GRBs shows that SHBs are on average harder. This result was used by Kouveliotou et al. (1993), together with the bimodal duration distribution, to suggest that SHBs and long GRBs are two distinctive populations. Figure 3 depicts T_{90} and the hardness (ratio between the 50 – 100 keV and the 25 – 50 keV fluence) of *BATSE*

⁶ The sample includes only long GRBs that have high resolution light curve and an initial pulse that is shorter than 2 s

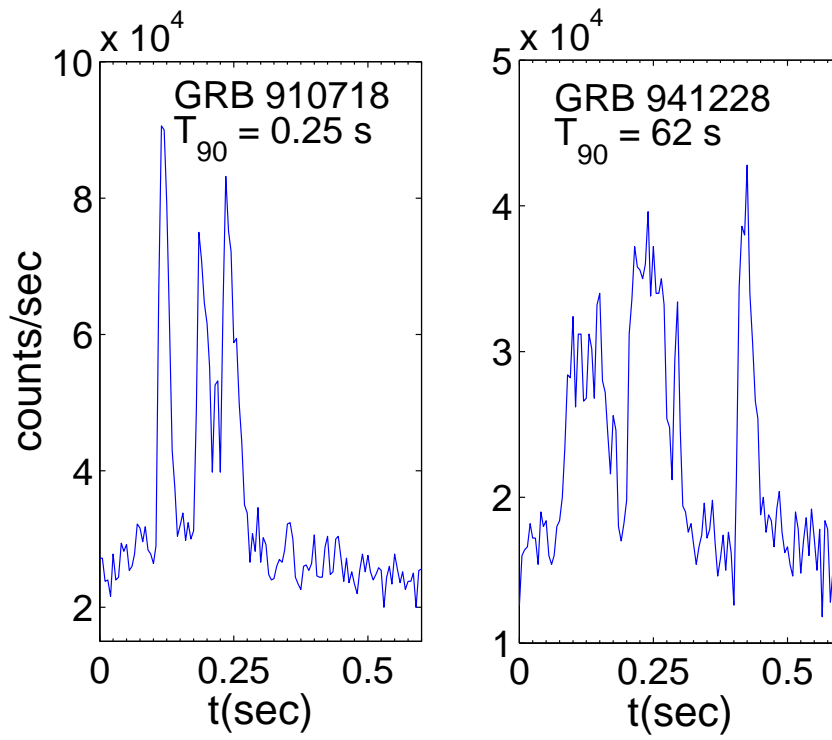


Fig. 2. **Left:** The light curve of GRB 910718, a bright SHB with $T_{90} = 0.25$ s. **Right:** The first 0.7 s of GRB 941228, a bright long GRB with $T_{90} = 62$ s. The figure demonstrates the similarity in short-time-scale structure in long and short GRBs. The resolution of both light curves is 5 ms. Both bursts show variability down to the resolution limit.

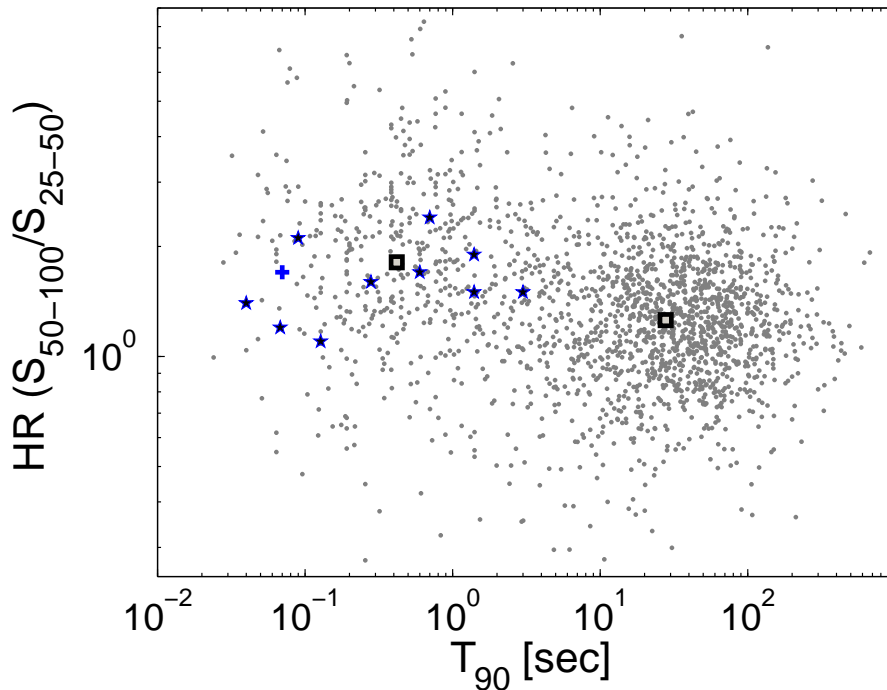


Fig. 3. The duration T_{90} and the hardness ratio of all GRBs with available data from the *BATSE* catalog (*dots*). *Swift* (*stars*) and *HETE-2* (*plus*) SHBs are marked as well. The average logarithmic values of *BATSE* bursts with $T_{90} > 2$ s and $T_{90} < 2$ s are marked by the two squares. The hardness ratio used here is the ratio of the fluence in the 50-100 keV and 25-50 keV energy bands. The *BATSE* data is taken from the current *BATSE* catalog and *Swift* and *HETE-2* data are taken from Table 2, where the hardness ratio is calculated using the photon index. Note that the fluence ratio that is used here is different than the typical hardness ratio, that uses counts.

GRBs. It is evident that while SHBs are on average harder, the variance in the hardness ratio is such that the two populations overlap and the distinction between them is not well determined.

Ghirlanda, Ghisellini & Celotti (2004) explore the time integrated spectra of 28 bright *BATSE* SHBs. They attempt to fit the spectrum of each burst with four different spectral models – a single power-law, a broken power-law, a Band function (a smoothly broken power-law; Band *et al.*, 1993) and a power-law with an exponential cut-off (PLE):

$$\frac{dN}{dE} = N_0 E^\alpha \exp[-E/E_0] \quad (1)$$

where N is the photon count and $E_p = (2 + \alpha)E_0$ is the peak of νF_ν . They find that PLE model (Eq. 1) provides the best fit to the data. The values of E_p that Ghirlanda, Ghisellini & Celotti (2004) find are in the range 50 – 1000 keV (mean value 355 ± 30 keV), which are comparable to values observed in long

GRBs. They find values of α between -2 and 0.5 (mean value -0.58 ± 0.1), which are significantly harder than those of long GRBs. These higher values of the low energy power-law index are the main driver of the higher hardness ratio of SHBs.

The *Konus-Wind* SHB catalog (Mazets *et al.*, 2004) contains 140 spectra of 98 SHBs (for some SHBs the spectrum is time integrated and for some it is given in two or three different time intervals). Mazets *et al.* (2004) use the same spectral models as Ghirlanda, Ghisellini & Celotti (2004) to fit the spectra of *Konus-Wind* SHBs. They fit 60% of the spectra with a PLE, 21% with a single power-law and 16% with a Band function. The average α value of the PLE spectra is -0.78 , rather similar to the one found by Ghirlanda, Ghisellini & Celotti (2004) for *BATSE* SHBs. The average E_p of PLE spectra is 837 keV, significantly higher than the value found for *BATSE* events. This difference is probably a result of the wider energy window of *Konus-Wind*, 15 – 10000 keV compared to 25 – 2000 keV for *BATSE*. The highest E_p value in the *Konus-Wind* catalog is 3.1 MeV. In about 30% of the sample photons are observed up to 5 MeV but only in $\approx 5\%$ of the bursts harder photons are observed. Only a single burst shows 10 MeV photons (the one with a PLE spectrum with $E_p = 3.1$ MeV).

An important point is that while most spectra are consistent with exponential cut-offs, the low energy spectrum of most SHBs is too soft to be consistent with a blackbody spectrum. Lazzati, Ghirlanda & Ghisellini (2005) studied the spectra of 76 *BATSE* SHBs and find that in more than 75% of the bursts the spectrum is inconsistent with a blackbody spectrum.

The fact that PLE provides the best fit to most SHB spectra is in contrast to long GRBs, where a Band function, with a rather shallow high energy power-law ($\sim E^{-2.25}$), provides the best spectral fit for most of the bursts (Preece *et al.*, 2000; Ghirlanda, Celotti & Ghisellini, 2002). This dissimilarity may reflect a genuine intrinsic difference between the spectra of short and long GRBs, in which case long GRBs are actually harder than SHBs at high energies (\gg MeV). However, this difference may also be a result of observational selection effects. A PLE fit may be preferred over a Band function fit in cases of low signal-to-noise ratio at high energies, as suggested by the results of Kaneko *et al.* (2006) that analyze the spectra of the 17 brightest *BATSE* SHBs and find that most of them are well fitted by a Band function or a broken power-law.

Among SHBs with known redshifts there are only two bursts with good spectral data (the spectral range of *Swift* alone is too narrow to constrain the broad band spectrum). The prompt emission time-integrated spectrum of *HETE-2* SHB 050709 is best fitted by a PLE with $E_p = 86.5_{-11}^{+16}$ keV and $\alpha = -0.82_{-0.14}^{+0.13}$ ($E_0 \approx 73$ keV; Villasenor *et al.*, 2005). The *Konus-Wind*

spectrum of SHB 051221A is fitted by a PLE with $E_p = 402_{-72}^{+93}$ keV and $\alpha = -1.08_{-0.14}^{+0.13}$ ($E_0 \approx 436$ keV; [Golenetskii *et al.*, 2005a](#)).

As I discuss below, the hardest observed non-thermal photons in the prompt emission play an important role in constraining the Lorentz factor of the prompt emission source (§3.2). The observations described above show that there are many SHB spectra that are consistent with having no non-thermal photons above ~ 1 MeV, while other bursts show non-thermal emission at least up to ~ 5 MeV. There is no published evidence that SHBs emit non-thermal photons above 10 MeV. This is in contrast to long GRBs where there are bursts that show > 100 MeV photons (e.g., [Schneid *et al.*, 1992](#); [Sommer *et al.*, 1994](#); [Hurley *et al.*, 1994](#)). The lack of observed $\gtrsim 100$ MeV photons from SHBs may be in part an observational selection effect as well. At very high energies the background is negligible on prompt emission time scales and therefore the detectability depends on the fluence and not on the flux. Hence, SHBs, which have a significantly lower fluence than long GRBs, are much harder to detect at these energies.

2.1.4 Isotropic equivalent energy

In the few cases where SHB redshifts are known, the isotropic equivalent gamma-ray energy, $E_{\gamma,iso}$, and luminosity, $L_{\gamma,iso}$, can be calculated (i.e., assuming that the source emission is constant over the whole 4π sr solid angle). These values are listed in Table 2. The isotropic equivalent energy of SHBs ranges between $10^{49} - 10^{51}$ erg, which is 2 – 3 orders of magnitude smaller than the energy range of long GRBs. The peak isotropic equivalent luminosity in most SHBs with known redshift is 10^{50} erg/s and in a single case (SHB 051221A) it is even larger than 10^{52} erg/s. These values are comparable to those observed in long GRBs (see Table 2).

[Amati *et al.* \(2002\)](#) have shown that there is a tight relation between $E_{\gamma,iso}$ and the redshift correct peak spectral energy, $E_p(1+z)$, of long GRBs with known redshifts (see also [Lloyd, Petrosian & Mallozzi, 2000](#); [Lloyd-Ronning & Ramirez-Ruiz, 2002](#); [Lamb, Donaghy & Graziani, 2004](#)). Even before redshifts of some SHBs were determined, it was shown that SHBs do not follow the Amati relation⁷ ([Ghirlanda, Ghisellini & Celotti, 2004](#); [Nakar & Piran, 2005](#)). The recent detection of SHB redshifts has shown that SHBs with known redshifts do not follow the Amati relation as well ([Amati, 2006](#)).

⁷ [Nakar & Piran \(2005\)](#) and [Band & Preece \(2005\)](#) have used the same method to show that many *BATSE* long GRBs do not follow the Amati relation as well.

2.2 Afterglow

The breakthrough in the study of SHBs came in the spring-summer of 2005 with the first detections of X-ray, optical and radio afterglow emission (Gehrels *et al.*, 2005; Castro-Tirado *et al.*, 2005; Prochaska *et al.*, 2005; Fox *et al.*, 2005; Hjorth *et al.*, 2005a,b; Bloom *et al.*, 2006b; Covino *et al.*, 2006; Berger *et al.*, 2005). This discovery was facilitated by timely and accurate localizations by *Swift* and *HETE-2*, and came 8 years after the first afterglow detection of a long GRB. The difficulty in detecting SHB afterglows is to achieve precise localization from a small number of photons (compared to long GRBs) and then to quickly point a sensitive X-ray instrument in order to detect the afterglow, which is significantly fainter relative to long GRB afterglows.

The importance of afterglow detection is twofold. First, afterglow detection enables sub-arcsecond localization and, possibly, unambiguous determination of the host galaxy and its redshift. Second, the afterglow itself can teach us about the processes that take place after the explosion and to provide clues about the physics of the central engine and about the properties and environment of the progenitor. Here I discuss the observational properties of the afterglows themselves, while the environmental properties are discussed later. The discussion below is based on the small sample of the SHBs with observed afterglows, and even within this small sample a large variance exists. It is likely that as more SHB afterglows will be observed, the discussion below will have to be updated or revised.

2.2.1 The late time afterglow

Figures 4a & 4b depict the X-ray and optical afterglow isotropic equivalent luminosities as a function of the source time of all SHBs with known redshift. The observed X-ray flux as a function of observer time is presented in Fig. 5. The light curves roughly show a power-law decay on scales of hours to days, with significant additional variability in some cases. After several hours, the X-ray and optical temporal power-law decay appear to be rather similar in all observed SHBs with indices in the range of $\alpha \sim 1 - 1.5$ ($F_\nu \propto t^{-\alpha} \nu^{-\beta}$). An exception is the X-ray afterglow of SHB 051210 (La Parola *et al.*, 2006), which decays as $t^{-2.57}$ during at least the first several hours (the redshift of this burst is unknown and therefore its afterglow is not in the figure). The optical and X-ray afterglows show power-law spectra with indices in the range $\beta \sim 0.5 - 1.5$. These general properties of late SHB afterglows are similar to those observed in long bursts.

Whenever a dense temporal sampling of the afterglow (mostly in X-rays) ex-

Table 2
Prompt emission and afterglow properties

SHB	T_{90}^a [s]	z	S_γ^b $\times 10^{-7}$	$E_{\gamma,iso}^c$ $\times 10^{49}$	$L_{\gamma,peak}^d$ $\times 10^{50}$	$f_b^{-1}{}^e$	$E_\gamma{}^f$ $\times 10^{49}$	F_{XE}^g $\times 10^{-11}$	Aft. ^h	ref.
050509B	0.04	0.225	0.23 ± 0.09	0.25	0.7[35ms]			0.06	XE	1
050709*	0.07	0.16	3 ± 0.38	1.6	3[60ms]			800	XE/L,O	2
050724	3	0.258	6.3 ± 1	9.1	1[0.8s]	< 13	> 0.7	1200	XE/L	3
**	[1.3]					[< 500]	[> 0.02]		O,R	
050813	0.6	0.7 or 1.8	1.24 ± 0.46	11 48	3[0.3s] 20[0.2s]			0.3	XE	4
050906	0.13		0.84 ± 0.46					< 0.007	None	5
050925†	0.07		0.92 ± 0.18					< 0.003	None	6
051105A	0.28		0.4 ± 0.09						None	7
051210	1.4		1.9 ± 0.3					40	XE	8
051221	1.3	0.546	22.2 ± 0.8 (32.2_{-17}^{+1})	130 250	(550[3ms])	80	1.5 3	10	XE/L O,R	9
060313	0.7	< 1.7	32.1 ± 1.4 (110 ± 20)					30	XE/L O	10
060502B	0.09	0.287(?)	1 ± 0.13	0.8(?)				0.1	XE	11
060801	0.04		0.8 ± 0.1					0.1	XE	12
061201‡	0.8		3.3 ± 0.3					~10	XE/L,O	13
061217‡	0.3		0.46 ± 0.08					~0.1	XE/L	14

Various properties of SHB prompt and afterglow emission as detected by *Swift* and *HETE-2*. All the quantities are in c.g.s units.

^a T_{90} as measured from *Swift* observations in the 15 – 350 keV energy band. This value is not strictly equivalent to the *BATSE* T_{90} , where the 20 – 2000 keV energy band is used.

^b Fluence [$\times 10^{-7}$ erg/cm²] in the 15 – 350 keV energy band (except for 060801, 061201 & 061217 - 15 – 150 keV). The fluence in the 20-2000 keV energy band is given in parentheses for bursts that are also detected by *Konus-Wind*.

^c Energy [$\times 10^{49}$ erg] in the source frame 15 – 350 (20 – 2000) keV energy band.

^d Peak isotropic equivalent luminosity [$\times 10^{50}$ erg/s] in the source frame 15 – 350 (20 – 2000) keV energy band. This luminosity is measured over the source frame time interval that is indicated in the brackets.

^e The inverse beaming factor, $f_b = \theta_j^2/2$, assuming a two sided 'top hat' jet with a half opening angle θ_j .

^f The beaming corrected γ -ray energy: $E_\gamma = f_b E_{\gamma,iso}$.

^g The early X-ray flux [$\times 10^{-11}$ erg/cm²/s] in the 0.3 – 10 keV energy band at $t \approx 100$ s (observer frame).

^h Detection of afterglow in: XE - early ($t \sim 100$ s) X-ray, XL - late ($t \sim 1$ d) X-ray, O - optical, R-radio.

* This burst was detected by *HETE-2*, so T_{90} , the fluence and the energy are given in the 30 – 400 keV energy band.

** T_{90} when calculated by simulating the *BATSE* algorithm. The maximal beaming factor and the minimal energy in the parenthesis are derived with the more conservative limit on the jet opening angle of SHB 050724(see §4.6).

† The galactic latitude (0.1) and the spectrum of this burst are consistent with an origin of a Galactic SGR. However, there is no known Galactic SGR at this location.

‡ These bursts were observed while the manuscript was in the refereeing process and are therefore not discussed in the text.

(?) Based on a low significance association ($\approx 90\%$ confidence).

References - 1. Gehrels *et al.* (2005); Bloom *et al.* (2006b) 2. Villasenor *et al.* (2005); Fox *et al.* (2005); Hjorth *et al.* (2005a) 3. Barthelmy *et al.* (2005); Berger *et al.* (2005); Krimm *et al.* (2005); Grupe *et al.* (2006) 4. Sato *et al.* (2005); Prochaska *et al.* (2005); Berger (2006) 5. Parsons *et al.* (2005) 6. Markwardt *et al.* (2005) 7. Barbier *et al.* (2005) 8. La Parola *et al.* (2006) 9. Cummings *et al.* (2005); Soderberg *et al.* (2006a); Burrows *et al.* (2006) 10. Roming *et al.* (2006) 11. Bloom *et al.* (2006a); Sato *et al.* (2006a) 12. Sato *et al.* (2006b) 13. Markwardt *et al.* (2006) 14. Parsons *et al.* (2006)

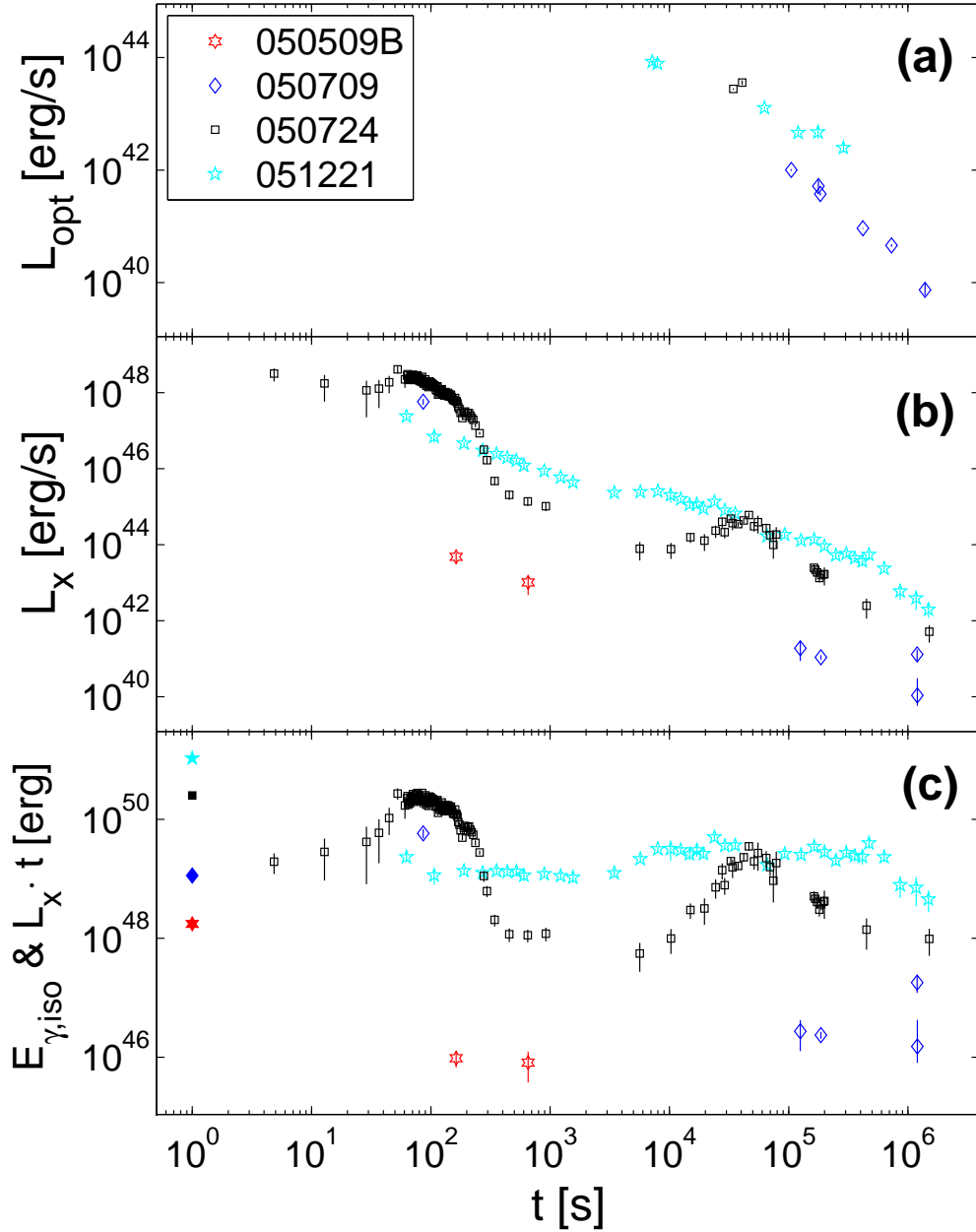


Fig. 4. The isotropic equivalent optical and X-ray luminosity as a function of the source frame time. Plotted are all SHB afterglows with a known redshift. **(a)** Optical luminosity (there was no optical detection of SHB 050509B). **(b)** X-ray luminosity. **(c)** X-ray luminosity multiplied by the time since the burst. This quantity illustrates the total energy emitted in the X-ray afterglow at a given time. The isotropic equivalent prompt emission fluence is plotted at $t = 1$ s (*solid symbols*). References: SHB 050509B: [Gehrels et al. \(2005\)](#); SHB 050709: [Villasenor et al. \(2005\)](#); [Fox et al. \(2005\)](#); [Hjorth et al. \(2005a\)](#); [Watson et al. \(2006\)](#); SHB 050724: [Barthelmy et al. \(2005\)](#); [Grupe et al. \(2006\)](#); [Berger et al. \(2005\)](#); SHB 051221A: [Soderberg et al. \(2006a\)](#); [Burrows et al. \(2006\)](#)

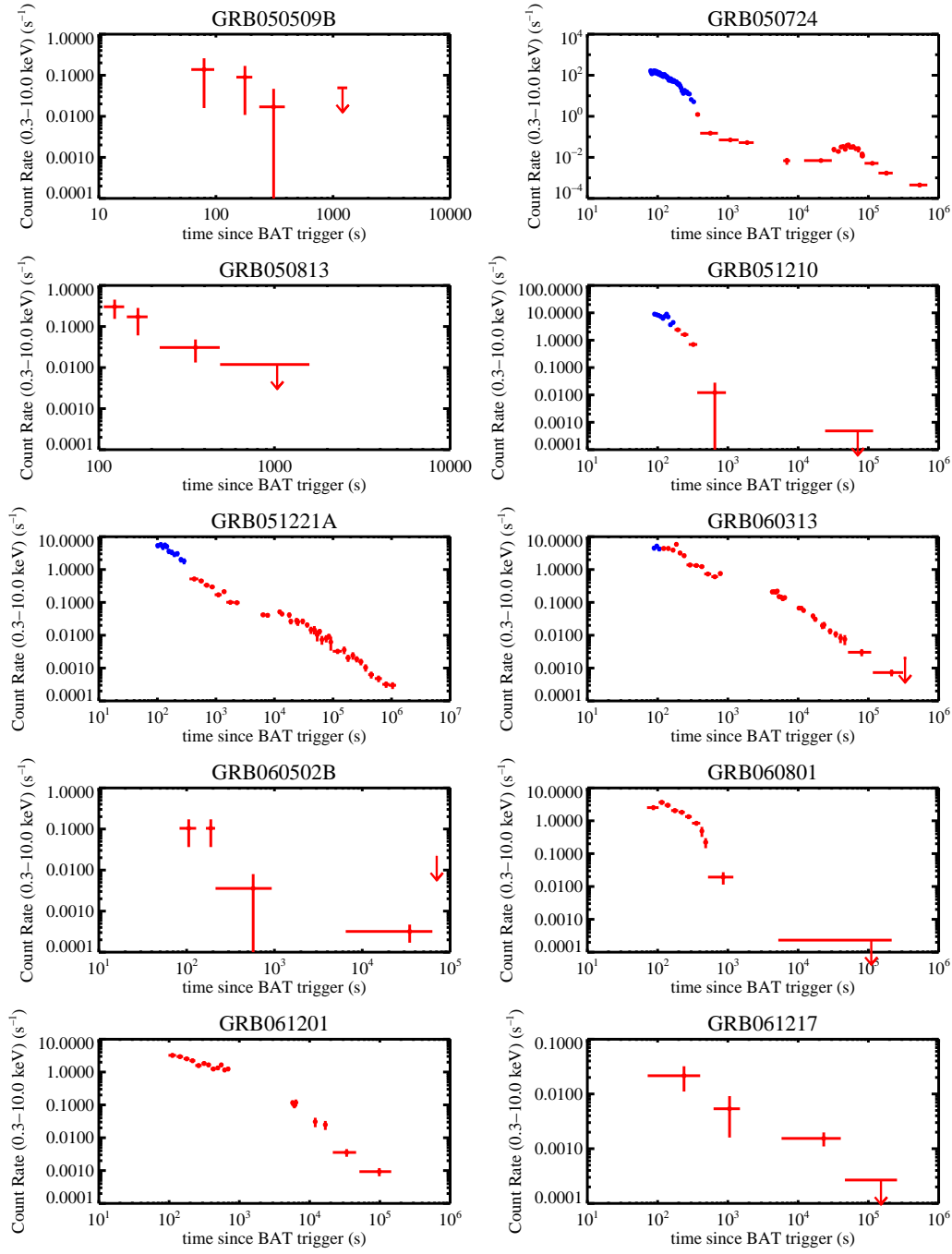


Fig. 5. SHB X-ray afterglow light curves observed by the *Swift* X-ray telescope (XRT; Windowed Timing mode in blue and Photon Counting mode in red). The light curves are given in units of count/s. The conversion factor to energy flux units is roughly $1 \text{ count/s} \approx 5 \times 10^{-11} \text{ erg/cm}^2/\text{s}$, where the exact conversion factor depends on the X-ray spectrum of each afterglow. *Courtesy of Judith Racusin and David Burrows.*

ists, significant superposed variability is evident, with diverse characteristics. The afterglow of SHB 051221 shows an X-ray brightening after ~ 2 hr, with a similar power-law decay before and after the brightening. A bright X-ray bump is observed, superimposed on a power-law decay, between 3 hr and 5 days after SHB 050724 occurred. In both of these cases no high-amplitude, rapid variability ($\Delta F/F \gg 1$ and $\Delta t/t \ll 1$) is seen. SHB 050709 does show rapid variability; after ≈ 15 days, a bright X-ray spike is observed ($\Delta F/F \approx 10$) that decays within 2 hr ($\Delta t/t \approx 0.01$). However, the detection of this spike is based on a single *Chandra* observation of nine photons (Fox *et al.*, 2005). This kind of variability, if confirmed, has far-reaching implications on theoretical models, as discussed in §4.

Observed SHB afterglows are significantly fainter than those of long GRBs. For example, after 1 day the SHB X-ray flux is fainter by more than an order of magnitude ($\sim 5 \cdot 10^{-14}$ erg/cm²/s in the four detected SHB late afterglows, compared to $\sim 5 \cdot 10^{-13}$ erg/cm²/s in long GRBs⁸). Moreover, early ($t \sim 100$ s) X-ray afterglow emission was detected in every long GRB that was observed at early times by *Swift*, while three out of the 11 SHBs observed by the *Swift* X-ray telescope (XRT) within ~ 100 s, lack detectable X-ray emission. If SHB afterglow flux is related to the flux of the prompt emission, as observed in long GRBs, then SHB afterglows are expected to be fainter (see §2.1.4). Fig. 4c shows that indeed this is part of the reason for the faintness of SHB afterglows. The figure presents SHB X-ray light curves multiplied by the time since the burst (illustrating the total energy emitted in the X-ray afterglow), as well as the prompt emission fluence (plotted at $t = 1$ s). This figure clearly shows that the X-ray afterglow is strongly correlated with the gamma-ray fluence and that the energy emitted in the X-ray afterglow is smaller than the gamma-ray energy by no more than a factor of ~ 10 . However, Fig. 6 shows that in SHBs in which the X-ray afterglow is not detected, the upper limits on the afterglows indicate that in these cases the emission is very faint, even compared to the gamma-ray fluence. See §4.5 for a discussion of the implications of this result.

We conclude that late SHB afterglows (hours-weeks) show roughly similar temporal and spectral properties to those observed in long GRBs, while being fainter on average. The afterglows of some SHBs are considerably fainter than these of long GRBs, even after correcting for the lower γ -ray energy output of these SHBs. The small number of SHB afterglows prevents a more detailed comparison. These observations are discussed in the context of the external shock model for GRB afterglows in §4.

⁸ Values are taken from the *Swift* archive, http://swift.gsfc.nasa.gov/docs/swift/archive/grb_table.

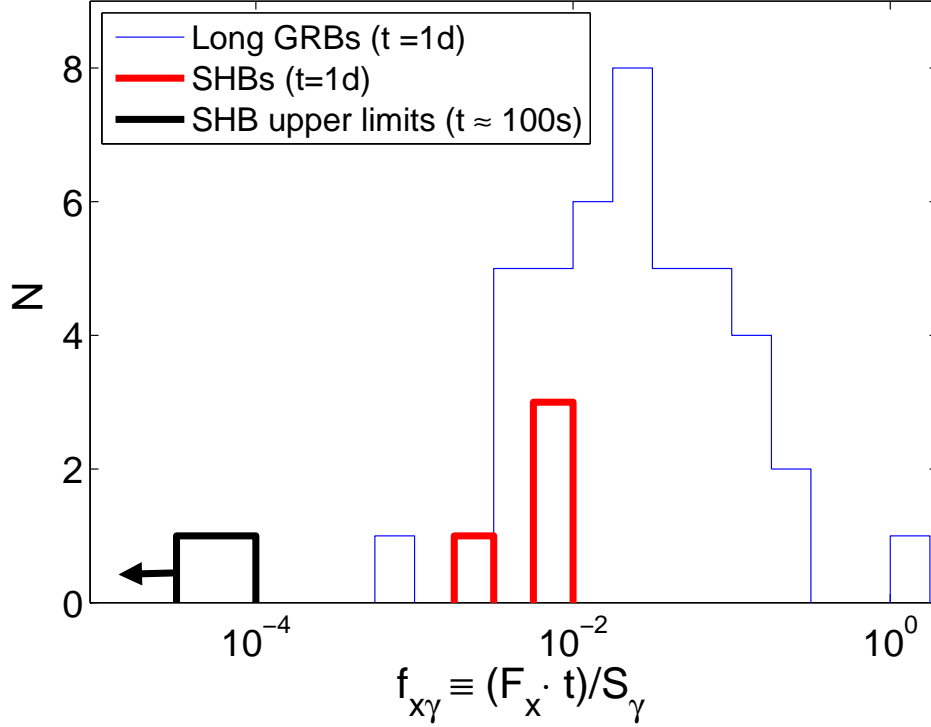


Fig. 6. A histogram of the ratio between the X-ray energy flux at time t multiplied by t and the prompt gamma-ray fluence. This is an estimate of the ratio between the energy emitted in the late X-ray afterglow and in the prompt emission. The ratio is given for *Swift* long bursts (*thin line*) and for SHBs with X-ray afterglow observed after ~ 1 day (*thick line*). The upper limit at $t \sim 100$ s for two *Swift* SHBs without detected X-ray afterglow is marked with arrow (*thick line + arrow*). The theoretical implications of this figure are discussed in §4.5. Reference: *Swift* archive, http://swift.gsfc.nasa.gov/docs/swift/archive/grb_table.

2.2.2 Soft X-ray “tails” of the prompt emission and the early afterglow

Several SHBs show a bright X-ray tail that follows the short prompt gamma-ray emission and lasts for ~ 100 s. This X-ray component is most prominent in SHBs 050709 and 050724, where its energy is comparable to (SHB 050724) or even larger by a factor of ~ 3 (SHB 050709) than the energy in the prompt gamma-rays (Barthelmy *et al.*, 2005; Villasenor *et al.*, 2005). This early luminous X-ray emission seems to be a common feature in SHBs, although there are cases in which the X-ray tail is either much weaker or does not exist at all (e.g. SHBs 050906 and 050925). An early hint to the existence of this component was found by Lazzati, Ramirez-Ruiz & Ghisellini (2001) that summed the gamma-ray light curves of 76 *BATSE* SHBs and detected an X-ray signal starting 30 s after the trigger and lasting for ~ 100 s (see also Connaughton, 2002; Frederiks *et al.*, 2004). The longer time scale and the softer spectrum of the X-ray tail, as well as the temporal gap from the short-hard prompt emission, clearly distinguishes it from the prompt emission. However, extrapolation of the late afterglow back to early times suggests that the X-ray tail is not the onset of the late afterglow. It is therefore unclear if the physical origin of this component is related to the prompt emission, to the afterglow or to a third process. In those cases where the energy in the X-ray tail is large, it may be detected also in gamma-rays, causing a SHB to look like a long GRB (see §2.7). Norris & Bonnell (2006) find eight *BATSE* GRBs with $T_{90} > 2$ s that show an initial short duration emission that is followed by a long episode of softer emission. The spectral lags of all these bursts are short, suggesting that these are SHBs. The extended emission in some of these bursts is highly variable and its energy is comparable to that of the initial spike. Based on comparison between their sample and the results of Lazzati, Ramirez-Ruiz & Ghisellini (2001), they suggest that the peak flux ratio between the initial spike and the extended tail can vary by a factor 10^4 between different bursts.

In bursts that exhibit a bright X-ray tail, it is followed by a steep temporal decay ($\alpha \gtrsim 2$; $\alpha \equiv -d\log(F_\nu)/d\log(t)$) before the typical late afterglow ($\alpha \sim 1$) is observed. This fast decay is clearly seen in SHBs 050709 and 050724. A fast decay phase is also observed in SHB 051210 (La Parola *et al.*, 2006). Here the first X-ray observation is after 80 s and the flux is already falling rapidly, until a flare is observed between 100 – 200 s. The energy in this X-ray flare is comparable to the prompt emission energy. After the flare the X-ray flux decays as $t^{-2.6}$ and there is no evidence for a regular late afterglow decay. In other bursts the regular X-ray decay ($\alpha \sim 1$) is observed starting at early times (e.g., SHB 050509B). Fig. 7 illustrates the main features observed in SHB X-ray afterglows.

The overall early X-ray emission of SHBs is different from the complex early X-ray afterglows of long GRBs (e.g., Nousek *et al.* 2006). Long GRBs do not

show similar X-ray tails, which are separated from the prompt emission⁹, and while there is a typical phase of fast X-ray decay in long GRBs, this decay marks the end of the prompt emission and is not the end of a distinctive X-ray component as it is in SHBs. The phase of shallow X-ray decay, which is often observed in long GRBs, was not observed so far in SHBs. Fig. 7 presents a qualitative comparison between the afterglows of long and short GRBs.

An early optical afterglow was detected so far only in one SHB (060313; Roming *et al.* 2006). In this burst the optical emission is constant at first ($t = 100 - 1000$ s) followed by a shallow decay, superimposed with rapid variability. The X-ray afterglow of this burst is uncorrelated with the optical emission.

2.3 Observed redshift distribution

It was suspected that SHBs take place at cosmological distances as soon as it was realized that they may be a distinct phenomenon from long GRBs. Indirect evidence for their cosmological origin were the nearly isotropic angular distribution in the sky (Briggs *et al.*, 1996; Balazs, Meszaros & Horvath, 1998) and the value of¹⁰ $\langle V/V_{max} \rangle < 0.5$ (Katz & Canel, 1996; Schmidt, 2001). These indicators also suggested that observed SHBs are closer than observed long GRBs. Guetta & Piran (2005) find that for SHBs $\langle V/V_{max} \rangle = 0.39 \pm 0.02$, which is significantly larger than the value $\langle V/V_{max} \rangle = 0.29 \pm 0.01$ they find for long GRBs. Magliocchetti, Ghirlanda & Celotti (2003) calculate the two-point angular correlation function for *BATSE* SHBs and find a $\sim 2\sigma$ deviation from isotropy on angular scales $\sim 2^\circ - 4^\circ$ (a similar deviation is not found for long GRBs). They suggest that this deviation is induced by nearby large-scale structure through a low-redshift population of SHBs.

The first limits on the distance to individual SHBs was obtained by examination of Interplanetary Network (IPN) localizations with small error boxes¹¹ (Nakar *et al.*, 2006). The lack of bright galaxies inside the small IPN error

⁹ Long GRBs do show X-ray flares but only rarely these have an energy that is comparable to that of the prompt emission

¹⁰ V/V_{max} is the ratio of the volume that is enclosed within the distance in which the event is actually observed, and the one which is enclosed within the maximal distance to which the same event would still be detectable, assuming an Euclidian space. Under the assumption that sources are distributed uniformly in distance, $\langle V/V_{max} \rangle = 0.5$ in Euclidian space. A smaller value, therefore, suggests sources at cosmological distances where the smaller the value of $\langle V/V_{max} \rangle$, the larger is the typical distance to the sources.

¹¹ Earlier examination of IPN error boxes was carried out by Schaefer *et al.* (1998), without deriving constraints on the bursts' distances. See also Schaefer (2006).

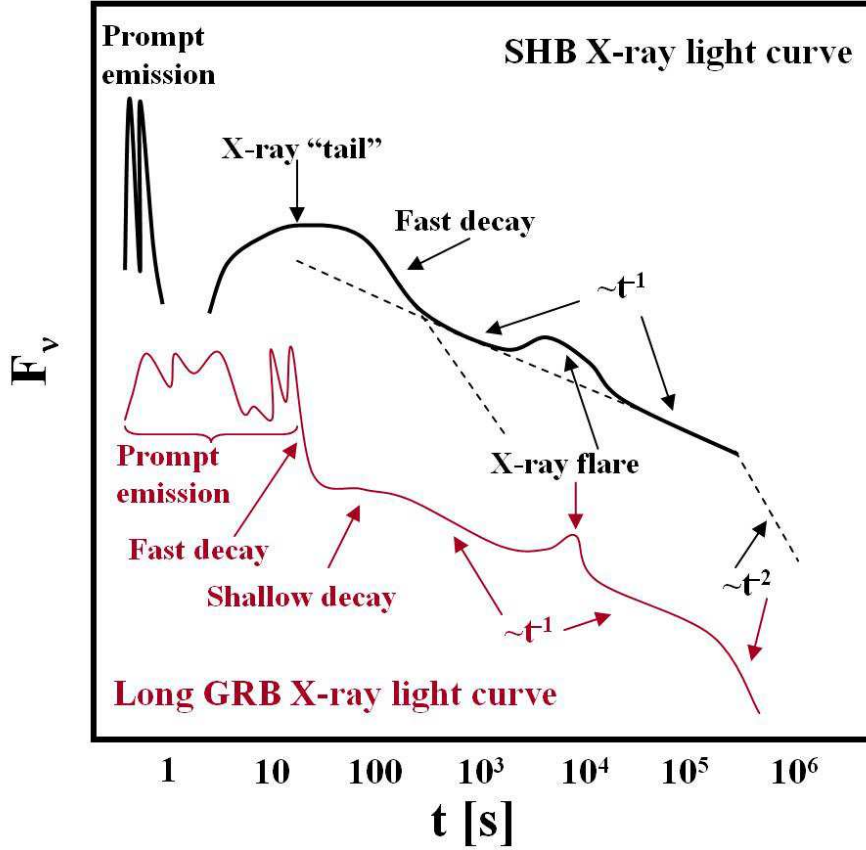


Fig. 7. An illustration of the main features observed in SHB X- and γ -ray light curves (*thick black line*) and comparison to long GRBs (*thin red line*). The dashed lines in the SHB light curve represent alternative features that are observed in some bursts. The hard SHB prompt emission is followed in some bursts by a soft X-ray tail. The tail is well separated both in time and in spectrum from the prompt emission. If a ‘tail’ is observed, it is followed by a steep decay that in most bursts turns into a shallower $\sim t^{-1}$ decay. Late X-ray flares can be observed at any time. So far a single SHB (051221A) has shown a late break in its light curve ($\sim t^{-2}$) that is interpreted as a jet break. Prompt emission of long GRBs, in contrast, is typically followed by a fast decay that flattens into a very shallow decay, before it steepens again to a $\sim t^{-1}$ decay. X-ray flares and late light curve breaks are observed in long GRBs as well.

boxes of six bright SHBs implied that the distances to these bursts exceed 100 Mpc (this limit was derived under the assumption that the SHB rate follows UV, blue or red light). The limits on the distances translate to energy output lower limits of order 10^{49} erg, implying that these bursts can be detected by *BATSE* at distances greater than Gpc. This result provided another strong indication that SHBs constitute a bone fide cosmological population.

The final confirmation of the cosmological origin of SHBs came with the secure identification of their host galaxies, following sub-arcsecond localizations of afterglows detected by *Swift* and *HETE-2*. The measured redshifts of the host galaxies are listed in Table 2. All together there are 3 SHBs (050709, 050724 & 051221) with sub-arcsecond localizations that fall on top of galaxies which are considered to be “securely” identified as the hosts. The afterglow of SHB 050509B was detected only by the *Swift* X-ray telescope (XRT) and therefore was localized only up to within several arcseconds. The error circle is located in the outskirts of a giant elliptical. The confidence that this is indeed the host galaxy is estimated to be $3 - 4\sigma$ (Gehrels *et al.*, 2005; Bloom *et al.*, 2006b). The XRT error circle of SHB 060502B is $\approx 20''$ from a bright early type galaxy at $z=0.287$. Bloom *et al.* (2006a) suggest that this galaxy is the host of SHB 060502B and they estimate the confidence of this association to be $\approx 90\%$. Finally, the afterglow of SHB 050813 was also detected only by the XRT and its location falls on the outskirts of an early type galaxy that is part of a group/cluster at $z = 0.72$ (Prochaska *et al.*, 2005) and on top of another, fainter, early type galaxy that is part of an apparent cluster at $z \approx 1.8$ (Berger, 2006). Therefore, this burst is most likely at redshift 0.72 or 1.8 and its host is an early type galaxy in a cluster or a group.

The cumulative distribution of the observed SHB redshifts (including the one detected by *HETE-2*) is compared in figure 8 to the distribution of *Swift* long GRBs. The most striking result of this comparison is that SHBs are detected at much lower redshifts than typical long GRBs - while the median redshift of SHBs is $z \approx 0.25$, the median redshift of *Swift* long GRBs is $z \approx 2.5$. Note that some of the observed SHBs are bright enough to be detected out to a much higher redshift. For example the prompt emission as well as the afterglow of SHB 051221 would be detected by *Swift* also at a redshift of $z \approx 2$. Nevertheless, caution is required when using the observed redshift distribution to draw quantitative conclusions. The redshifts of more than half of the *Swift* SHBs are unknown and thus the observed distribution is likely to be biased by selection effects that are needed to be quantified before the entire sample can be used.

Gal-Yam *et al.* (2005) study the four best-localized IPN SHBs (< 10 arcmin²), searching for significant luminosity overdensities inside the error boxes. They identify two putative host/cluster associations with SHBs. SHB 790613 is found to be significantly (3σ c.l.) associated with the rich galaxy cluster Abell

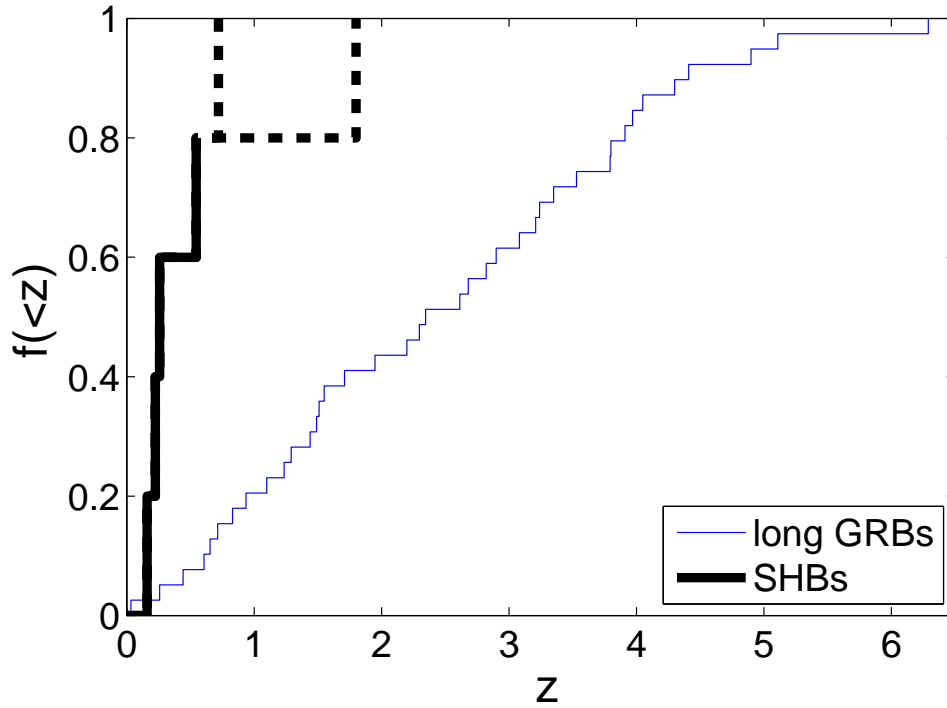


Fig. 8. The cumulative distribution of observed SHB redshifts (including *HETE-2* SHB 050709 and not including the low significance redshift association of SHB 060502B) [*thick line*] compared to the of cumulative distribution of *Swift* long GRBs with known redshifts [*thin line*]. The dashed thick lines corresponds to the two possible values of the redshift of SHB 050813 (0.72 or 1.8).

1892 ($z = 0.09$) while SHB 000607 is found to be associated (at the 2σ c.l.) with a bright galaxy at $z = 0.14$. They derive lower limits on the redshifts of the two other bursts they examine of $0.25[0.06]$ at $1[2]\sigma$ c.l.

Further clues about the redshift of SHBs are found by correlating their locations with volume limited samples of galaxies and clusters. [Tanvir *et al.* \(2005\)](#) find a correlation between the locations of *BATSE* SHBs and the positions of galaxies in the local Universe, suggesting that between 10 and 25 percent of *BATSE* SHBs originate at very low redshifts ($z < 0.025$). These SHBs do not seem to be extra-galactic versions of the giant flares from SGR 1806-20 (see §2.9.1) as they are correlated with early-type galaxies as well. So far, none of the well localized SHBs (≈ 15 bursts) are associated with such a nearby galaxy. [Ghirlanda *et al.* \(2006\)](#) find a positive 2σ angular cross-correlation signal, on scales $< 3^\circ$, between SHBs and galaxy clusters at $z < 0.45$. The significance of the signal increases when only clusters at $z < 0.1$ are considered.

[Berger *et al.* \(2006b\)](#) explore the XRT error circles of SHBs with detected early X-ray afterglows but without identified hosts. They find that the galaxies within these error circles are fainter than 23-26 mag, and therefore are most likely at higher redshifts than the identified SHB hosts. Based on comparison to the redshifts of galaxies in the GOODS ([Cowie *et al.*, 2004](#); [Wirth *et al.*, 2004](#)) and the HUDF ([Coe *et al.*, 2006](#)) [Berger *et al.* \(2006b\)](#) conclude that at least 1/4 of the Swift SHBs are at $z > 0.7$. This conclusion is valid if the progenitors of these SHBs did not travel long distances from their hosts so these are still within the XRT error circles.

We conclude that SHBs were shown to be genuine cosmological events which are observed, on average, at significantly lower redshifts than long GRBs. Indirect methods suggest that a non-negligible fraction of SHBs originate even closer - in the local universe, while non-detection of bright galaxies in some XRT error circles suggest that a significant fraction of the SHBs originate at $z \sim 1$. These results still require validation by future observations. The conclusions that can be drawn from the observed redshift distribution on the *intrinsic* redshift distribution of SHBs are discussed in §5.1.2.

2.4 Host galaxies and cluster associations

Various properties of known SHB host galaxies are listed in Table 3 (see [Berger, 2006](#); [Bloom & Prochaska, 2006](#), for recent SHB host galaxies brief reviews). Host galaxies include both early- and late-type galaxies, as well as field and cluster galaxies. This diversity is in striking contrast to the properties of the host galaxies of long GRBs, which are typically dwarf starburst galaxies and are always (so far) found in the field. Moreover, the typical spe-

cific star-formation rate (SFR) in a long GRB host is $\approx 10 M_{\odot} \text{ yr}^{-1} (L/L_*)^{-1}$ (Christensen, Hjorth & Gorosabel, 2004) while the specific SFR of SHB late-type hosts is significantly smaller, $\lesssim 1 M_{\odot} \text{ yr}^{-1} (L/L_*)^{-1}$. A conservative comparison between the typical stellar ages in the hosts of long and short GRBs rejects the null hypothesis that the two populations are drawn from the same parent distribution at 99.75% confidence (Gorosabel *et al.*, 2006). These differences between the host galaxies of short and long GRBs are among the main foundations of the recent validation that long and short GRBs are two different physical phenomena.

SHBs that take place in early-type galaxies are clearly associated with an old stellar population. SHBs in late-type star-forming galaxies, on the other hand, are not necessarily associated with young stars. The hosts of both SHBs 050709 and 051221 show evidence for a significant population of old (~ 1 Gyr) stars (Covino *et al.*, 2006; Soderberg *et al.*, 2006a). Moreover, an examination of the exact location of SHB 050709 within its host shows that it is not associated with the main star-forming regions in that galaxy (Fox *et al.*, 2005).

Berger *et al.* (2006a) explore the association of *Swift* SHBs with clusters. They determine, using optical spectroscopy, that SHBs 050709, 050724 and 051221A are not associated with galaxy clusters. Using X-ray observations they find that except for SHB 050509B there is no evidence for other associations of *Swift* SHBs with clusters that are brighter than $3 \cdot 10^{-14} \text{ erg/s/cm}^2$, or with mass $M > 5 \cdot 10^{13} M_{\odot}$, assuming a typical redshift $z = 0.3$. These results suggest that about 20% of SHBs are associated with massive clusters, which is consistent, within the uncertainties, with the fraction of stellar mass in such clusters (Fukugita, Hogan & Peebles, 1998).

Finally, it is important to remember that since host galaxies were identified only for less than half of the *Swift* bursts, this sample likely suffers from selection effects. The distribution of the SHB offsets from their host centers (Table 3) is also expected to be biased by similar selection effects. As we discuss later (§5.2.3), some progenitor models predict brighter afterglows within late-type galaxies, making such hosts easier to detect (Belczynski *et al.*, 2006). Additionally, the most popular progenitor model (compact binary merger) predicts that some of the events will take place far from their host galaxies ($\gtrsim 100$ kpc). This idea is also supported by the large possible offset of SHB 050509B (see Table 3). In such cases the afterglow is expected to be very dim and even when an afterglow is detected, the association with the parent host can be unclear.

Table 3
Putative host galaxy properties

SHB	z	Type ^a	L/L_* ^b	SFR M _⊙ /yr	Offset (kpc)	Offset (r/r_e)	Assoc. ^c	SN ^d limit	Ref.
050509B	0.225	E(c)	3	< 0.1	44 ⁺¹² ₋₂₃	13 ⁺³ ₋₇	3 – 4σ	-13	1
050709	0.16	Sb/c	0.1	0.2	3.8	1.8	Secure	-12	2
050724	0.258	E/S0	1.5	< 0.03	2.6	0.4	Secure		3
050813	0.72 or 1.8	E/S0(c/g) E/S0(c)							4
051221A	0.546	Late	0.3	1.4	0.76	0.29	Secure	-17.2	5
060502B	0.287(?)	Early	1.6	0.6	73 ± 19		≈ 90%		6
IPN SHBs:									
790613	0.09	E/S0(c)					3σ		7
000607	0.14	Sb	1	0.3			2σ		7

^a Hubble type of the host galaxy. (c)[(g)]: The host belong to a galaxy cluster [group].

^b Early-type: the rest frame K-band host luminosity in units of K-band L_* . Late-type: the rest frame B-band host luminosity in units of B-band L_* .

^c The confidence level of the association between the putative host galaxy and the SHB. The association is considered to be secured when a sub-arcsecond localization of the afterglow coincides with the putative host.

^d The limit on the rest-frame absolute magnitude after $\approx 7 - 14$ days (M_R for SHBs 050509B and 050709 and M_V for SHB 051221) of a supernova associated with the SHB.

References - 1. Gehrels *et al.* (2005); Fox *et al.* (2005); Bloom *et al.* (2006b) 2. Fox *et al.* (2005); Prochaska *et al.* (2005); Covino *et al.* (2006) 3. Berger *et al.* (2005) 4. Prochaska *et al.* (2005); Berger (2006) 5. Soderberg *et al.* (2006a) 6. Bloom *et al.* (2006a) 7. Gal-Yam *et al.* (2005)

2.5 Limits on a supernova component

Despite the low redshifts of the first two SHB afterglows and the extensive optical follow-up, no associated supernova was detected. The limits are so deep (see Table 3) that an object that is ~ 10 times fainter than the faintest observed supernova (of any type) would have been detected. These observations are again in striking contrast to the observations of long GRBs. So far a supernova was detected in almost any long GRB with a redshift low enough to enable such a detection (see a discussion of GRBs 060505 and 060614 in §2.8). The lack of associated supernovae is another line of evidence that support the distinct nature of long and short GRBs.

2.6 Observed rate

The whole-sky detection rate of *BATSE* was ≈ 170 SHBs per year (Meegan *et al.*, 1997). This rate can be translated to an observed local rate ($z \ll 1$) using the observed *Swift* redshift distribution. The first three *Swift* SHBs with known redshift constitutes a complete sample (see discussion in §5.1.1), unbiased by selection effects other than the *Swift* sensitivity, which is roughly comparable to that of *BATSE* for SHBs (Band, 2006). Two out of these three bursts are within a distance of 1 Gpc, implying that at least 15% of all *Swift* SHBs are within this distance (at the 2σ c.l.). Since the SHB redshift distributions of *Swift* and *BATSE* bursts are not expected to be very different (given the similar detector thresholds) the observed local rate is $\mathcal{R}_{SHB,obs} \sim 10 \text{ Gpc}^3 \text{ yr}^{-1}$ (Nakar, Gal-Yam & Fox, 2006). This rate is larger by about an order of magnitude than estimated local rate of the long GRB (Guetta, Piran & Waxman, 2005). It is also higher than estimates of the SHB rate that were done before the detection of SHB afterglows (Schmidt, 2001; Ando, 2004; Guetta & Piran, 2005) by a factor of 10 – 100.

2.7 Identifying an SHB

An important observational challenge is to be able to distinguish between SHBs and long GRBs on a burst-to-burst basis¹². This was not so important prior to the detection of afterglows, when SHBs were studied statistically, using mainly prompt emission observations. However, now, when most recent scientific progress is based on a small sample of bursts with afterglows, this

¹² Here, the term SHB refers to any burst that is physically associated with the population that constitutes the majority of *BATSE* GRBs with $T_{90} < 2$ s. Note that such a burst may not have $T_{90} < 2$ s.

topic becomes crucial. It will probably remain an important issue even when the sample size of SHBs with afterglows will increase significantly if, as happened for long GRBs, much of the progress will be based on a few bursts with unique properties (e.g., very low redshifts).

Currently, no satisfactory tests can provide a definite burst classification based on the prompt emission properties alone. The test which is commonly used ($T_{90} < 2$ s) is based on the *BATSE* duration distribution and, as evident from Fig. 1, is rough and somewhat arbitrary ($T_{90} < 3$ s would serve just as well). Clearly, there are long GRBs with $T_{90} < 2$ s and SHBs that last longer than 2 s. Usage of this criterion is further complicated by the possible contribution of the X-ray tail, which follows some SHBs, to T_{90} (Norris & Bonnell, 2006). As demonstrated in Fig. 3, considering the hardness ratio does not significantly improve the ability to make a correct identification. A third prompt emission property that can be used is the spectral lag (see §2.1.2; Norris, Scargle & Bonnell, 2001), which in long GRBs is typically positive and, on average, longer than in SHBs. Unfortunately, the lag distributions of the two populations overlap as well. While a burst with a long ($\gtrsim 0.1$ s) positive lag probably belongs to the long group, the opposite is not true, since there are long GRBs with short lags. Here, the lag-luminosity anti-correlation that was found for long GRBs may be of help (Norris, Marani & Bonnell, 2000). Long GRBs with short spectral lags (~ 10 ms) tend to be the brightest ones ($\gtrsim 10^{52}$ erg/s). Therefore, SHBs seem to occupy a separate region in lag-luminosity space - short lags ($\lesssim 10$ ms) and lower luminosity ($\lesssim 10^{52}$ erg/s). This method, although promising, still needs to be validated by increasing the sample size of SHBs with known luminosity. Finally, since there are outliers to the lag-luminosity relation of long GRBs, even this method cannot provide absolute classification.

Tests that assign probability to the classification using the prompt emission alone (e.g., as suggested by Donaghy *et al.* 2006) are also questionable. First, the sample that is currently used to derive such tests is the *BATSE* sample, while the tests are applied to bursts detected by other detectors (e.g., *Swift* and *HETE-2*). Such an application may be compromised since statistical properties of an observed sample depend strongly on detector properties. Second, any decomposition of the observed distribution to a sum of underlying distributions (e.g., Horváth, 2002) depends on the assumed shape of the underlying functions, which is not uniquely determined. For example, the X-ray tails observed in some SHBs suggest that the duration distribution of SHBs alone may be bimodal - one peak corresponds to SHBs with faint X-ray tails and the other includes SHBs for which the X-ray tails are bright enough to affect T_{90} (according to this speculation, the second longer peak is not observed because long GRBs dominate the observed distribution above ~ 2 s).

Based on the small sample of SHBs with afterglows it seems that a much

better classification can be done based on environmental properties (Donaghy *et al.*, 2006), i.e., the host galaxy type, its star-formation rate, the location of the burst within the host (§2.4), and on the existence of an accompanying supernova (§2.5). This classification is also based on physical grounds – progenitors of long GRBs are associated with massive stars, while SHBs occur preferentially (according to the current small sample) in places where the probability to find massive stars is small. Put differently, if a burst with a duration of 100 s will be detected in an early type galaxy and without an accompanying supernova, it is most likely related physically to SHBs and not to long GRBs (see discussion about GRBs 060505 and 060614 in §2.8).

A more quantitative test can be carried out when the afterglow is imaged by the *Hubble Space Telescope (HST)*. Fruchter *et al.* (2006) explored 42 *HST* images of long GRB host galaxies and found that afterglow locations within the hosts are more concentrated in bright blue pixels than those of core-collapse supernovae. This concentration is most likely a result of the very short lifetime of the progenitors of long GRBs. A quantitative test to determine if a burst is long can be done by analyzing its *HST* image in the same way Fruchter *et al.* (2006) did, and comparing the result with the known distribution of long GRB locations.

GRB 050416A demonstrates the difficulty to use the prompt emission properties to classify an event. It is a soft burst with a border-line duration ($T_{90} = 2.4$ s) and a negative spectral lag (Sakamoto *et al.*, 2006). As it turns out, this specific burst took place in the brightest blue *HST* pixel of a star-forming galaxy ($\approx 4 M_{\odot}/\text{yr}/(L/L_*)$) and its afterglow shows the probable signature of a supernova component (Soderberg *et al.*, 2006b), implying that it is most likely a long burst.

In this review I used the “classical” criterion, namely $T_{90} < 2$ s, when compiling Table 2 and as the sample of SHBs with afterglows or significant afterglow constraints. Most of the bursts in this sample are short enough, $T_{90} \ll 1$ s, to confidently assume that they are bone fide SHBs. The only two SHBs that have border-line durations and that have significant effect on theoretical interpretation are SHBs 050724 and 051221A. The former is observed within an early-type galaxy and therefore is not a long GRB. SHB 051221A has a short spectral lag compared to long GRBs, even when its high luminosity is considered (Gehrels *et al.*, 2006), supporting its classification as a SHB. Nevertheless, the possibility that GRB 051221A is not a genuine SHB cannot be excluded.

Table 4
GRBs with $T_{90} \geq 2$ s that were proposed to be SHBs

SHB	T_{90}^a [s]	z	$E_{\gamma,iso}$ 10^{49} erg	Ref.
050911 [†]	16	0.165(?)	2(?)	Tueller <i>et al.</i> (2005); Berger <i>et al.</i> (2006a)
051114A	2.2			Sakamoto <i>et al.</i> (2005)
051211A	4.2			Kawai <i>et al.</i> (2005)
051227	8			Hullinger <i>et al.</i> (2005)
060121 ^{††}	2	4.6[1.7]	$24[4] \times 10^3$	de Ugarte Postigo <i>et al.</i> (2006); Levan <i>et al.</i> (2006a)
060505	4	0.089	1.2	Fynbo <i>et al.</i> (2006); Ofek <i>et al.</i> (2006a)
060614	102	0.125	80	Gal-Yam <i>et al.</i> (2006); Fynbo <i>et al.</i> (2006) Della Valle <i>et al.</i> (2006); Gehrels <i>et al.</i> (2006)
061006	130			Krimm <i>et al.</i> (2006)
061210	85			Palmer <i>et al.</i> (2006)

A compilation of *Swift* GRBs that were appeared in the literature as putative SHBs although their duration is 2 s or longer. *HETE-2* GRB 060121 is included as well since its redshift is constrained.

^a - T_{90} as measured from *Swift* observations in the 15 – 350 keV energy band.

[†] - The putative redshift is based on a possible association with the cluster EDCC 493 (Berger *et al.* , 2006a).

^{††} - A photometric redshift. Both $z \approx 4.6$ and $z \approx 1.7$ are consistent with the observations (de Ugarte Postigo *et al.* , 2006).

2.8 Additional putative SHBs

Given the difficulty to identify SHBs, a growing number of GRBs that do not pass the rough cut of $T_{90} < 2$ s were suggested, for various reasons, to physically belong to the SHB population. Table 4 lists all such *Swift* GRBs as well as *HETE-2* GRB 060121.

The most interesting bursts in this sample are GRBs 060121, 060505 and 060614. Each one of these bursts affects the SHB theory if it is related physically to this population. Unfortunately, it is unlikely that an unambiguous classification will ever be achieved in any of the cases. I mention some of the relevant theoretical implications of these bursts being SHBs in the theoretical sections.

GRB 060121 is a border line burst ($T_{90} = 1.97 \pm 0.06$ s; Donaghy *et al.* , 2006) with an optical afterglow (Levan *et al.* , 2006a) and a faint host with a photometric redshift probability with two peaks $z = 1.7 \pm 0.4$ and $z = 4.6 \pm 0.5$ (de Ugarte Postigo *et al.* , 2006). The source rest-frame duration is therefore less than 1 s. This burst also has short spectral lag, however, this cannot be used here to support the suggestion that it is a SHB, since short lags are expected in long bursts with similar peak flux ($\approx 3 \cdot 10^{53}$ erg/s at $z=1.7$).

GRB 060505 is another border-line GRB ($T_{90} = 4 \pm 1$ s) which is located on top of a highly star forming knot in the spiral arm of a galaxy at $z = 0.089$ (Fynbo

et al., 2006; Ofek *et al.*, 2006a). This burst does not show any evidence of supernova emission down to a very strict limit of $M_B > -12.6$ and therefore was suggested as putative SHB.

The duration of GRB 060614 is 102 s putting it, as long as duration is concerned, safely in the long GRB group (Gehrels *et al.*, 2006). However, Gal-Yam *et al.* (2006) do not find any supernova emission down to $M_B > -12$ in *HST* images of this $z=0.125$ burst (see also Fynbo *et al.*, 2006; Della Valle *et al.*, 2006). Moreover, the star-formation rate of the host is low ($< 1 M_\odot/\text{yr}/(L/L_*)$) and its lag-luminosity puts it away from the long GRB population and together with the other *Swift* SHBs. Additionally, its location in the *HST* image is on a faint pixel compare to the long GRB sample of Fruchter *et al.* (2006). Finally, the light curve of this burst is composed of an initial hard episode, which lasts ~ 5 s, that is followed by a variable soft emission that lasts ≈ 100 s. Based on these observations Gal-Yam *et al.* (2006) and Gehrels *et al.* (2006) suggest that this might be a long duration burst that is associated physically with the SHB population.

2.9 SHB interlopers

It is possible that the SHB population defined according to its *BATSE* duration, contains sub-classes which are not physically associated with the dominant SHB population, or with long GRBs. Actually, the recent γ -ray giant flare from SGR 1806-20 implies that this is indeed the case. Such possible sub-classes are discuss below.

2.9.1 Extra-galactic SGR giant flares

Soft gamma-ray repeaters (SGRs) are compact sources of persistent X-ray emission and repeating bursts of soft gamma-rays (see Woods & Thompson 2004 for a review), which are believed to be highly-magnetized young neutron stars (known as magnetars; e.g., Duncan & Thompson 1992; Paczyński 1992). At infrequent intervals, these sources emit extreme flares of high energy radiation, releasing more than 10^{44} ergs in the form of gamma-rays alone. These “giant flares” are characterized by a short (~ 0.1 sec), hard (~ 300 keV) and very intense spike that is followed by a long (~ 300 sec) pulsating soft “tail” (not to be confused with the X-ray tail observed in some SHBs). The maximal observed isotropic equivalent luminosity of such giant flares is $\sim 10^{47}$ erg/s following the eruption of SGR 1806–20 on December 2004 (Hurley *et al.*, 2005; Palmer *et al.*, 2005, for as short review of this event see Taylor & Granot 2006).

Only the initial short and hard spike of an extragalactic giant flare would have

been detected by *BATSE* because its luminosity is much higher than that of the pulsating tail, in which case it would be classified as a SHB (Duncan, 2001; Eichler, 2002). With a luminosity of $\sim 10^{47}$ erg/s such flares can be detected by *BATSE* up to ≈ 50 Mpc, suggesting that a significant fraction of the *BATSE* SHB sample is comprised of similar extra-galactic flares (Dar, 2005a,b; Palmer *et al.*, 2005; Hurley *et al.*, 2005; Nakar *et al.*, 2006). This fraction, however, cannot be very large given that none of the current *Swift* SHBs took place in a nearby galaxy, and therefore they are all much more energetic than the giant flare from SGR 1806-20. Additional constraints on the rate of SGR giant flares was obtained by exploration of IPN error boxes (Nakar *et al.*, 2006; Ofek, 2006), the lack of a *BATSE* SHB overdensity toward the virgo cluster (Palmer *et al.*, 2005; Popov & Stern, 2006) and the small fraction of SHBs with a blackbody spectrum (Lazzati, Ghirlanda & Ghisellini, 2005, ; the spectrum of the SGR giant flare is consistent with a blackbody). All these methods yield an upper limit on the fraction of giant flares out of the *BATSE* SHB sample, f_{SGR} , while the single observed event puts a lower limit on this fraction. Having the most stringent and least assumption dependent result, Ofek (2006) finds that $0.01 < f_{SGR} < 0.14$ at 95% confidence.

Interestingly, Tanvir *et al.* (2005) find evidence that a local population (within ≈ 100 Mpc) of SHBs may constitute $\approx 10\%$ of the total SHB population. At first glance it looks as if these are the expected extra-galactic SGR Giant flares. However, the results of Tanvir *et al.* (2005) suggest that a large fraction of these nearby bursts reside in early type galaxies. SGRs are thought to be produced by core collapse of young stars and to be associated with star forming regions, as supported by the Galactic SGRs (e.g., Gaensler *et al.*, 2001). Therefore, extra-galactic SGRs are expected to be found in late type galaxies only. Following these observations Levan *et al.* (2006b) discussed an alternative channel to produce SGRs, a merger of two white dwarfs, which should take place also in early-type galaxies (see also Thompson & Duncan, 1995; King, Pringle & Wickramasinghe, 2001). If a large fraction of the SGRs are formed in this way than the SHB sub-population found by Tanvir *et al.* (2005) may be extra-galactic SGR giant flares.

Distinguishing between an SGR giant flare and a SHB is not trivial, even if the location of the burst coincides with a nearby galaxy. An example is GRB 051103, localized by the IPN (Golenetskii *et al.*, 2005b) in the vicinity of M81 and M82 (≈ 3.6 Mpc from Earth). The error box includes one of the star forming arms of M81 (Ofek *et al.*, 2006b; Frederiks *et al.*, 2006). Lacking additional observations, it is currently unknown whether this was an SGR giant flare in M81/82 or a background SHB.

2.9.2 Very short GRBs

Cline, Matthey & Otwinowski (1999, 2001) and Cline *et al.* (2005) suggest that SHBs with $T_{90} < 0.1$ s compose a sub-class that is distinct from the rest of the SHB population. The main evidence that they present are a value of $\langle V/V_{max} \rangle \approx 0.5$ and an anisotropic distribution on the sky of the very short GRBs. Both properties suggest a nearby population and are different than those of longer SHBs. They also find that *Konus-Wind* very short GRBs show on average harder spectrum above 3 MeV than longer SHBs. Cline, Matthey & Otwinowski (2001) and Cline *et al.* (2005) suggest that these events may be produced by primordial black hole evaporations or by nearby extra-galactic SGR giant flares. Note that these observations suggest that if indeed this is a subclass, very short GRBs take place in the local universe. So far there are 5 *Swift* SHBs with $T_{90} < 0.1$ s, none of which are associated with a nearby galaxy.

3 Relativistic outflows and the prompt emission

The theory of long GRB prompt and afterglow emission was explored extensively. The generally accepted picture is that a stellar object undergoes a catastrophic event leading to the formation of a central engine. The engine rapidly releases energy in a compact region ($\sim 10^6 - 10^7$ cm). This energy is deposited in the form of radiation, heat and/or electromagnetic field and leads to the acceleration of an ultra-relativistic outflow. At first, this flow is optically thick and it “carries” the energy out, while cooling adiabatically, to large distances ($\gtrsim 10^{13}$ cm), where it becomes optically thin. From this point and on, dissipation of the flow’s energy, most likely by internal processes (i.e., without interaction with the ambient medium), results in observed radiation. The dissipation heats electrons to highly relativistic velocities and these radiate in the presence of magnetic field and/or radiation field (e.g., synchrotron and inverse compton radiation) that is either advected by the flow from the source or generated by the dissipation process. This emission is observed as the prompt gamma-rays. At larger radii ($10^{16} - 10^{18}$ cm) the energy that remains in the relativistic flow is transferred into the circum-burst medium, generating a decelerating blast wave. This blast wave, which propagates into the external medium, is the source of the afterglow emission.

This picture is based on the observed luminosity, time scales and spectral and temporal evolution of long GRB prompt and afterglow emission. Since most of these properties are common to long and short GRBs, the same model is applied also to SHBs and appears to give an adequate explanation to their observations¹³.

¹³ This is true only for the physical processes that produce the prompt and afterglow emission. There are two separate branches of theoretical research of short and long

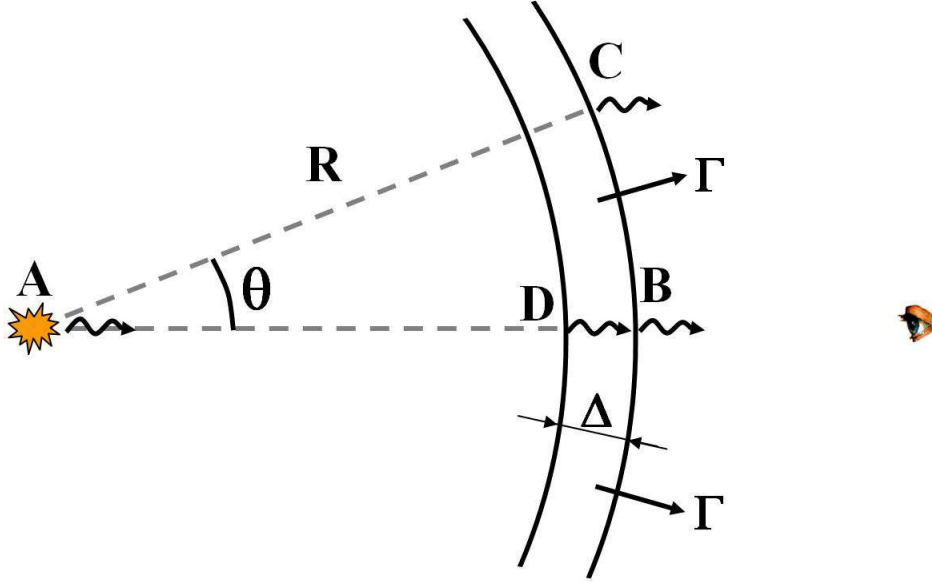


Fig. 9. Illustration of the emission sites of four photons from a relativistic spherical shell with a width Δ that expands with a Lorentz factor Γ . These photons set three typical time scales (see the text). Photon ‘A’ is emitted from the origin at the time of the explosion. Photons ‘B’, ‘C’ and ‘D’ are all emitted when the shell front is at radius R . ‘B’ is emitted from the front of the relativistic shell on the line-of-sight. ‘C’ is emitted from the front of the shell at an angle θ . ‘D’ is emitted from the rear of the shell on the line-of-sight.

Numerous review articles describe GRB theory, focusing on the general model outlines described above (e.g., Piran, 1999, 2005b; Mészáros, 2006). I will review here only the main theoretical aspects of this model while quantitatively confronting it (in several cases for the first time) with SHB observations.

3.1 Relativistic effects

The ultra-relativistic velocity of the source of the prompt and afterglow emission directly affects their observational properties. I briefly describe here some of these effects, serving as a basis for further discussion.

3.1.1 Time scales

Consider a spherical shell with a width Δ that is expanding with a relativistic Lorentz factor $\Gamma \gg 1$ and emits photons at radius $r = R$ from points ‘B’, ‘C’ & ‘D’ (Fig. 9). Photon ‘A’ is emitted from the origin at the time of the

GRBs that explore the progenitors and the processes that lead to the formation of the central engine (see §5).

explosion (when the shell is ejected; Fig. 9). The different arrival times of these four photons to the observer set three different time scales:

Line-of-sight time: t_{AB} is the time interval between two photons emitted by the shell front along the line-of-sight one when the shell is ejected, $r = 0$, and the second when the shell is at $r = R$:

$$t_{los} = \frac{R}{2c\Gamma^2}. \quad (2)$$

This time scale is also comparable to the time between any two photons that are emitted over the expansion time, i.e., the time over which the radius doubles (which is also the adiabatic cooling time). If the Lorentz factor of the emitting shell is not constant, but decays as $\Gamma \propto R^{-g}$ (e.g., during SHB external shock $g = 3/2$) then $t_{los} = R/(2[1 + 2g]c\Gamma^2)$.

Angular time: $t_{BC} = R\theta^2/2c$ is the time interval between two photons emitted at radius R , one along the line of sight and the other at an angle $\theta \ll 1$. Light aberration from relativistic sources implies that most of the photons that arrive to the observer are from angles $\lesssim 1/\Gamma$. This sets the angular time over which photons that are emitted from the shell at radius R arrive to the observer:

$$t_{ang} = \frac{R}{2c\Gamma^2}. \quad (3)$$

Shell width time: The time scale that is set by the shell width is not affected by the relativistic motion:

$$t_{\Delta} = \Delta/c. \quad (4)$$

Note that if we set $t = 0$ to the arrival time of photon ‘A’ then photons from radius R arrive to the observer between t_{los} and $\sim 2t_{los}$ ($t_{los} \approx t_{ang}$). As I will discuss later, this property makes it difficult for a single spherical shell to produce high amplitude rapid variability in the light curve (§3.4.1).

In the scenario discussed above the emitting material and the emission front are propagating at the same Lorentz factor Γ . This is not always the case. For example, according to the afterglow theory the emission is generated by a blast wave (i.e., emission front) that propagates at a Lorentz factor that is larger by a factor of $\sqrt{2}$ than the fluid that is crossing the shock (i.e., emitting material). In such case the line-of-sight time (Eq. 2) depends on the emission front Lorentz factor while the angular time (Eq. 3) depends on the Lorentz factor of the emitting material.

3.1.2 Causal connection and quasi-sphericity

Consider a spherical shell that is expanding at a Lorentz factor $\Gamma \gg 1$, and a signal (e.g., a sound wave) that is propagating on its surface at velocity $c\beta_s$ (as measured in the local rest frame). Between the radius R and $R + dR$ this signal propagates an angular distance $d\theta_s = \beta_s dR/(\Gamma R)$. Therefore, during the

expansion time (i.e., the time over which the radius doubles) the signal propagates $\theta_s \approx \beta_s/\Gamma$ (logarithmic terms are neglected). Since $\beta_s \leq 1$ the angular size of a causally connected patch of the shell is $\sim 1/\Gamma$. Therefore, a relativistic shell is ‘frozen’ over angular scales that are larger than $1/\Gamma$. Relativistic light aberration implies that most of the photons that are emitted from an angle $\gtrsim 1/\Gamma$ with respect to the line-of-sight as observed from the origin, do not reach the observer. The combination of the two effects implies that any event occurring at angles that are larger than $1/\Gamma$ cannot be observed directly and are also causally disconnected from the region that can be seen. Thus, the observer is completely ignorant of anything outside of the $1/\Gamma$ angular region.

While this property makes it difficult to study the angular structure of relativistic outflows, it makes the early stages of GRBs considerably simpler to model. As long as the angular structure of the flow varies over angles that are larger than $1/\Gamma$, each part of the outflow behaves as if it was a part of a spherical flow with the local properties. Thus we can apply spherically symmetric models to the prompt emission and to the initial phases of the afterglow. Throughout the paper I will refer to this property as quasi-sphericity.

3.1.3 High latitude emission

Consider an infinitesimally thin spherical shell that expands relativistically with a Lorentz factor $\Gamma = (1 - \beta^2)^{-1/2}$ and radiates an arbitrarily short pulse at radius R . What would be the observed shape of this pulse? The first photons that arrive to the observer are emitted on the line-of-sight and therefore arrive at t_{los} . At later times photons arrive from larger and larger angles with respect to the line-of-sight, θ , such that any given observer time is mapped onto a given angle (‘latitude’). The relativistic blueshift decreases with increasing latitude (and time) resulting in a decay of the energy flux. Additionally, due to the decreasing blueshift, a given observer frequency corresponds to an emitted rest frame frequency that increases with latitude. Therefore, the observed pulse shape at a given frequency window depends on the emitted spectrum. In the case of a power-law spectrum ($F_\nu \propto \nu^{-\beta}$) the observed flux depends on the Lorentz boost as $F_\nu \propto \mathcal{D}^{-(2+\beta)}$ where $\mathcal{D} = \Gamma(1 - \beta \cos \theta)$ is the inverse of the Doppler factor. Using the relation between the observer time and the emission angle, $t - t_{los} = 1 - R \cos(\theta)/c$, one obtains $\mathcal{D} \propto 1 + (t - t_{los})/t_{ang}$ in the limit of $\Gamma \gg 1$, implying (Kumar & Panaitescu, 2000; Nakar & Piran, 2003a):

$$F_\nu \propto \left(1 + \frac{t - t_{los}}{t_{ang}}\right)^{-(2+\beta)}. \quad (5)$$

At late times ($t \gg t_{los}$ and $t \gg t_{ang}$) the light curve decays as $t^{-(2+\beta)}$. This relativistic high latitude emission is important since it predicts a prolonged observed flux, with decreasing peak frequency, even in the case of an arbi-

trary short burst of emission (e.g., a ‘naked’ afterglow, see §4.4; [Kumar & Panaitescu, 2000](#)). It also constrains the amount of possible variability from a spherically symmetric source ([Nakar & Piran, 2003a](#), see §4.7).

3.2 *The Lorentz factor of the outflow*

Perhaps the most prominent feature of GRBs is that they are (special) ultra-relativistic sources. This is a well-established result, relying on several independent indications, some of which are (almost) model independent. Here I discuss two methods, starting with the opacity constraint, the most robust and model independent method¹⁴, where a lower limit on the Lorentz factor is set by requiring that the source of the prompt emission is optically thin. The second method provides a measurement of the Lorentz factor Γ during the early afterglow and can be applied when the onset of the afterglow is observed. It depends on the afterglow model and is valid only when the observed afterglow emission is produced by an external shock (see §4).

These two methods (as well as several others) were used to carefully analyze only long GRB observations and therefore the Lorentz factor of SHBs was never properly constrained. Here I briefly present the derivation of the theoretical constraints and then apply them to the observations of SHBs. The main result is that, like long GRBs, SHBs are ultra-relativistic. However, while observations of long GRBs require $\Gamma \gtrsim 100 - 300$, for most of the SHBs $\Gamma \gtrsim 10 - 50$ is consistent with the observations.

3.2.1 *Opacity constraints*

The prompt emission of GRBs (long and short) is non-thermal (§2.1.3), implying that the source is optically thin to the observed photons. On the other hand, if a non-relativistic source is assumed, a calculation of the optical depth to Thomson scattering, τ_T , based on the enormous observed luminosity of MeV γ -rays, results in $\tau_T \sim 10^{13}$ ([Schmidt, 1978](#)). This discrepancy was known as the compactness problem and at first was used to argue that GRBs are Galactic. This conflict was alleviated when it was realized that the source of the emission may be moving at relativistic velocities towards the observer (e.g., [Guilbert, Fabian & Rees, 1983](#); [Piran & Shemi, 1993](#)). The most comprehensive calculation of the opacity limit on the Lorentz factors of long bursts appears in [Lithwick & Sari \(2001\)](#). Here I carry out similar analysis, adapting it to the possibly different prompt emission spectra of SHBs.

¹⁴In the case of long GRBs the most direct evidence of a mildly relativistic motion during the afterglow phase are the resolved radio images of the afterglow of GRB 030329 ([Taylor *et al.*, 2004, 2005](#)).

The non-thermal spectrum of GRBs implies that the source is optically thin to Thomson scattering on e^-e^+ pairs¹⁵. An inevitable source for such pairs is the annihilation of photons with rest frame energy $\epsilon'_{ph} > m_e c^2$, where m_e is the electron mass. Therefore, the Thomson optical depth for a given pulse during the prompt emission phase is¹⁶:

$$\tau_T \approx \frac{\sigma_T N_{ph} f(\epsilon'_{ph} > m_e c^2)}{4\pi R^2}, \quad (6)$$

where σ_T is the Thomson cross-section, N_{ph} is the total number of emitted photons within the pulse, $f(\epsilon'_{ph} > m_e c^2)$ is the fraction of photons that create pairs and R is the radius of the source. Relativistic motion of the source has two effects. First, it reduces the energy of the photons in the rest frame, thereby reducing f . Second, for a given observed time of the pulse, δt , it increases the emission radius as $R \sim c\delta t\Gamma^2$. The time scales and the luminosities of individual pulses in long and short GRBs are similar (see §2.1.2), but the spectrum may be different. While the spectrum of most long GRBs is best described by a Band function (smoothly broken power-law; [Preece et al., 2000](#); [Ghirlanda, Celotti & Ghisellini, 2002](#)), the best fits spectrum of most SHBs is a low energy power-law and an exponential cut-off ([Ghirlanda, Ghisellini & Celotti, 2004](#), PLE; see §2.1.3). While this spectral difference may be a result of observational selection effects, PLE spectrum should be used when conservatively deriving the lowest Lorentz factor that is consistent with all current observations. The reason is that PLE spectrum is consistent with all available data of most bursts and it is less constraining than spectra with high energy power-law. Note also that GeV photons, which support spectral high-energy power-law, were observed in several long GRBs (e.g., [Schneid et al., 1992](#); [Sommer et al., 1994](#); [Hurley et al., 1994](#)) while there is no report in the literature of a photon harder than 10 MeV that was observed from a SHB. Hopefully, *GLAST* observations will unambiguously determine the high energy spectra of SHBs, enabling more stringent limits on SHB Lorentz factors.

Using a power-law spectrum with index α and an exponential cut-off at E_0 (Eq. 1), Eq. 6 becomes:

$$\tau_T \approx 10^{14} S_{\gamma,-7} d_{L,28}^2 \delta t_{-2}^{-2} \frac{m_e c^2}{E_0} \Gamma^{-(4-\alpha)} \exp \left[-\frac{\Gamma m_e c^2}{E_0(1+z)} \right], \quad (7)$$

where S_{γ} is the observed gamma-ray fluence of the pulse, d_L is the luminosity distance to the burst (at redshift z) and throughout the paper N_x denotes

¹⁵ Opacity to $\gamma\gamma$ pair production provides less stringent constraints on SHB Lorentz factors.

¹⁶ Here I assume that the source is moving directly toward the observer. If the source is moving at some angle with respect to the line of sight then the optical depth increases and so does the lower limit on Γ .

$N/10^x$ in c.g.s units (except for E_0 which is traditionally used in this context as the spectral cutoff energy). Requiring $\tau_T < 1$ results in the following constraint on the Lorentz factor:

$$\frac{\Gamma m_e c^2}{E_0(1+z)} + (4-\alpha)\ln(\Gamma) + \ln\left[\frac{E_0}{m_e c^2}\right] \gtrsim 30. \quad (8)$$

The logarithmic dependence on S_γ , δ_t and d_L is neglected in Eq. 8 (the range of the observed values of SHB pulses may affect the value of Eq. 8 by less than 50%). Figure 10 presents the lower limit on Γ as a function of E_0 for three values of α . This lower limit is $\Gamma \gtrsim 15$ for the majority of the bursts analyzed by Ghirlanda, Ghisellini & Celotti (2004), assuming that they are cosmological, while for SHBs 051221 and 050709 the opacity lower limits are $\Gamma > 25$ and $\Gamma > 4$ respectively. These lower limits are significantly lower than those obtained for long GRBs ($\Gamma \gtrsim 100$; e.g., Lithwick & Sari, 2001). Note however that for both populations only lower limits on the Lorentz factor are available and, while the typical Lorentz factor of SHBs could be lower than that of long GRBs, a precise comparison between the real values of Γ is impossible. Additionally, the smaller lower limits on SHB Lorentz factors depend on the best-fit function of their spectra which might be affected by observational selection effects. Hopefully the high energy spectra of SHBs will be securely determined by the upcoming *GLAST* mission.

3.2.2 Constraints from the onset of the afterglow

Within the framework of all the models discussed in this review, the afterglow is produced by a blast wave that propagates into the circum-burst medium, which is generated by the interaction of the relativistic outflow with the ambient medium. Once most of the energy is deposited into the external medium the blast wave assumes a self-similar profile (Blandford & McKee, 1976) and the X-ray and optical emissions are expected to decay as power-laws (roughly as t^{-1} , where t is the observer time since the trigger of the prompt emission; see §4). During the self similar phase:

$$\Gamma(t) \approx 40 \left(\frac{E_{k,iso,50}}{n_0}\right)^{1/8} \left(\frac{t}{100 \text{ s}}\right)^{-3/8} (1+z)^{3/8}, \quad (9)$$

Where $E_{k,iso}$ is the isotropic equivalent kinetic energy that remains in the relativistic outflow after the prompt emission phase and n is the density of the external medium, which is taken to be constant (as expected in the environment of SHBs; see §5). Note that the dependence on both $E_{k,iso}$ and n is weak. Plugging the earliest observed time at which the afterglow shows a regular decay that fits the self-similar model into Eq. 9 provides a lower limit on the Lorentz factor of the outflow.

Figure 4 shows three SHBs for which a regular afterglow, decaying as $\sim t^{-1}$, is

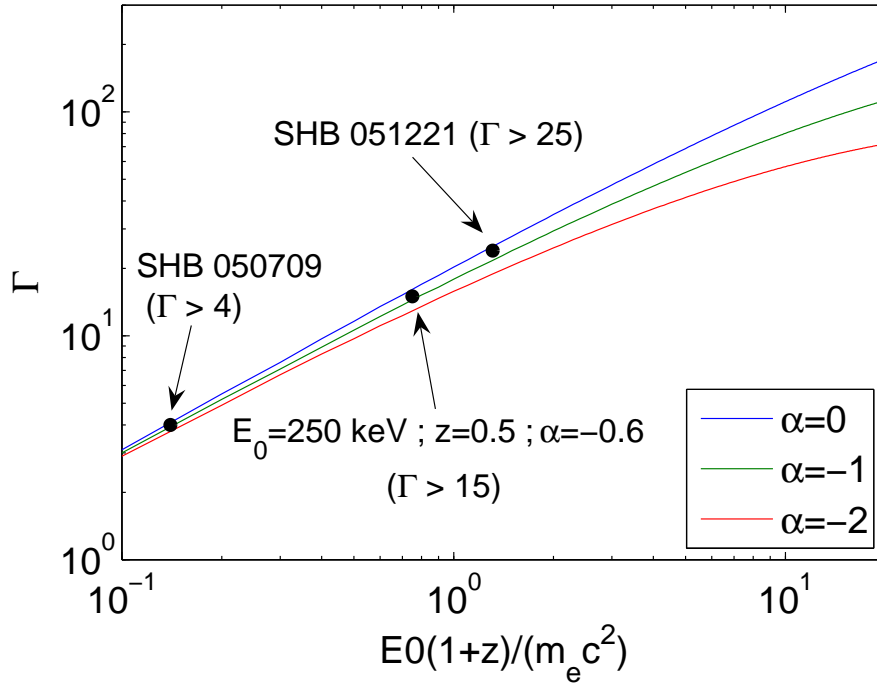


Fig. 10. The lower limit on the Lorentz factor of the prompt emission source as a function of the rest frame spectral typical energy $E_0(1+z)$ in units of $m_e c^2$. The limit is derived by the opacity constraint (Eq. 8) using three different low energy power-law slopes α . The dots mark three bursts, SHB 050709, SHB 051221A, and a typical SHB (according to Ghirlanda, Ghisellini & Celotti, 2004) at $z=0.5$. (prompt emission properties are taken from Villasenor *et al.*, 2005; Golenetskii *et al.*, 2005a)

observed at $t \approx 100$ s. Therefore, assuming that this emission results from an external shock, the Lorentz factor of the ejecta in these bursts is constrained to be $\Gamma \gtrsim 40$ (e.g., [Lee, Ramirez-Ruiz & Granot, 2005](#), use this method to constrain the Lorentz factor of SHB 050509B). This lower limit is similar to the one obtained by the prompt emission opacity. Note that the Lorentz factor of SHB 050709 is not well constrained by this method, since the first observations of “regular” afterglow decay in this burst is more than a day after the burst.

3.3 *The composition of the relativistic outflow*

One of the main open questions about the physics of GRBs (long and short) as well as that of other relativistic astrophysical phenomena (e.g., micro-quasars and active galactic nuclei) is how to launch (and often collimate) a relativistic outflow. Most models of the “engine” that produces the flow are composed of different combinations of rotation, accretion and magnetic fields, where the energy source of the flow can be any one of the above. Whatever the energy source is, the outflow starts its way when a vast amount of energy is deposited in a relatively baryonic free compact environment. The evolution of the flow depends on the composition of the deposited energy (heat, magnetic field, etc.) and the environment in which the outflow propagates. Almost all suggested models are applicable for both long and short GRBs, where the main difference is the duration over which the engine is active, which is roughly comparable to the observed duration of the burst (§3.4.1). Another difference is that the engine of long GRBs is believed to operate at the center of a collapsing star, while in all current SHB progenitor models the engine is “exposed” (§5). Thus, relativistic ejecta from SHBs do not have to penetrate through several solar masses of surrounding material, and can be launched directly.

The relativistic outflow composition is currently unknown. The main candidates are baryonic plasma (protons, electrons and likely neutrons) and magnetized plasma (at various ratios of magnetic to particle energy). Currently no observations of either long or short bursts conclusively point towards one of these cases. Since there are no studies of this topic that are specific for SHBs, and given that this topic is well covered elsewhere ([Zhang & Mészáros, 2004](#); [Piran, 2005b,a](#); [Mészáros, 2006](#); [Lyutikov, 2006](#)), I provide here only a brief overview.

3.3.1 *Baryonic flow*

In this case the engine energy is deposited at the end of acceleration into an extremely small load of baryons, thereby accelerating the baryons to ultra-relativistic velocities. The most basic model of pure baryonic outflow suggests

that the outflow is accelerated by radiation pressure. It was realized early on that releasing the observed luminosity in the form of pairs and/or radiation in a compact region (< 0.001 light sec) results in the relativistic expansion of a pairs-radiation fireball (Goodman, 1986; Paczynski, 1986). If there is a negligible load of baryons in such a fireball, most of the energy escapes as quasi-thermal radiation. However, if the proton load is high enough, then the accompanying electrons increase the optical depth and the fireball remains optically thick until almost all the the energy is converted into bulk motion kinetic energy (Shemi & Piran, 1990; Piran, Shemi & Narayan, 1993; Mészáros, Laguna & Rees, 1993; Grimsrud & Wasserman, 1998; Daigne & Mochkovitch, 2002b; Nakar, Piran & Sari, 2005; Li & Sari, 2006). The minimal (isotropic equivalent) proton load that results in full conversion of radiation to bulk motion energy corresponds to a maximal Lorentz factor:

$$\Gamma_{max} \approx 1000 E_{50}^{1/4} R_{0,6}^{-1/4} T_{-1}^{-1/4}, \quad (10)$$

Where R_0 is the radius in which the energy is released (comparable to the engine size) and T is the duration over which the energy, E , is isotropically deposited. Together with the lower limit on the Lorentz factor (~ 30 ; see §3.2) the allowed range of baryonic mass is ($E = \Gamma M_{ej} c^2$):

$$5 \cdot 10^{-8} M_{\odot} E_{50}^{3/4} R_{0,6}^{1/4} T_{-1}^{1/4} \lesssim M_{ej} \lesssim 2 \cdot 10^{-6} M_{\odot} E_{50}. \quad (11)$$

Note that while the mass lower limit (and the Lorentz factor upper limit) is model dependent and valid only in this scenario, the upper limit on the baryonic mass is generic since it is derived by the Lorentz factor opacity constraint (§3.2). This implies that in any model, the region in which the ejecta is accelerated must be almost completely clean of baryons.

This simple model does not discuss collimation of the flow, which may be done by a hydrodynamic interaction with the environment or by magnetic forces. In both cases the interaction may affect the final Lorentz factor (as discussed below). Additionally, any variability of the outflow in this quasi-spherical model is generated by varying the deposition rate of the energy and/or the baryonic loading. If neutrons are present in the fireball as well, as expected if the engine is driven by accretion onto a compact object (e.g., Beloborodov, 2003b), these will be dragged by nucleon collisions along with the protons up to high Lorentz factor and may affect the evolution of the fireball at late times (e.g., Derishev, Kocharovsky & Kocharovsky, 1999a,b; Pruet & Dalal, 2002; Beloborodov, 2003a,b; Vlahakis, Peng & Königl, 2003a; Peng, Königl & Granot, 2005; Rossi, Beloborodov & Rees, 2006). In this case the mass limit is roughly applicable to the total baryonic mass.

An additional, purely hydrodynamic acceleration mechanism of a non-magnetized plasma flow was discussed recently by Aloy & Rezzolla (2006) (see also Aloy, Janka & Müller 2005). The acceleration is powered by rarefaction waves that

propagate into a relativistic flow in the presence of large velocities tangential to a discontinuity. Such hydrodynamical conditions are expected to be generated by the interaction of the flow with a thick accretion torus that feeds the compact engine. Thus, once the flow achieves a moderate Lorentz factor (e.g., by radiation pressure as discussed above) additional acceleration is provided by this process. As a result, the maximal Lorentz factor in this model is not set by transparency considerations and can significantly exceed the upper limit in Eq. 11. Rarefaction waves also provide natural collimation to the flow and [Aloy, Janka & Müller \(2005\)](#) find that for the observed SHB parameters, the resulting flow is a narrow jet (~ 0.1 rad) with a core Lorentz factor of ~ 1000 and rather sharp edges.

3.3.2 Magnetized flow

Many authors suggested models in which magnetic fields play an important role in the dynamics (acceleration and possible collimation) as well as in the final energetic content of the outflow (e.g., [Usov, 1992](#); [Levinson & Eichler, 1993](#); [Usov, 1994](#); [Thompson, 1994, 2006](#); [Katz, 1997](#); [Mészáros & Rees, 1997b](#); [Kluźniak & Ruderman, 1998](#); [Drenkhahn & Spruit, 2002](#); [Vlahakis & Königl, 2003a,b](#); [Lyutikov & Blandford, 2002, 2003, 2004](#); [Lyutikov, 2004, 2006](#)). These models differ in the initial ratio of magnetic to particle energies and in the large scale magnetic field configuration. During the evolution of the flow the energy can be transferred between the different components of the flow (bulk, heat and magnetic) and different models predict different final flow compositions (in the sense that there are different final energy ratios between these components). Some models predict that by the time that the prompt emission is generated, most, or comparable amount, of the energy is in a baryonic component (e.g., [Katz 1997](#); [Vlahakis & Königl 2003a,b](#)) while in other models the magnetic field is the dominant component at all times (e.g., [Mészáros & Rees 1997b](#); [Lyutikov & Blandford 2003](#)).

Introducing magnetic fields enables models to achieve final Lorentz factors that are significantly higher than the one obtained in pure baryonic models (e.g., $\sim 10^6 - 10^7$ in [Mészáros & Rees 1997b](#)) and it also relaxes the constraints on the minimal baryonic load, allowing for a pure magneto-leptonic flow (e.g., [Thompson, 1994](#)). Another example is [Vlahakis, Peng & Königl \(2003a\)](#) that suggest a scenario in which the interplay between the magnetic and baryonic energy making it possible to increase the baryonic load in the form of neutrons that decouple from the flow while its Lorentz factor is still moderate.

Regardless of the acceleration mechanism, the final composition of the flow is the relevant initial condition for the prompt emission phase. As we see below it mainly affects the dissipation process that gives rise to the prompt emission.

3.4 *The prompt emission*

The prompt emission is generated (or at least re-processed) at a radius in which the optical depth of the relativistic flow is low. Any heat that is generated in the flow while it is optically thick is quickly lost to adiabatic expansion, and therefore the outflow energy must be dissipated into internal heat near the radius in which the emission takes place. Dissipation processes vary according to the composition of the flow. In a baryonic or weakly-magnetized plasma the dissipation may result from strong shocks, while in Poynting-flux-dominated flows the heat is produced by dissipation of the magnetic field (e.g., via reconnection).

3.4.1 *Internal or external dissipation?*

The dissipation can be done either by processes that are internal to the flow (e.g., internal shocks) or by interaction with an external medium (e.g., external shock). In the case of a baryonic flow an important difference between the two dissipation modes is their implications for the central engine. In internal dissipation models of baryonic outflow the duration of the burst, T , is related to the duration of the engine activity. Since the light-crossing time of the engine is shorter by many orders of magnitude than the burst duration, a long-lived engine is required. In these models the observed variability time scale, δt , reflects the variability of the flow, induced either by the engine itself or by interactions at the base of the flow during the acceleration. On the other hand, the external shock model (e.g., Rees & Mészáros, 1992; Katz, 1994; Dermer & Mitman, 1999), which is the most popular of the external dissipation models of baryonic outflow, allows for an explosive source, i.e., the energy can be released on an engine dynamical time scale. If the source is explosive, the duration of the burst in this model is determined by the radius in which the interaction takes place ($T \sim R/c\Gamma^2$), while the variability time scale may be determined by the size of density fluctuations in the external medium.

In long GRBs the consensus is that if the outflow is baryonic the prompt emission results from internal dissipation (see however Dermer & Mitman 2004; for a comprehensive discussion of the topic see Piran 2005b). The main argument in favor of internal dissipation is the rapid, high amplitude variability observed during the prompt emission of long GRBs. Namely, the prompt emission flux varies by $\sim 100\%$ over time scales, $\delta t \ll T$. The main obstacle to highly variable emission from external shocks is the angular smoothing (Fenimore, Madras & Nayakshin, 1996) and detailed hydrodynamical analysis shows that quasi-spherical external shocks cannot produce the observed variability (Sari & Piran, 1997). In quasi-spherical symmetry the angular time (t_{ang}) is always

the longest observed time scale and therefore it is comparable to the total duration of the burst, thereby washing out any variability that arises during the emission (for a definition of quasi-sphericity and relevant time scales see §3.1). Thus, viable external shock models must invoke spatial variability on small angular scales ($\ll 1/\Gamma$). The main attempt to do so suggests a clumpy external medium (Dermer & Mitman, 1999, 2004). In the context of long GRBs this model encounters difficulties with achieving the required variability together with a reasonable efficiency (Sari & Piran, 1997; Nakar & Piran, 2002c). Furthermore, in this model the width of the relativistic shell, Δ , sets a lower limit on the variability time scale ($\delta t \gtrsim \Delta/c$) implying $\Delta \ll R/\Gamma^2$. Any variability during the acceleration of the flow will result in $\Delta \sim R/\Gamma^2$ and therefore this model requires the source of the flow to be extremely, some may say unphysically, steady.

Many SHBs show variability that is similar to the one observed in long bursts (§2.1.2; Nakar & Piran, 2002b) and therefore the arguments discussed above in favor of internal dissipation if the outflow is baryonic are applicable in the case of variable SHBs as well. In the case of SHBs there are additional arguments against external shock as the prompt emission dissipation process. First, variable external shocks require the ambient medium to have numerous dense clumps. Such an environment may be formed by winds from massive stars, the progenitors of long GRBs. However, the proposed progenitor models for SHBs predict a rather smooth circum-burst medium. Second, the afterglow is most likely produced by external shock. Therefore, if the prompt emission arises from an external shock as well, then the afterglow is expected to join smoothly with the prompt emission. However, the observed afterglows show a clear distinction between the prompt emission, the following X-ray tail and the late X-ray afterglow (Fig. 4). To produce all these phases by external shocks, even if the prompt emission is not variable, requires a contrived external density profile. Finally, as discussed in §2.2, there are SHBs with very faint X-ray afterglows. These bursts lack bright external shock emission following the prompt emission and therefore, for any reasonable external density profile, the prompt emission should arise from a different process.

If the outflow is Poynting-flux-dominated then the prompt emission energy is generated by dissipation of the outflow magnetic energy. This dissipation may be affected by interaction with the external medium (e.g., Thompson, 2006). The observed prompt emission variability can be generated in a Poynting-flux-dominated flow by emission process that is not isotropic in the rest frame of the expanding outflow (e.g., Lyutikov & Blandford, 2003; Thompson, 2006). In such case not all the $1/\Gamma$ angular region is observed but only small regions within it where the emission happens to point towards the observer. This way the angular smoothing is avoided and high variability may be archived also in external dissipation process (see more details in §3.4.3). Note that in the two specific models of the prompt emission in a Poynting-flux-dominated

flow that are currently available (Lyutikov & Blandford, 2003; Thompson, 2006), the duration of the burst reflects that activity time of the engine.

To conclude, if the outflow is baryonic then variable SHBs (which are the majority) are most likely produced by internal dissipation. In a Poynting-flux-dominated flow the dissipation process can be either internal or external. All viable models in both flow types relate the observed duration of the burst to the engine activity duration (e.g., Kobayashi, Piran & Sari, 1997; Nakar & Piran, 2002a; Janka *et al.*, 2005; Lyutikov, 2006; Thompson, 2006). SHB that shows a smooth prompt emission light curve may arise from an external shock in case that the afterglow joins smoothly with the prompt emission (no such cases were observed so far).

3.4.2 Internal shocks

In a baryonic or weakly magnetized flow the suggested dissipation process is internal shocks (e.g., Rees & Mészáros, 1994; Narayan, Paczynski & Piran, 1992; Paczynski & Xu, 1994), namely, shocks that arise in a variable flow when plasma portions with different velocities collide. In this model each pulse in the light curve corresponds to a single episode of collision that takes place at a radius $R \sim c\delta t\Gamma^2 = 3 \cdot 10^{12} \text{ cm } \delta t_{-2}\Gamma_2^2$. The total duration of the burst corresponds to the total width of the outflow, and is therefore not related to R . At these radii the plasma density is low enough so the flow is optically thin to Thomson scattering, as implied by the observations. The low plasma density also implies that the mean free path for a binary collision between plasma particles (e.g., protons) is much larger than R and therefore these shocks are collisionless and are mediated by collective electromagnetic plasma instabilities (§4.10). Collisionless shocks are believed to efficiently accelerate particles to relativistic velocities (§4.10) and the propagation of the accelerated relativistic electrons in the plasma magnetic field is thought to be the source (via e.g., synchrotron process) of the observed prompt emission.

The main advantage of internal shocks is that they are expected to arise naturally in the baryonic outflow and that they can easily reproduce the observed variable light curve (e.g., Kobayashi, Piran & Sari, 1997). In fact the observed variability reflects the variable activity of the engine¹⁷ and the duration of the burst is comparable to, or at most larger by an order of magnitude than (Janka *et al.*, 2005), the duration of engine activity. Additionally, the simplest inter-

¹⁷ If the flow is accelerated by radiation pressure alone than the prompt emission light curve directly reflects the energy deposition rate and/or baryonic load modulation at the base of the flow (Kobayashi, Piran & Sari, 1997; Nakar & Piran, 2002a). If the flow is accelerated continuously also at large radii (e.g., by rarefaction waves as discussed in §3.3.1) then it reflects the structure of the flow at the end of the acceleration phase (Janka *et al.*, 2005; Aloy & Rezzolla, 2006).

pretation of the emission as synchrotron radiation roughly predicts the correct observed frequency. The relative velocities between different plasma portions are mildly relativistic and therefore internal shocks heat the protons to mildly relativistic temperatures. Assuming that the shocks couple the electron and magnetic energies to the proton energy, the electrons have typical Lorentz factor $10^2 - 10^3$, and gyrate in a $\sim 10^6$ G magnetic field (in the plasma rest frame) producing ~ 100 keV synchrotron emission (in the observer frame)¹⁸.

The main disadvantage of the internal shocks model is its efficiency. Internal shocks are expected to radiate only a small fraction of the total flow energy, $\sim 1\%$ (e.g., Kobayashi, Piran & Sari, 1997; Daigne & Mochkovitch, 1998; Kumar, 1999). Being mildly relativistic, internal shocks convert only a small fraction of the bulk kinetic energy into internal energy, and only a fraction of this internal energy is carried by radiating electrons. As a result, most of the flow energy is not radiated and remains to be dissipated by an external shock, resulting in a bright afterglow. In long GRBs the afterglow is not as bright as expected, suggesting that typically as much as 10 – 50% of the relativistic flow energy is emitted in the form of gamma-rays and in some cases the gamma-ray efficiency may even be higher (Freedman & Waxman, 2001; Lloyd-Ronning & Zhang, 2004; Granot, Königl & Piran, 2006; Fan & Piran, 2006). As I show in §4.5 the efficiency of the prompt emission in SHBs is most likely high as well (see also Bloom *et al.*, 2006b). Therefore, efficiency is potentially a problem of this model in SHBs as well. The same extensions of the internal shocks model that were suggested in order to resolve this issue in the context of long GRBs are applicable to SHBs as well, e.g., very large amplitude Lorentz factor variability (Beloborodov, 2000; Guetta, Spada & Waxman, 2001) and repeated shock crossings (Kobayashi & Sari, 2001).

The interpretation of the prompt emission as optically thin synchrotron radiation predicts a spectrum that is softer than $dN/d\nu \propto \nu^{-2/3}$ (Rybicki & Lightman, 1979). This prediction is in conflict with the observed spectrum of most SHBs (§2.1.3; Ghirlanda, Ghisellini & Celotti, 2004). This problem, raised by Preece *et al.* (1998) in the context of long GRBs, is more severe in short GRBs where the low energy spectrum is harder. Again, different models that were put forward to explain the hard spectrum of long GRBs are also applicable here. Some of these models are: random magnetic fields on very short length-scales, leading to jitter radiation instead of synchrotron (Medvedev, 2000), effects of synchrotron self absorption or anisotropic electron pitching angles (Lloyd & Petrosian, 2000; Granot, Piran & Sari, 2000), Upscatter of optical self-absorbed photons by inverse Compton (Panaitescu & Mészáros, 2000) and Photospheric effects (Mészáros & Rees, 2000).

¹⁸Note however that this model predicts larger variance in the observed typical frequency than suggested by *BATSE* observations.

On the high energy end, most SHB spectra are consistent with having an exponential cut-off, while long GRBs show a power-law (§2.1.3; Ghirlanda, Ghisellini & Celotti, 2004). If this cut-off is intrinsic, and not an observational selection effect, then it most likely reflects the energy distribution of radiating electrons, suggesting that in SHBs, unlike in long GRBs, the electrons are not accelerated to very high energies during the prompt emission phase. In fact, the observed spectrum in most SHBs can be produced by a mildly relativistic shocks that only couple the electrons and the protons, without further accelerating electrons to higher (power-law) energies as required in long GRBs. In this case there are no electrons with Lorentz factors above $10^2 - 10^3$ and an exponential cut-off in the spectrum is expected at ~ 100 keV. I speculate here that such difference may arise from different magnetization level of the outflow, where collisionless shocks during the prompt emission of SHBs are magnetized while those in long GRBs are not. Numerical simulations (Spitkovsky, 2005) suggest that first order Fermi acceleration of particles may not take place in magnetized shocks while it has been recently suggested (Lyubarsky, 2006) that in such magnetized shocks the electrons can reach equipartition with the protons (with a quasi-thermal energy distribution) through the the synchrotron maser instability. The reason that strong magnetic fields at the shock front may suppress electron acceleration is that they prevent downstream thermal electrons from crossing the shock back into the upstream, thereby suppressing the Fermi process. On the other hand, theoretical considerations (Milosavljević, Nakar & Spitkovsky, 2006) and numerical simulations (Spitkovsky, 2005) suggest that in unmagnetized shocks some of the thermalized downstream electrons can cross the shock back into the upstream and thus start the Fermi acceleration cycles (see §4.10).

3.4.3 *Prompt emission from a magnetized flow*

If the outflow energy is carried mostly by Poynting flux up to the point where the interaction with the external medium starts, the dissipation of the bulk energy into internal energy cannot occur through internal shocks¹⁹. In this case the energy source of the radiation is most likely magnetic dissipation processes (e.g., reconnection). Currently there are two models of magnetized flows treating the prompt emission in some detail.

Lyutikov & Blandford (2003) suggest that electromagnetic current-driven instabilities dissipate magnetic energy into heat and high energy particles (see also Lyutikov, 2006). The propagation of these high energy particles within a strong magnetic field, naturally present in this model, is the source of the ob-

¹⁹Note that outflow models that are dominated by magnetic energy at small radii but convert their energy into particle kinetic energy during the acceleration, can use internal shocks to produce the prompt emission.

served prompt γ -ray emission. In this model the dissipation takes place close to the deceleration radius ($\sim 10^{15} - 10^{16}$ cm) while the outflow Lorentz factor is $\Gamma \sim 100 - 1000$. Therefore, the observed variability time scale implies that the emission is not spherical (the observed variability, δt , is much shorter than t_{ang} in this case). Lyutikov & Blandford (2003) suggest that the reconnection of the magnetic field produces, additionally to high energy particles, also relativistic turbulence with a Lorentz factor $\gamma_t \gg 1$, as measured in the rest frame of the expanding shell. This bulk relativistic motion of the emitting matter causes the radiation to be beamed into an angle of $\approx 1/(\Gamma\gamma_t) \ll 1/\Gamma$. This way, each observed pulse is coming from a small angular region ($\ll 1/\Gamma$) on the expanding shell, allowing $\delta t \ll t_{ang} = R/(2c\Gamma^2)$. In this model the burst duration is greater or equal to t_{ang} , so that $\delta t \ll T$.

Thompson (2006) suggests a flow which is a combination of a strong magnetic field and pair-radiation plasma. In this model the radius in which the outflow becomes optically thin is determined by the pair enrichment of the ambient medium through the interaction with the flow radiation (Thompson & Madau, 2000; Mészáros, Ramirez-Ruiz & Rees, 2001; Beloborodov, 2002; Kumar & Panaitescu, 2004). The magnetic dissipation is triggered by the interaction with the pair loaded external medium and is regulated to take place around the radius where the outflow becomes optically thin. The prompt emission in this model is generated by inverse Compton scattering of the seed photons that are carried in the flow by pairs which are accelerated by the reconnecting magnetic field. Highly variable light curve is obtained by emission that is directed in the rest frame of the relativistic outflow. The peak spectral energy of the prompt emission (observed at ~ 500 keV) reflects the temperature of these seed photons (Lorentz boosted to the observer frame). Therefore, it is determined by the radius at which the flow starts expanding freely, and by the Lorentz factor at this radius. In long GRBs the observed spectrum corresponds to a Lorentz factor of a few at a radius of $\sim 10^{10}$ cm which may be naturally explained as the radius of the progenitor star. It is unclear at this point if this model can be applied to SHBs as well, since the recent observations indicate that in SHBs the free expansion should also start at a large radius. For example, Thompson, Mészáros & Rees (2006) find that in the case of SHB 050709 the peak spectral energy corresponds to a flow that is still mildly relativistic and thermalized at $\sim 10^{10}$ cm. Currently it is unclear how the thermalization radius can be so high in SHBs.

3.5 High energy Cosmic-rays and neutrinos

3.5.1 High energy Cosmic-rays

Cosmic-ray acceleration is typically discussed in the context of long GRBs (for a recent review see [Waxman, 2004](#)). Long GRBs were suggested as the source of extra-galactic ultra-high energy cosmic rays, with observed energies between $10^{18} - 10^{20}$ eV (UHECRs; [Waxman, 1995](#); [Milgrom & Usov, 1995](#); [Vietri, 1995](#); [Wick, Dermer & Atoyan, 2004](#); [Dermer & Atoyan, 2006](#)). This idea is supported by the similar total flux of long GRB gamma-rays and UHECR and by the small number of other candidate UHECR sources. Cosmic rays are suggested to be accelerated in long GRB internal and reverse shocks, where diffusive shock acceleration (a.k.s first order Fermi acceleration; §4.10) may be able to accelerate particles to 10^{20} eV. External shocks are not a promising UHECR acceleration site via diffusive shock acceleration ([Gallant & Achterberg, 1999](#); [Milosavljević & Nakar, 2006a](#)) and therefore long GRBs are expected to be UHECR sources only if the outflow is baryonic (§3.3), unless particles are accelerated in the external shock by an alternative mechanism (e.g., second order Fermi acceleration; [Dermer & Mitman, 1999](#); [Dermer, 2006](#)).

The three major factors that limit shock acceleration are time, confinement and cooling. Assuming that the coherence length of the magnetic field in the upstream (unshocked wind) is larger than R/Γ , the criterion that the acceleration is faster than adiabatic cooling is $R_L < R/\Gamma$ where R_L is the Larmor radius of accelerated particles in the upstream field and R [Γ] is the radius [Lorentz factor] of the relativistic wind (note that the shock itself is mildly relativistic in the wind rest frame). This condition also guarantees that the accelerated particle is confined and that it has sufficient time to be accelerated. Writing this condition using the parameters of relativistic winds one obtains ([Waxman, 1995](#)):

$$E_{p,max} \approx 10^{20} \text{ eV} \sqrt{\varepsilon_{B,-1}^{us}} \Gamma_2^{-1} L_w^{1/2}, \quad (12)$$

where $E_{p,max}$ is the maximal energy to which protons can be accelerated and L_w is the wind luminosity. ε_B^{us} is the fraction of magnetic field energy density in the unshocked wind²⁰ out of the total wind energy density (including rest mass energy) as measured in the wind rest frame. The requirement that the acceleration is faster than synchrotron cooling is satisfied for $R > 10^{13} \text{ cm } E_{p,20}^3 \Gamma_2^{-2}$ ([Waxman, 1995](#)). If SHB winds are baryonic then both conditions can be satisfied during the internal shocks and the reverse shock,

²⁰ ε_B^{us} is not to be confused with the magnetic field density in the shocked downstream, ε_B , which is the site of synchrotron emission.

given that $100 \lesssim \Gamma \lesssim 1000$ and that the wind is mildly magnetized. Therefore, SHBs may be able to accelerate 10^{20} eV cosmic rays just like long GRBs. However, The total SHB gamma-ray energy flux is lower by two orders of magnitude than that of long GRBs and the observed UHECRs (Table 1). Therefore, while SHBs may be sources of high energy cosmic rays, they are unlikely to be the dominant source of the observed UHECRs.

3.5.2 High energy neutrinos

High energy neutrinos (\gtrsim TeV) are also usually discussed in the context of long GRBs (for reviews see [Waxman, 2000](#); [Mészáros & Razzaque, 2006](#)). In long GRBs, four sites were suggested as primary sources of high energy neutrinos: (i) Acceleration of a neutron rich outflow ([Bahcall & Mészáros, 2000](#); [Derishev, Kocharovskiy & Kocharovskiy, 1999a](#)). (ii) Internal shocks ([Waxman & Bahcall, 1997, 1999](#); [Rachen & Mészáros, 1998](#); [Dermer & Atoyan, 2003](#)) (iii) Reverse shocks ([Waxman & Bahcall, 2000](#)). (iv) In the course of a long GRB jet drilling through the envelope of its massive-star progenitor ([Mészáros & Waxman, 2001](#)).

The last site is irrelevant for SHBs, as the progenitors are not massive stars. All other processes may take place in SHBs if their outflow is baryonic. If the outflow is Poynting-flux-dominated then large neutrino flux is unexpected unless neutrinos are efficiently produced in the forward shock ([Dermer, 2002](#); [Li, Dai & Lu, 2002](#)). This may be possible in the less likely case that $\sim 10^{19}$ eV protons are accelerated in the forward shock.

The energy of neutrinos produced during the acceleration of a neutron rich outflow is ~ 10 GeV and therefore these are hard to detect (due to neutrino detector sensitivity at this energy range). Reverse shock neutrinos are produced by interaction of $\sim 10^{20}$ eV cosmic rays with UV photons. The UV flux in SHB reverse shocks is significantly fainter compare to long GRBs (§4.3) and therefore this process is inefficient in SHBs. Internal shock neutrinos are produced by interaction of $\gtrsim 10^{16}$ eV cosmic rays with the prompt gamma-rays. The neutrinos are produced by the decay of pions that result from this interaction. The efficiency of this process depends on the efficiency of the cosmic ray acceleration, the observed gamma-ray flux and the variability time scale, all of whom may be similar in both phenomena. In long GRBs [Waxman & Bahcall \(1997\)](#) estimate that in optimal conditions about 10% of the burst energy is in the form of $\sim 10^{15}$ eV neutrinos. Assuming a similar efficiencies for long and short GRBs out of the total gamma-ray emission (Table 1) implies that the neutrino flux from short GRBs is:

$$\epsilon_\nu^2 \Phi_\nu(\epsilon_\nu \approx 10^{15} \text{ eV}) \sim 5 \cdot 10^{-11} \text{ GeV/cm}^2/\text{s/sr}. \quad (13)$$

4 The afterglow - Theory

X-ray and optical emission observed hours, days and weeks after some SHBs resemble the afterglow observed in long GRBs. Any GRB model that is not 100% efficient in converting energy into gamma-rays predicts an interaction of the remaining relativistic ejecta with the external medium, which is expected to produce radiation at longer wavelengths. Therefore, various models of the prompt emission, that were developed for long GRBs and are applicable to SHBs as well, also predict similar afterglow emission. Indeed, the existence of SHB afterglows was predicted long before these were observed (Panaitescu, Kumar & Narayan, 2001; Nakar & Piran, 2002b). Differences between long and short GRB afterglows are expected mostly due to different total energies, different properties of the ambient medium and, possibly, different outflow geometries. I give here a brief description of the standard external shock afterglow model and emphasize the interpretation of observed SHB afterglows in this context. I extend and adjust the basic model in places where the specific SHB parameter space requires it. The reader is referred to Piran (1999, 2005b) and Mészáros (2006) for further details on the model²¹.

4.1 Standard model - synchrotron radiation from a spherically symmetric adiabatic blast wave

The remaining relativistic flow energy, after the end of the prompt emission phase, is transferred to the external medium by driving a shock-wave into it - the external shock. At early times the energy content in the ejecta and the freshly-shocked external medium is comparable. At this time the ejecta composition has a strong effect on the dynamics and the emission. I discuss this early, but more complicated, phase later (§4.3). After all the energy is dissipated into the external medium the only memory of the initial conditions is the total amount of energy and its angular distribution (i.e. the initial geometry of the flow). This phase, generally referred to as the late afterglow, is discussed here.

Consider an adiabatic and spherical²² blast wave with energy E that propagates with Lorentz factor Γ into an external medium composed of proton-

²¹ SHB afterglow models that I do not cover here are the “cannonball” model (for review see Dar & de Rújula, 2004) and a cylindrical external shock model (Wang, Cheng & Tam., 2005)

²² The spherical approximation can be used here as long as the blast wave properties do not vary over angles that are smaller than $1/\Gamma$ (quasi-sphericity of relativistic flows). E in this model corresponds to the isotropic equivalent kinetic energy of the outflow.

electron plasma with a constant density n . The random motion Lorentz factor of the shocked plasma in the blast wave rest frame is $\approx \Gamma$ and therefore the total blast wave energy, as measured in the observer frame, is $\approx M(R)\Gamma^2 c^2$, where $M(R)$ is the mass accumulated by the blast wave up to a radius R . Energy conservation dictates (e.g., [Sari, Piran & Narayan, 1998](#)):

$$\gamma \approx 50 \left(\frac{E_{50}}{n_{-2}} \right)^{1/2} R_{17}^{-3/2} \approx 6 \left(\frac{E_{50}}{n_{-2}} \right)^{1/8} \left(\frac{t_d}{1+z} \right)^{-3/8}, \quad (14)$$

$$R \approx 4 \cdot 10^{17} \text{ cm} \left(\frac{E_{50}}{n_{-2}} \right)^{1/4} \left(\frac{t_d}{1+z} \right)^{1/4}, \quad (15)$$

where γ is the Lorentz factor of the freshly-shocked external medium (the Lorentz factor of the shock itself is $\Gamma = \sqrt{2}\gamma$) and t_d is the observer time in days ($t \approx R/4\gamma^2$; [Waxman, 1997a](#); [Sari, 1997](#)). Conservation of mass, momentum and energy fluxes across the shock imply that the proper number and energy density of the freshly shocked plasma (in the plasma rest frame) are $4\gamma n$ and $4\gamma^2 n m_p c^2$ respectively. The profiles of the hydrodynamic quantities (pressure, density and velocity) behind the shock are self similar ([Blandford & McKee, 1976](#)) and the entire shock energy is concentrated in a very thin shell with a width $\Delta \approx R/10\Gamma^2$. The simplest model assumes that the shock couples the electrons to the proton energy and accelerates all the electrons to a power-law $dN/dE \propto E^{-p}$ starting at a minimal Lorentz factor $\gamma_{e,m} = \gamma \varepsilon_e (m_p/m_e)(p-2)/(p-1)$, where $p > 2$ and ε_e is the fraction of the internal energy that is carried by the electrons. After crossing the shock the electron and the proton temperatures are not coupled any more, and the electrons cool down by radiation and pdV work. This model assumes further that the magnetic field in the shocked plasma carries a constant fraction ε_B of the internal energy, where the magnetic field of freshly shocked plasma is $B = (32n m_p c^2 \varepsilon_B)^{1/2} \gamma$. Note that by definition $\varepsilon_e + \varepsilon_B < 1$.

This model has five free parameters: E , n , ε_e , ε_B and p . These parameters can, in principle, take almost any value, but observation of long GRBs together with the properties of the host galaxies of SHBs suggests a “natural” range for these parameters. Assuming that the processes that produce the prompt emission in long and short GRBs are similar, we expect similar efficiency, implying that the γ -ray isotropic equivalent energy output is a reasonable estimator of E ([Freedman & Waxman, 2001](#); [Granot, Königl & Piran, 2006](#); [Fan & Piran, 2006](#)), and therefore $E \sim 10^{50}$ erg (see Table 2). Observed SHB host galaxies, and the location of the bursts within them, indicate that the progenitors are associated with an old stellar population. Moreover, various progenitor models suggest that the peculiar velocity of the progenitors can be high enough to escape from the gravitational potentials of their hosts. Therefore, possible environments of SHBs are the inter-stellar medium (ISM), intra-cluster medium (ICM) or the inter-galactic medium (IGM). In all of these cases the gas density would be rather constant on the scales relevant

for SHBs, and the corresponding density values are $10^{-2} - 1 \text{ cm}^{-3}$ (ISM), $10^{-3} - 10^{-2} \text{ cm}^{-3}$ (ICM) and $\sim 10^{-6} \text{ cm}^{-3}$ (IGM). Finally, the values of ε_e , ε_B and p are determined by collisionless shock physics, which take place on microphysical scales and are therefore unlikely to depend on global properties such as the total energy, the density profile, etc. It is therefore reasonable to use the values observed in long GRBs (see also §4.10): $\varepsilon_e = 0.05 - 0.5$, $\varepsilon_B = 10^{-3} - 0.1$ and $2 \lesssim p \lesssim 3$ (e.g., Panaitescu & Kumar, 2001; Yost *et al.*, 2003).

Within this parameter range the radio to X-ray afterglow is dominated by synchrotron radiation. The synchrotron spectrum has three characteristic frequencies (e.g., Mészáros & Rees, 1997a; Waxman, 1997b; Sari, Piran & Narayan, 1998; Granot, Piran & Sari, 1999b): ν_m - the typical synchrotron frequency ($\propto \gamma B \gamma_e^2$) that corresponds to the synchrotron frequency of an electron with Lorentz factor $\gamma_{e,m}$; ν_c - the synchrotron frequency that corresponds to $\gamma_{e,c}$, which is the Lorentz factor above which radiative cooling is significant; and ν_a - the synchrotron self-absorption frequency. The observed spectrum is usually four-segment broken power-law with breaks at the characteristic frequencies, where the power-law indices depend on the order of these frequencies. The value of ν_a and of the peak value of F_ν depend on the order of the characteristic frequencies as well. In the parameter range relevant for SHBs the typical frequency order would be $\nu_a < \nu_m < \nu_c$ during the relativistic phase (i.e., cooling is slow). In this case the characteristic frequencies are²³:

$$\begin{aligned}
\nu_a &\approx 0.2 \text{ GHz } (1+z)^{-1} \varepsilon_{e,-1}^{-1} \varepsilon_{B,-2}^{1/5} E_{50}^{1/5} n_{-2}^{3/5}, \\
\nu_m &\approx 5 \cdot 10^{10} \text{ Hz } (1+z)^{1/2} \varepsilon_{e,-1}^2 \varepsilon_{B,-2}^{1/2} E_{50}^{1/2} t_d^{-3/2}, \\
\nu_c &\approx 8 \cdot 10^{18} \text{ Hz } (1+z)^{-1/2} \varepsilon_{B,-2}^{-3/2} E_{50}^{-1/2} n_{-2}^{-1} t_d^{-1/2}, \\
F_{\nu,m} &\approx 5 \text{ } \mu\text{Jy } (1+z) \varepsilon_{B,-2}^{1/2} E_{50} n_{-2}^{1/2} d_{L,28}^{-2},
\end{aligned} \tag{16}$$

where $F_{\nu,m}$ is the flux at ν_m . The observed flux is a broken power-law with the following spectral and temporal indices:

$$F_\nu \propto \begin{cases} \nu^2 t^{1/2} & \nu < \nu_a \\ \nu^{1/3} t^{1/2} & \nu_a < \nu < \nu_m \\ \nu^{-\frac{p-1}{2}} t^{-\frac{3}{4}(p-1)} & \nu_m < \nu < \nu_c \\ \nu^{-\frac{p}{2}} t^{-\frac{3p-2}{4}} & \nu_c < \nu \end{cases}. \tag{17}$$

A detailed discussion of the light curve in cases of other orders of the break frequencies can be found in Granot & Sari (2002) while the case of $1 < p < 2$

²³ Eq. 16 is generalized to include self-synchrotron Compton cooling (see §4.2) by taking $\nu_c \rightarrow \nu_c(1+Y)^{-2}$ where Y is defined in Eq. 22. As I show, in SHBs $Y \ll 1$.

is discussed in [Dai & Cheng \(2001\)](#).

Once the blast wave accumulates enough mass it decelerates to non-relativistic velocities and makes a transition from the relativistic self-similar Blandford-Mackee solution ([Blandford & McKee, 1976](#)) to the Newtonian self-similar Sedov-Von Neumann-Taylor solution ([Sedov, 1946](#); [von Neumann, 1947](#); [Taylor, 1950](#)). The transition between the two solutions is gradual and takes about one decade in time around:

$$t_{NR} \sim 0.5 \text{ yr} \left(\frac{E_{50}}{n_{-2}} \right)^{1/3} (1+z) \quad (18)$$

At $t \gg t_{NR}$ the blast wave velocity is $v \propto t^{-3/5}$ and the flux at the radio frequencies, ν_R , which is typically the only observed wavelengths at this time, behaves as: ([Waxman, Kulkarni & Frail, 1998](#); [Frail, Waxman & Kulkarni, 2000](#)):

$$F_{\nu,R} \propto \nu^{-\frac{p-1}{2}} t^{-\frac{3(p-1)}{2} + \frac{3}{5}}; \quad \nu_a, \nu_m < \nu_R < \nu_c \quad \& \quad t \gg t_{NR} \quad (19)$$

4.1.1 Comparison to the observations

The handful of observed SHB afterglows were analyzed within the framework of the standard afterglow model in several papers ([Hjorth *et al.*, 2005b](#); [Fox *et al.*, 2005](#); [Berger *et al.*, 2005](#); [Lee, Ramirez-Ruiz & Granot, 2005](#); [Bloom *et al.*, 2006b](#); [Panaitescu, 2006](#); [Campana *et al.*, 2006](#); [Burrows *et al.*, 2006](#); [Grupe *et al.*, 2006](#); [Soderberg *et al.*, 2006a](#)). The simple model gives a reasonable explanation of the general properties of most of the observed afterglows. Moreover, most of the observed properties were predicted by the standard model (e.g., [Panaitescu, Kumar & Narayan, 2001](#)) and while the current observations are too sparse to confirm its validity, they are certainly encouraging. For example, this model predicts that the emitting electrons are accelerated in unmagnetized relativistic collisionless shocks to a power-law distribution with index p . Long GRB afterglow observations as well as theory of particle acceleration in relativistic shocks suggests $2 \lesssim p \lesssim 3$ (§4.10). This prediction determines, with little freedom, the optical and X-ray spectral and temporal evolution (Eq. 17). Most SHB afterglows conform with the evolution of the afterglow as predicted by this range of p values. A few examples are SHBs 050709 ($p \approx 2.5$; [Fox *et al.*, 2005](#); [Panaitescu, 2006](#)), 050724 ($p=2-3$; [Berger *et al.*, 2005](#); [Panaitescu, 2006](#)) and 051221 ($p \approx 2.2$; [Soderberg *et al.*, 2006a](#); [Burrows *et al.*, 2006](#)) where broad-band modeling (radio to X-ray) gives a reasonable description of the observed afterglows.

Unfortunately, the current quality of the data is not sufficient to break all the degeneracies between the other four parameters of the model (E , n , ε_e and ε_B), and to determine their values. Nevertheless, in most cases where the simple

standard model fits the data, the default parameters that were predicted based on the observations of long GRBs (i.e., $E \sim E_{\gamma,iso}$, $n < 1 \text{ cm}^{-3}$ and ε_e and ε_B not much smaller than equipartition), give a satisfactory description of the data (e.g., [Panaitescu, 2006](#)).

On the other hand, some of the observed details cannot be explained by the simple, spherically symmetric, self-similar model. The most prominent features that require deviation from the basic model are the early X-ray tail (see §2.2.2), the late flares observed in the X-ray afterglows of several bursts (Fig. 4) and the late break in the light curve of SHB 051221. Extensions of the basic model that can explain at least some of these features are discussed below.

4.2 *Synchrotron self-Compton*

The same electrons that produce synchrotron radiation also upscatter synchrotron photons by the inverse Compton process (synchrotron self-Compton - SSC; e.g., [Mészáros, Rees & Papathanassiou 1994](#); [Waxman 1997c](#); [Panaitescu & Kumar 2000](#); [Dermer, Chiang & Mitman 2000](#); [Sari & Esin 2001](#); [Zhang & Mészáros 2001b](#)). SSC photons themselves are upscattered again by the same relativistic electrons to even higher energies producing a second generation of inverse Compton photons. The process continues to higher and higher generations until the photon energies, as seen in the electrons' rest frame, are above the Klein-Nishina energy ($m_e c^2$), where the scattering cross-section drops rapidly (roughly linearly) with photon energy. For typical long GRB parameters the first generation of the SSC is below the Klein-Nishina limit and is usually calculated without considering the effect of the Klein-Nishina cross-section. This first SSC generation is predicted to produce bright GeV emission that would be detected by sensitive GeV future observatories (e.g., *GLAST*). The second SSC generation for long GRB afterglows is well above the Klein-Nishina limit and is completely suppressed. As I show below for SHBs the situation is different as the first generation SSC component is already affected by the Klein-Nishina cross-section, though it is not entirely suppressed. I therefore repeat the analysis presented in [Sari & Esin \(2001\)](#) augmented by a simple estimate of the effect of the Klein-Nishina cross-section (c.f., [Li & Waxman, 2006](#)). The result is that in all but the brightest SHBs the SSC emission is expected to be significantly less energetic than the synchrotron emission.

Photons that are scattered by an electron with a Lorentz factor γ_e are below the Klein-Nishina limit as long as the observed frequency satisfies:

$$h\nu \lesssim h\nu_{KN}(\gamma_e) = m_e c^2 \frac{\Gamma}{\gamma_e} \quad (20)$$

where h is the Planck constant and Γ is the plasma Lorentz factor (γ_e is measured in the plasma rest-frame). In the slow cooling regime (i.e., $\nu_m < \nu_c$, as expected for SHBs) most of the synchrotron energy is emitted around ν_c and most of the SSC energy is emitted by $\sim \gamma_c$ electrons that upscatter $\sim \nu_c$ photons. Therefore, the Klein-Nishina limit can be neglected only if $\nu_c/\nu_{KN}(\gamma_c) \lesssim 1$:

$$\frac{\nu_c}{\nu_{KN}(\gamma_c)} \approx 10^4 E_{50}^{-1} n_{-2}^{-3/2} \varepsilon_{B,-2}^{-5/2} (1+Y)^{-2}. \quad (21)$$

Here I included the effect of SSC cooling on ν_c using the Y parameter (defined in Eq. 22 and found to be small). Eq. 21 shows clearly that in SHBs the Klein-Nishina limit cannot be neglected and that the first SSC branch in this case is strongly affected by the Klein-Nishina cross-section²⁴.

The total energy in the first SSC generation can be estimated as follows. In the relevant parameter space $\nu_m < \nu_{KN}(\gamma_c) < \nu_c$ where $F_\nu \propto \nu^{(1-p)/2}$, implying that for $2 < p < 3$ most of the upscattered energy is emitted by $\sim \gamma_c$ electrons that upscatter $\sim \nu_{KN}$ photons. Therefore, the ratio of the SSC luminosity to the synchrotron luminosity is (c.f. Eq. 3.1 of Sari & Esin 2001):

$$Y \equiv \frac{L_{IC}}{L_{syn}} = \frac{U_{syn}(\nu < \nu_{KN}[\gamma_c])}{U_B} = \frac{\eta_{rad}\eta_{KN}U_e}{(1+Y)U_B} = \frac{\eta_{rad}\eta_{KN}\varepsilon_e}{(1+Y)\varepsilon_B}, \quad (22)$$

where U_{syn} , U_B and U_e are the energy density of the synchrotron emitted photons, the magnetic field, and the relativistic electrons respectively (measured in the plasma rest frame). η_{rad} is the fraction of the electrons' energy that is radiated:

$$\eta_{rad} = \left(\frac{\nu_m}{\nu_c}\right)^{\frac{p-2}{2}} \quad ; \quad \nu_m < \nu_c. \quad (23)$$

η_{KN} is the fraction of the radiated energy which is in frequencies smaller than $\nu_{KN}(\gamma_c)$:

$$\eta_{KN} = \left(\frac{\nu_{KN}(\gamma_c)}{\nu_c}\right)^{\frac{3-p}{2}} \quad ; \quad \nu_m < \nu_{KN}(\gamma_c) < \nu_c. \quad (24)$$

Expressing Eqs. 23 & 24 using the five free parameters of the model and plugging them into Eq. 22 yields:

$$Y = 0.01 e^{4.3(2.5-p)} \varepsilon_{e,-1}^{p-1} \varepsilon_{B,-2}^{\frac{3-p}{4}} E_{50}^{1/2} n_{-2}^{\frac{5-p}{4}} t_d^{-\frac{p-2}{2}} \quad (25)$$

This equation is valid for $2 < p < 3$ and as long as $\nu_m < \nu_{KN}(\gamma_c) < \nu_c$, as expected in SHBs. Note that in this range of p values the dependence on

²⁴ In long GRBs the isotropic equivalent blast wave energy is larger by 2–3 orders of magnitude and the external medium density is usually higher. Therefore, the Klein-Nishina cross-section can usually be neglected for the first SSC generation.

ε_B and t is very weak while by definition $\varepsilon_e < 1$. Therefore, $Y \ll 1$ in all SHBs but the most energetic ones that happens to explode in relatively dense environments. The implications of such low Y values is that SSC cooling is inefficient and can be ignored in Eq. 16 and that in general SSC GeV emission from most SHB late afterglows will be dim and is unlikely to be detected by planned GeV observatories.

4.3 *Early afterglow and the reverse shock*

According to the internal-external dissipation model, between the prompt emission and the late afterglow there is an intermediate phase, during which the energy in the ejecta is dissipated into the external medium. The composition of the ejecta plays an important role in the physical evolution during this phase. In long GRBs a baryonic flow may show a clear observable signature (the reverse shock optical flash and radio flare) which is not expected in a Poynting flux dominated flow. As I show below for SHBs, even if the flow is baryonic and there is a strong reverse shock, bright early optical emission is not expected.

Interaction of baryonic ejecta with the external medium generates two shocks. One is propagating into the external medium (forward shock) and the other is propagating back into the ejecta (reverse shock). Between these two shocks there are two shocked regions that are separated by a contact discontinuity. Similar shock structure can be found in many astrophysical environments such as supernova remnants and stellar winds. As I show below, in SHBs the reverse shock is mildly relativistic. This implies that during a single crossing the shock dissipates most of the bulk motion energy of the outflow into internal energy. After the shock crosses the outflow once and a rarefaction wave is reflected, only the forward shock remains, and is the source of the late afterglow. The reverse shock is short-lived and might produce an observable signature which may be distinguishable from the late afterglow emission. If, however, the outflow is dominated by Poynting flux, then the large magnetic pressure prevents the formation of a strong reverse shock. The exact prediction for magnetized flow depends on the magnetization level of the plasma (e.g., [Lyutikov, 2006](#); [Zhang & Kobayashi, 2005](#)).

Observed signatures of reverse shocks were explored extensively in the context of long GRBs (e.g., [Mészáros & Rees, 1997a](#); [Sari & Piran, 1999](#); [Kobayashi & Sari, 2000](#); [Sari & Mészáros, 2000](#); [Fan *et al.*, 2002](#); [Soderberg & Ramirez-Ruiz, 2002](#); [Zhang, Kobayashi & Mészáros, 2003](#); [Nakar & Piran, 2004](#); [Beloborodov, 2005](#); [McMahon, Kumar & Piran, 2006](#)) and the same results are applicable, with some minor changes, to SHBs. I summarize the predictions for reverse shock emission, making the required adjustments to SHBs.

Consider a homogenous cold baryonic shell expanding relativistically into homogenous cold ambient medium. The problem is well defined by the shell (isotropic equivalent) energy E , width Δ in the lab frame, initial Lorentz factor Γ_0 and the ambient density n . As the ejecta plow through the external medium, a forward shock and a reverse shock are produced. The strength of the reverse shock is determined by the dimensionless parameter (Sari & Piran, 1995):

$$\xi \equiv (l/\Delta)^{1/2}\Gamma_0^{-4/3} \quad (26)$$

where $l \equiv (3E/(4\pi n m_p c^2))^{1/3}$ is the Sedov length. If $\xi \lesssim 1$ the reverse shock is relativistic and the shell decelerates, while dissipating most of its bulk motion energy, within a single shock crossing of the shell at $R_\Delta \approx l^{3/4}\Delta^{1/4}$. In this case $R_\Delta = R_{dec}$, where R_{dec} is the deceleration radius, namely the radius in which all the ejecta decelerates by a factor of two or more. For $\xi \gg 1$ the RS is Newtonian and many crossings are required to decelerate and shock dissipate a significant fraction of the ejecta energy. In this case R_{dec} is the radius in which the forward shock collects an amount of mass that is equivalent to $\sim E/(c^2\Gamma_0^2)$.

The Lorentz factor of the outflow is expected to vary by at least a factor of order unity, causing the shell to expand once it gets out to a radius $R_{spread} \approx \Delta_0\Gamma_0^2$ where $\Delta_0 \approx cT$ is initial width of the shell (T is the burst duration):

$$\Delta \approx \max(\Delta_0, R/\Gamma_0^2), \quad (27)$$

Correspondingly, ξ is constant up to R_{spread} , and it decreases at larger radii. The value of $\xi_0 \equiv \xi(\Delta_0)$ determines the evolution of the reverse shock. If $\xi_0 < 1$ then $R_{dec} < R_{spread}$ and the relativistic reverse shock crosses the shell before it starts spreading. If $\xi_0 \gg 1$ the reverse shock is initially Newtonian and the shell begins to spread during the first crossing of the reverse shock. As the shell spreads the reverse shock grows stronger and at the radius where the reverse shock finally crosses the shell, $\xi \approx 1$ and the reverse shock is mildly relativistic (its Lorentz factor is ≈ 1.25).

For typical SHB parameters,

$$\xi_0 = 43 \left(\frac{E_{50}}{n_{-2}} \right)^{1/6} \Gamma_{0,2}^{-4/3} T_{-1}^{-1/2} \gg 1. \quad (28)$$

Therefore, in most (and maybe all) SHBs the reverse shock is mildly relativistic ($\xi \approx 1$) and does not depend on the initial Lorentz factor, the total energy or the burst duration. The deceleration radius in this case is:

$$R_{dec} \approx 5 \cdot 10^{16} \text{ cm} \left(\frac{E_{50}}{n_{-2}} \right)^{1/3} \Gamma_{0,2}^{-2/3} \quad (29)$$

Corresponding to an observer time:

$$t_{dec} \approx \frac{R_{dec}}{2c\Gamma_0^2}(1+z) \approx 90 \text{ s } (1+z) \left(\frac{E_{50}}{n_{-2}} \right)^{1/3} \Gamma_{0,2}^{-8/3}. \quad (30)$$

At t_{dec} the reverse shock dies away and its optically thin synchrotron emission (at $\nu > \nu_a$) peaks and then starts fading rapidly (e.g., Sari, 1997). t_{dec} also marks the onset of the “late” afterglow - a self similar adiabatic solution - as the forward shock turns into a single blast wave (and indeed Eqs. 30 and 9 are similar). Note that in SHBs t_{dec} does not depend on T and that $t_{dec} \gg T$. This is different than long GRBs where Δ_0 is significantly larger and $\xi_0 \lesssim 1$, in which case $t_{dec} \approx T$. Thus, in SHBs a gap is expected between the prompt emission and the afterglow while in long GRBs the two are expected to overlap.

The emission from the reverse shock is calculated as in the standard afterglow model, taking into account that the reverse shock is mildly relativistic while the forward shock is ultra-relativistic. The strength of the shock defines the typical energy per particle in the shocked region. This in turn sets the typical frequency of the emitted synchrotron radiation. Thus, while the forward shock is radiating in the X-ray band, the reverse shock is radiating at low frequencies. The reverse shock signature in long GRBs is an optical flash that peaks soon after, or during, the prompt GRB emission and then decays as $\sim t^{-2}$ (e.g., Sari & Piran, 1999). $R \sim 18$ mag is expected from the reverse shock of a typical long GRB and in extreme cases it can be brighter by several orders of magnitude (Nakar & Piran, 2004). An accompanying radio flare is expected to peak hours to days later (e.g., Kulkarni *et al.*, 1999; Nakar & Piran, 2004). In SHBs, where the energy and typical density are lower and the reverse shock is not expected to be very strong, the predictions are different. For SHB “canonical” parameters ($E_{50} = 1$, $n = 0.01 \text{ cm}^{-3}$, $\epsilon_e = 0.1$, $\epsilon_B = 0.01$) most of the reverse shock emission is radiated around ~ 100 GHz and the early optical emission is faint, $\sim 2 \mu\text{Jy}$ ($R \sim 23$ mag) at $z = 0.2$ ²⁵. In this case the optical emission from the forward shock is expected to be brighter than the reverse shock emission. Actually, the reverse shock emission from SHBs is more likely to be detected by early radio observations. In the above case a peak flux of ~ 0.1 mJy is expected in 8 GHz at $t \approx 20$ min.

To conclude, early reverse shock optical flash is not expected from most SHBs (assuming canonical parameters), even if the ejecta is baryonic. A reverse shock signature might however be detected by very early deep radio observations.

²⁵ If the ejecta is mildly magnetized so the reverse shock is still mildly relativistic but $\epsilon_B 1/3$, then the optical emission from the reverse shock is brighter ($F_{\nu,opt}$ is roughly linear with ϵ_B at this parameter range). Additional increase in the reverse shock optical luminosity is expected if only a small fraction of the electrons is accelerated, thereby significantly increasing ν_m .

4.4 “Naked” afterglow

When the relativistic outflow that produces the prompt emission is quasi-spherical, an afterglow (late soft emission) is expected even if no emission from the external shock is observable (e.g., due to low external density). This is the high latitude emission of the prompt gamma-rays source (§3.1.3), that decays at late times ($t \gg t_{los}$ and $t \gg t_{ang}$; §3.1.1) as $F_\nu \propto \nu^{-\beta} t^{-(2+\beta)}$. This type of afterglow (“naked”; Kumar & Panaitescu, 2000; Dermer, 2004; Page *et al.*, 2006) is suggested to be responsible for the first phase of long GRB X-ray afterglows²⁶ (Nousek *et al.*, 2006; Zhang *et al.*, 2006).

SHBs 051210 (La Parola *et al.*, 2006) and 050813 (Roming *et al.*, 2006) show X-ray afterglows that may be high latitude emission. The afterglow of 051210 also shows a flare at $t \sim 100$ s. Assuming that no external shock emission exists, this flare is probably a result of the engine activity, in which case $t_{los} \sim 100$ s. La Parola *et al.* (2006) find that assuming this value of t_{los} , the late time decay is consistent with high latitude emission. In order for external shock emission to be fainter than the high latitude emission, they estimate that the external density is lower than $n < 4 \cdot 10^{-3} \text{ cm}^{-3}$.

4.5 X-ray dark afterglows and γ -ray efficiency

Figure 6 presents the distribution of the dimensionless ratio $f_{x\gamma} \equiv F_x t / S_\gamma$, where F_x is the X-ray (0.2 – 10 keV) energy flux at time t and S_γ is the prompt emission gamma-ray fluence (15 – 150 keV), of *Swift* long and short GRBs at one day (§2.2.1). Within the framework of the standard afterglow model (§4.1) and as long as the blast wave is quasi-spherical:

$$f_{x\gamma} \equiv \frac{F_x t}{S_\gamma} \approx \begin{cases} 10^{-2} \kappa^{-1} \varepsilon_{e,-1}^{3/2} \varepsilon_{B,-2} E_{k,50}^{1/3} n^{1/2} & \nu_x < \nu_c \\ 2 \cdot 10^{-3} \kappa^{-1} \varepsilon_{e,-1}^{3/2} t_d^{-1/3} & \nu_x > \nu_c \end{cases} \quad (31)$$

where,

$$\kappa \equiv \frac{E_\gamma}{E_k} \quad (32)$$

represents the γ -ray efficiency of the prompt emission. E_k (equivalent to E in 4.1) is the kinetic energy of the blast wave and E_γ is the energy emitted in γ -rays (all energies in this section are isotropic equivalent). The exact power

²⁶ Note that identification of high latitude emission can be tricky. At early times it requires an identification of t_{los} of the specific shell that dominates the late naked afterglow emission. As evident from Eq. 5, a significant underestimate of t_{los} leads to an overestimate of the decay index at early time.

of the parameters in Eq. 31 (e.g., ε_e) depends weakly on p (assuming here $2.1 < p < 3$). For simplicity I use approximate power values. I also neglect weak dependence (power-law indices below 1/4) on parameters, since these cannot affect the result significantly (the lack of dependence on n is exact). Following §4.2 the SSC cooling is neglected as well.

Assuming that microphysics of collisionless shocks does not vary significantly between bursts (either long or short) $\varepsilon_e \approx 0.1$ and $\varepsilon_B \approx 0.01$ are adopted. Under this assumption, for long GRBs at late time (~ 1 d; but before the jet-break), one expects $\nu_c < \nu_x$ in which case $f_{x\gamma}$ is almost a direct measure of the γ -ray efficiency, κ . As evident from Fig. 6, for long GRBs $f_{x\gamma}(1d) = 0.1 - 10^{-3}$ implying $\kappa_{LGRB} \approx 0.01 - 1$. This result is well known (Freedman & Waxman, 2001; Lloyd-Ronning & Zhang, 2004; Granot, Königl & Piran, 2006; Fan & Piran, 2006). Figure 6 also shows that the values of $f_{x\gamma}$ for SHBs with observed X-ray afterglows are comparable to those of long GRBs, ~ 0.01 .

For some SHBs the circum-burst density can be low, in which case it is not clear whether ν_c is above or below the X-ray band at 1 day. If $n \gtrsim 0.01 \text{ cm}^{-3}$ then $\nu_x \lesssim \nu_c$ and $\kappa_{SHB} \approx 0.1$. If the density is significantly smaller then $\nu_x > \nu_c$ and κ decreases as $n^{1/2}$. Since SHBs with observed afterglows are typically located within their host galaxy light, most likely $n \gg 10^{-4} \text{ cm}^{-3}$, so $\kappa \approx 0.01 - 0.1$. We can conclude that at least some SHBs (those with observed X-ray afterglow) the gamma-ray efficiency is most likely similar to that of long GRBs (see Bloom *et al.*, 2006b; Lee, Ramirez-Ruiz & Granot, 2005, for a specific exploration of the efficiency of SHB 050509B).

Early X-ray afterglow from long GRBs is always detected. In contrast, there are several SHBs with tight upper limits on any early (< 100 s) X-ray emission. The values of $f_{x\gamma} \lesssim 5 \cdot 10^{-5}$ for these bursts are exceptionally low (Fig. 6). Making the plausible assumptions that the gamma-ray efficiency of these bursts is typical ($\kappa \sim 0.1$) as are the initial Lorentz factor and the microphysical parameters, these values of $f_{x\gamma}$ indicate that these events occurred in extremely low density environments, $n \lesssim 10^{-5} \text{ cm}^{-3}$, typical for the inter galactic medium. As I will discuss below this result suggests a long-lived progenitor with high natal velocity (§5.2.3). An alternative would be to relax any of the above assumptions. For example, assuming an inter-stellar density ($n \gtrsim 0.01 \text{ cm}^{-3}$), the low $f_{x\gamma}$ value can be explained by ultra-efficient gamma-rays production ($\kappa \gtrsim 100$), by unusually low electron and magnetic field energies ($\epsilon_e^{3/2}\epsilon_B \lesssim 10^{-6}$) or by low initial Lorentz factor $\Gamma_0 \lesssim 20$. The latter case can explain the faint early afterglow because if Γ_0 is low the deceleration time (and therefore the afterglow onset) is at $t \gg 100$ s.

4.6 Angular structure of the outflow

The angular structure of the relativistic outflow is of great physical interest. As discussed in §3.1.2, during the prompt emission phase the observer is sensitive only to a small patch of the flow (a solid angle of $\sim 1/\gamma^2$ sr), and is ignorant to any of the flux emitted outside of this patch. This flux determines the total energy emitted by the burst as well as the range of the viewing angles over which a given burst can be detected. Therefore the angular structure is a crucial ingredient in determining the total burst energy and in extracting the total SHB rate out of the observations. Furthermore, the structure of the jet is most likely determined by the engine, and different progenitor and central engine models predict different angular structures.

Currently, the small number of SHB afterglows prevents the determination of the exact angular structure of the outflow (even in long GRBs it is still an open question). Therefore, I discuss here only the simplest jet structure: a uniform energy over a half opening angle $\theta_j \ll 1$ and no energy outside of this angle (a.k.a 'top hat')²⁷. This simple model turns out to be consistent with the few available observations (excluding the observed flares discussed in §4.7) and it is also supported by numerical simulations (Janka *et al.*, 2005). A comprehensive review of jets in GRBs can be found in Granot (2006), where the dynamics and observational signatures of relativistic blast waves with different angular structures are discussed.

Two key processes govern the observational signatures of a decelerating collimated relativistic blast wave. The first is relativistic beaming of the radiation from an emitting element with a Lorentz factor Γ to an angle of $1/\Gamma$. This implies that the radiation from a jet with half opening angle θ_j is confined to an angle $\theta_j + 1/\Gamma$. The second process is hydrodynamic lateral spreading of the jet, which is limited by the angular size of causally connected regions (see §3.1.2), $\approx 1/\Gamma$. Therefore, the half opening angle of a jet with an initial half opening angle $\theta_{j,0}$ is: $\theta_j \lesssim \theta_{j,0} + 1/\Gamma$. If the observer viewing angle (with respect to the axis of the jet), θ_{obs} , is smaller than $\theta_{j,0}$, the two effects combine to produce a light curve that is initially similar to that of the spherical blast wave discussed in §4.1. Only when the blast wave decelerates and Γ becomes comparable to $1/\theta_{j,0}$ the jetted nature of the blast wave “reveals” itself to the observer in the form of a light curve break (Rhoads, 1997, 1999; Sari, Piran

²⁷ Observational signatures of the ‘top hat’ jet are very similar to those of a structured jet where the energy per solid angle is $\propto \theta^{-2}$, if the jet opening angle is replaced by the viewing angle (Lipunov, Postnov & Prokhorov, 2001; Rossi, Lazzati & Rees, 2002; Zhang & Mészáros, 2002). Therefore, all the discussion here is valid for this case as well (replacing θ_j with the viewing angle). Note that such a structured jet results in a larger beaming-corrected energy and lower beaming-corrected rate than top hat jet.

& Halpern, 1999).

This jet-break in the light curve results from a combination of the two processes discussed above. When the radiation beaming angle becomes wider than the jet size, the “missing” emission manifests itself as a faster decay of the light curve. Simultaneously, when the jet center become causally connected with the jet edges, the jet spreads sideways and the energy per solid angle decreases resulting in a faster deceleration with the radius. Therefore, at:

$$t_j \approx 2 \text{ d} (1+z) \left(\frac{E_{k,iso,50}}{n_{-2}} \right)^{1/3} \left(\frac{\theta_{j,0}}{0.2} \right)^{8/3} \quad (33)$$

the light curve ‘breaks’ roughly simultaneously in all observed bands. The asymptotic decay at $t_j \ll t \ll t_{NR}$ (defined in Eq. 18) is²⁸ (Sari, Piran & Halpern, 1999):

$$F_\nu \propto \begin{cases} \nu^2 t^0 & \nu < \nu_a \\ \nu^{1/3} t^{-\frac{1}{3}} & \nu_a < \nu < \nu_m \\ \nu^{-(p-1)/2} t^{-p} & \nu_m < \nu < \nu_c \\ \nu^{-p/2} t^{-p} & \nu_c < \nu \end{cases}. \quad (34)$$

Comparison with the temporal decay at $t \ll t_b$ (Eq. 17) shows that in the optical and the X-ray (where $\nu > \nu_m$) a roughly similar break is expected from $\alpha \approx 1$ to $\alpha \approx 2$. Therefore, when an achromatic break, with roughly the predicted power-law indices, is observed, it is usually interpreted as an indication that the outflow was initially collimated to a half opening angle:

$$\theta_{j,0} \approx 0.15 \text{ rad} \left(\frac{E_{k,iso,50}}{n_{-2}} \right)^{-1/8} \left(\frac{t_j/(1+z)}{1 \text{ d}} \right)^{3/8}. \quad (35)$$

To date, three SHBs have known redshift and late afterglow light curves (Fig. 4). The limits on the opening angle of these bursts are:

SHB 050709: In this burst there are optical and X-ray detections at several different epoches (Fox *et al.*, 2005; Hjorth *et al.*, 2005b). Fox *et al.* (2005) suggest an optical break based on three *HST* observations, but Watson *et al.*

²⁸ The hydrodynamics of lateral spreading is a major open question. Numerical simulations (Granot *et al.*, 2001; Cannizzo, Gehrels & Vishniac, 2004) and approximate analytical treatment (Kumar & Granot, 2003) suggest that the spreading velocity in the co-moving fluid frame is significantly smaller than c . The details of the lateral spreading determine the relative importance of each one of the two processes that cause the observed break. In any case, observational signatures do not depend strongly on the spreading details. Eq. 34 is derived assuming maximal lateral spreading (comparable to the light speed), but is a fairly good approximation for spreading at any other velocity (including no spreading at all).

(2006) have shown that when additional optical data are considered, the optical data set cannot be fitted by a single or a broken power-law. Additionally, the last X-ray observation ($t = 16$ d) shows evidence of an intense flare. Given the small number of observations and the apparent variability, it is impossible to reliably determine an underlying power-law behavior that is consistent in all wavelengths. Therefore, unfortunately, the opening angle of this burst cannot be constrained.

SHB 050724: Observations include a detailed X-ray light curve (Campana *et al.*, 2006; Grupe *et al.*, 2006) but only sparse detections in the IR, optical and radio (Berger *et al.*, 2005). At early times the X-rays are dominated by the X-ray tail (§2.2.2), and following its decay two flares are observed, one at ~ 1000 s and the other around $\approx 10^4 - 10^5$ s. Between the two flares the power-law decays as $\sim t^{-1}$ and late *Chandra* observations at $t \approx 3$ weeks show that after the second flare the afterglow resumes its shallow $\sim t^{-1}$ decay. These observations suggest that $t_j > 20$ d as there is no evidence for a jet-break in the data, implying (Grupe *et al.*, 2006): $\theta_{j,0} \gtrsim 0.4$ rad $(E_{k,iso,50}/n_{-2})^{-1/8}$. Possible caveats are that a jet signature may have been obscured by the flaring activity or, if the density is indeed as high as suggested by Panaitescu (2006), $\gtrsim 0.1$ cm $^{-3}$, the Newtonian transition may already affect the light curve after 3 weeks, preventing the detection of a jet. If instead one adopts the beginning of the second flare ($\approx 10^4$ s) as a lower limit on the jet-break time, the opening angle is $\theta_{j,0} \gtrsim 0.06$ rad $(E_{k,iso,50}/n_{-2})^{-1/8}$. Assuming ‘top hat’ jet structure these limits imply a total (beaming corrected) energy of $E_{\gamma,tot} = E_{\gamma,iso}\theta_j^2/2 \gtrsim 0.7[0.02]10^{49}$ erg $(E_{k,iso,50}/n_{-2})^{-1/4}$ (the bracketed value is for the more conservative limit on $\theta_{j,0}$).

SHB 051221: Observations include a detailed X-ray light curve (Burrows *et al.*, 2006) and continuous optical monitoring (Soderberg *et al.*, 2006a). This afterglow shows a continuous X-ray decay as $t^{-1.2}$ between 100 s and 4 d with a short episode of flattening around $t = 1$ hr. At $t \approx 5$ d the X-ray decay becomes much steeper (roughly as t^{-2}). The optical light curve decays as $\approx t^{-0.9}$ until 4 d where it falls below the detection limit. The 3σ optical upper limits after four days require a simultaneous optical break. Here the interpretation of the break at 4 d as a jet signature seems quite suggestive given its achromatical nature and the regular decay before and after the break at the predicted decay rates. The corresponding jet opening angle is $\theta_{j,0} \approx 0.16$ rad $(E_{k,iso,51}/n_{-2})^{-1/8}$ implying a total energy $E_{\gamma,tot} \approx 3 \cdot 10^{49}$ erg $(E_{k,iso,51}/n_{-2})^{-1/4}$.

Since there is only one “clean” case (SHB 051221) for which a reasonable constraint on the beaming can be obtained, the opening angle distribution of SHB jets is not well constrained. Current observations suggest that the average beaming factor ($f_b \equiv 1 - \cos\theta_j$) satisfies $1 \ll \langle f_b^{-1} \rangle < 100$, but at this point no secure conclusion can be drawn. The fine details of the outflow angular structure remain obviously unconstrained.

4.7 Afterglow variability

Afterglow model ingredients discussed so far are regular and as such they predict smooth and regular light curves (smoothly broken power-law). These models are simplified and the true physical environment is expected to be more complicated with irregularities giving rise to light curve variability. Thus, afterglow variability, or the lack of it, can probe irregularities in the external shock and late engine activity.

The external shock cannot produce large amplitude, rapid flux variability ($\delta F/F \gtrsim 1$ over $\delta t/t \ll 1$ where F is the afterglow flux and t is the time since the burst). The reason is that during the external shock $t_{ang} \sim 10t_{los} \sim 10t_{\Delta}$ (the width of the emitting shell following the external shock is $\Delta \approx R/(10\Gamma^2)$; §3.1.1). Emission from a radius R is observed between $t = t_{los}$ and $t \approx t_{ang} + t_{los} \approx t_{ang}$ and therefore spherical variations are smoothed over t_{ang} , implying $\delta t \sim t_{ang} \sim t$. Even variations in a well localized angular region will be smoothed over t_{Δ} implying $\delta t \gtrsim t/10$. For an external shock to produce high amplitude variability on shorter time scales a very small region (relative to Δ and R/Γ) should increase its luminosity so that it becomes much brighter than the remainder of the observed shell, and then quickly decay without affecting the emissivity of its vicinity. Such behavior is not expected from hydrodynamical processes. Producing significant variability even over time scales as short as t_{Δ} requires a unique configuration. On the other hand, if the engine is active at late times, it can easily produce variability with arbitrary amplitude on time scales as short as its dynamical time (< 1 ms), just as we observe during the prompt emission. Therefore, whenever a high amplitude, rapid variability is observed, it is likely a result of late engine activity.

High latitude emission (§3.1.3) from a quasi-spherical shell sets another interesting constraint on the variability induced by an external shock (Nakar & Piran, 2003a). A spherical external shock cannot produce light curves that decay faster than $F_{\nu} \propto \nu^{-\beta} t^{-(2+\beta)}$. Rapidly decaying light curves must result either from late engine activity or from an aspherical blast wave on angular scales $\lesssim 1/\Gamma$.

Alternative explanations for afterglow temporal variability are:

(i) *Variable external density* (e.g., Wang & Loeb, 2000; Lazzati *et al.*, 2002; Ramirez-Ruiz *et al.*, 2001; Dai & Lu, 2002; Nakar, Piran & Granot, 2003; Nakar & Piran, 2003a; Ramirez-Ruiz *et al.*, 2005; Ioka, Kobayashi & Zhang, 2005; Eldridge *et al.*, 2006; Pe’er & Wijers, 2006; Nakar & Granot, 2006): This variability source is discussed mostly in the context of turbulent ISM or massive stellar wind environment. In the case of SHBs massive stellar winds are most likely irrelevant (§5), while density inhomogeneities resulting from ISM turbulence are expected to have a low amplitude (of order unity). The main

distinction of density induced variability is that it is chromatic. The light curve varies both above and below ν_c , but these variations are uncorrelated (Nakar & Granot, 2006). The resulting fluctuations can be either ‘bumps’ or ‘dips’ (relative to the unperturbed light curve). A turbulent ISM can produce only rapid, low amplitude, fluctuations on top of a smooth power law decay (Wang & Loeb, 2000). Significant density fluctuations, which are not expected in the case of SHBs, can produce high amplitude light curve variability but only over a long duration ($\delta t \sim t$). Detailed limits on the light curve fluctuations in the case of increasing density are discussed in Nakar & Granot (2006).

(ii) *angular variability of the ejected energy* (“patchy shell” e.g., Kumar & Piran, 2000b; Nakar, Piran & Granot, 2003; Nakar & Oren, 2004; Ioka, Kobayashi & Zhang, 2005): If the outflow energy has an intrinsic angular structure it will produce a variable afterglow light curve. As the blast wave decelerates, the angular size of the observed region ($\sim 1/\gamma$) increases. As a result, the effective (average) energy of the observed region, and hence the observed flux, vary. If the angular structure has a typical scale then the fluctuation amplitude decreases with time as more patches enter the observed region. Averaging over larger random structures leads to a decay of the fluctuation envelope as $t^{-3/8}$ (Nakar, Piran & Granot, 2003; Nakar & Oren, 2004). A surprising result is that although the variability is not limited by the angular time, the gradual change in the visibility of the patches dictates that the variability time scale is $\Delta t \sim t$ (Nakar & Oren, 2004). An important feature in this scenario is the break of the axial symmetry and therefore the possible production of linear polarization. Both the amplitude and the angle of polarization are correlated with the light curve variations (Granot & Königl, 2003; Nakar & Oren, 2004).

(iii) *Energy injection* (e.g., “refreshed shocks” Rees & Mészáros, 1998; Kumar & Piran, 2000a; Sari & Mészáros, 2000; Granot, Nakar & Piran, 2003; Fox *et al.*, 2003; Nousek *et al.*, 2006; Zhang *et al.*, 2006; Granot & Kumar, 2006): Energy can be injected into the external blast wave by late-arriving shells. Such shells can be produced by late engine activity, or a slow shell, ejected during the initial burst, can overtake the decelerating material behind the (initially faster) afterglow shock. In both of these cases the blast wave energy increases monotonically and, therefore, the observed flux is expected to rise above the unperturbed light curve, in all wavelengths, during energy injection. When the injection stops the original decay is resumed. The resulting light curve in the case of discrete episodes of energy injection has a distinctive step-like structure. The time scale of the steps (δt) depends on their timing relative to the jet-break. $\delta t \sim t$ before the brake and $\delta t < t$ is possible after the jet-break (Granot, Nakar & Piran, 2003). In any case δt is limited by the time associated with the width of the shell behind the afterglow shock, t_Δ , implying $\delta t \gtrsim t/10$. A variant of this model is the two-component jet model (e.g., Berger *et al.*, 2003; Königl, 2004; Peng, Königl & Granot, 2005; Granot,

2005; Wu *et al.*, 2005; Jin *et al.*, 2006) where the opening angle of the slow ejecta is larger than the opening angle of the fast ejecta.

(iv) *Microensing event* (Loeb & Perna, 1998; Garnavich, Loeb & Stanek, 2000; Granot & Loeb, 2001; Mao & Loeb, 2001; Gaudi, Granot & Loeb, 2001; Koopmans & Wambsganss, 2001; Ioka & Nakamura, 2001; Baltz & Hui, 2005): The apparent radius of the afterglow ($\sim R/\Gamma$) increases with time (as $t^{5/8}$ in the quasi-spherical phase) and at cosmological distances its angular size after a day is $\sim \mu\text{as}$, comparable to the Einstein radius of a solar mass gravitational lens at these distances (Loeb & Perna, 1998). Therefore, a microlensing event may induce afterglow brightening, which is expected to be seen simultaneously in all wavelengths. Some color dependence is expected as a result of the color dependent afterglow surface brightness (Granot, Piran & Sari, 1999a; Granot & Loeb, 2001). Note that the probability for an afterglow microlensing is small (Koopmans & Wambsganss, 2001; Baltz & Hui, 2005) and therefore only a small fraction of the observed afterglow variability may be attributed to microlensing.

All well-sampled SHB X-ray afterglows show strong variability. In almost all cases $\delta t \sim t$, implying that the source of the variability is not necessarily late engine activity (although it may be). An exception is SHB 050709 where Fox *et al.* (2005) find that during the last *Chandra* observation (exposure time of 5 hr, taken at $t = 16$ d) most of the flux arrived during the first 6 ks (a constant emission rate is rejected at 99.9% confidence), suggesting a high amplitude flare, $\Delta F/F \approx 10$, with very rapid variability $\delta t/t \approx 0.005$. Such a flare, if real, requires a source that is still active 16 days after the burst. Note that the energy emitted in this X-ray flare was $\sim 10^{45}$ erg, about four orders of magnitude below that of the GRB itself.

Large flares observed in other bursts (e.g., SHBs 050724, 051221 and 060313) are too bright and rapid to be explained by external density enhancement (Nakar & Granot, 2006) and most likely result from energy fluctuations of the external shock (either a patchy shell or refreshed shocks) or by internal dissipation of flow ejected during late engine activity. Note that SHB 051221 shows the very indicative step-like light curve expected by refreshed shocks (Burrows *et al.*, 2006; Soderberg *et al.*, 2006a) while flux in SHB 050724 afterglow returns to its original level after it flares (assuming a constant underlying decay; Campana *et al.*, 2006; Grupe *et al.*, 2006) suggesting that the flares result from hot spots on the blast wave, or that they are unrelated to the external shock (i.e., late engine activity). Interestingly, similar variable afterglows are observed in long GRBs, such as the step-like light curve of GRB 030329 (e.g., Lipkin *et al.*, 2004) or the X-ray flares after which the original underlying flux level and decay rate are resumed in many *Swift* X-ray afterglows (e.g., Nousek *et al.*, 2006).

4.8 The early X-ray “tail”

Currently, two *Swift* and *HETE-2* SHBs (050709 & 050724) exhibit soft X-ray tails, which last for ~ 100 s and are separated by ~ 10 s from the short and hard bursts of prompt gamma-rays (§2.2.2). The variability of such a tail is an important clue to its origin. Similarly to the prompt emission, rapid high amplitude variability implies continuous engine activity, while low variability emission can be explained by external interaction. In these two bursts no apparent rapid variability is seen, although the low signal to noise ratio in these two bursts may hide such variability, if it exists. Among the several *BATSE* bursts identified by Norris & Bonnell (2006) to have a similar temporal structure, there are some in which the soft tail is highly variable. Similarly, the X-ray tail of the nearby GRB 060614, which may be an extreme member of the SHB family (Gal-Yam *et al.*, 2006; Gehrels *et al.*, 2006), is also highly variable. Therefore, while at this point continuous engine activity is not absolutely necessary to explain the observed X-ray tails, there are suggestive hints in this direction. Note that X-ray flares observed hours and days after the bursts, might require late engine activity as well.

If the X-ray tail can be explained by external dissipation then it is intriguing that its duration and timing are similar to the expectation from reverse shock emission (Eq. 30). According to the canonical microphysical assumptions, reverse shock emission is not expected to contribute to the X-ray emission (§4.3). However, it is possible that the composition of the outflow (e.g., its magnetization level) can affect particle acceleration or the magnetic field of the shocked plasma in a way that results in bright X-ray emission. For example, a large ϵ_B together with effective acceleration of only a small fraction of the electrons (resulting in a high value of γ_m) can produce soft X-ray emission that begins ~ 10 s after the prompt emission, lasts for ~ 100 s and has a comparable energy to the one observed in the prompt emission.

MacFadyen, Ramirez-Ruiz & Zhang (2005) suggest a binary SHB progenitor that is composed of a neutron star and a non-compact companion (§5.3.1). In this model the SHB takes place once the neutron star collapses to a black hole (driven by accretion). The X-ray tail is produced by interaction of relativistic ejecta with the non-compact companion. The time scale as well as the typical emission frequency and the total radiated energy from this interaction can fit observed X-ray tails. This model, however, can explain only a single smooth episode.

If however X-ray tails are produced by extended engine activity then there are several different schemes that were suggested in order to extend the duration of hyperaccretion of $\sim 0.1 M_\odot$ onto a black hole (the most popular central engine model) beyond the natural timescale of $\lesssim 1$ s (§5.2.1). Examples in-

clude magnetic barrier that chokes the accretion (van Putten & Ostriker, 2001; Proga & Zhang, 2006), disk fragmentation (Perna, Armitage & Zhang, 2006) and a complex evolution of the neutron star disruption in a NS-BH binary (Faber *et al.*, 2006a). Alternatively, viscosity that is lower than expected can prolong the accretion time (§5.2.1). Fan, Zhang & Proga (2005) argue that if the X-ray tail results from a low accretion rate, the energy of the accretion cannot be extracted by neutrino-anti neutrino annihilation, since the efficiency of this process falls rapidly when the accretion rate is lower than $0.01 M_{\odot}/s$. For a detailed discussion of accretion disk lifetime and the efficiency of different energy extraction mechanisms see §5.2.1. A different solution may be that the central engine is a hyper-magnetized neutron star (e.g., Usov, 1992, §5.3.2 and §5.2.II). The activity duration of this type of engine may be significantly longer than several seconds (e.g. Dai *et al.*, 2006).

4.9 Macronova

An interesting possible source of late time emission is radioactive decay of matter that was ejected sub-relativistically during the burst. There are several possible scenarios in which such ejecta are launched along with the relativistic outflow that produce the SHB. For example, during the coalescence of a neutron star with another compact object (neutron star or a black hole) considerable amount of mass, of the order of $0.01 M_{\odot}$, may be ejected from the system (e.g., Rosswog *et al.*, 1999; Ruffert & Janka, 2001). During the merger the density and temperature of the ejected mass can be high enough to produce heavy neutron rich elements, most of them radioactive (e.g., Lattimer & Schramm, 1974, 1976; Symbalisty & Schramm, 1982; Eichler *et al.*, 1989; Rosswog *et al.*, 1999; Ruffert & Janka, 2001). Another example of a source of radioactive sub-relativistic ejecta may be nucleosynthesis in the wind that is driven by a neutrino-dominated hyper-accreting disk, which is the leading central engine model (e.g., MacFadyen, 2003).

Sub-relativistic radioactive ejecta also power the emission from supernova explosions. The higher expected velocities in the SHB case, together with the lower amount of mass, lead to a fainter and faster evolving, yet supernova reminiscent, emission. Radioactive energy dominates the observed emission of sub-relativistic ejecta since initial thermal energy is quickly lost to expansion. The properties of the observed emission are determined by the interplay between the typical radioactivity lifetime (which depends on the nuclear composition of the outflow), and the maximal time (and radius) at which the ejecta are still dense enough to reprocess this energy into a blackbody radiation. If a significant amount of radioactive heat is generated while the ejecta are dense enough we may detect the emitted blackbody emission. If most of the energy is released at later times the radioactively generated photons may be observed

directly.

Li & Paczyński (1998) were the first to discuss this possibility. Having the unknown composition ejected matter during a compact binary merger in mind, they postulate a radioactive source which decays as a power-law in time. Assuming that $0.01 M_{\odot}$ is ejected at a velocity of $c/3$, and that 0.1% of the rest mass energy is converted to heat, they find that after one day the bolometric luminosity can be as high as 10^{44} erg/s ($M_{bol} \sim -21$). Such a bright emission is already ruled out by tight constraints on the optical emission from SHB 050509B (Hjorth *et al.*, 2005a).

Kulkarni (2005), introducing the term “Macronova”, presents detailed light curve calculations for two specific nuclear heat sources, free neutron decay and radioactive Ni 56. He finds that neutron-heated ejecta may generate an optical emission that peaks hours after the SHB with a luminosity of $\sim 10^{41}$ erg/s ($M \sim -14$). Such emission can be detected from $z = 0.2$ by a 10-meter-class telescope. Ni 56 heated ejecta, on the other hand, are very hard to detect in optical observations, unless the velocity of the ejecta is unreasonably slow (much below the escape velocity from a neutron star surface), otherwise the ejecta becomes optically thin before most of the Ni 56 decay. Most of the radioactive energy in this case would escape as hard X-ray photons.

To conclude, macronova emission may be detected if SHBs eject a significant amount of radioactive mass with a favorable decay time, and even then only by rapid (less than 1 d post burst) and deep optical observations. The characterizing signatures of macronova optical emission are blackbody colors and non-correlated optical and X-ray emission.

4.10 Relativistic collisionless shocks

The microphysics of collisionless shocks is a major open question in GRB physics (for a recent review see Waxman, 2006). The mean free path of a proton to undergo a binary collision of any type during GRB external or internal shocks is larger by many orders of magnitude than the size of the system. Therefore, any interaction between the particles must be due to collective processes. Such electromagnetic interactions are known to take place in anisotropic plasma and they give rise to collisionless shocks in GRBs. The external shock is ultra-relativistic and the “upstream” (e.g., the unshocked ISM) is unmagnetized. Internal shocks, if they take place, are mildly relativistic and the upstream may be magnetized by magnetic field that is advected all the way from the central engine.

Afterglow observations require collisionless shocks to generate the two major ingredients of the observed emission: (i) The shock should generate a near

equipartition magnetic field while a μG upstream field is some eight orders of magnitude below equipartition (the fraction of the generated magnetic energy out of the total energy is parameterized by ε_b). The generated field must be sustained along the downstream. (ii) The shock should accelerate electrons to Lorentz factors that are much higher than the thermal temperature of the “downstream” (the shocked ambient medium). The outcome of the acceleration process is parameterized by ε_e and p (see §4.1).

There is currently no complete “first principles” theory that explains how collisionless shocks accelerate particles or generate and sustain the magnetic field. ε_b , ε_e and p are simply phenomenological (almost certainly oversimplified) model parameterizations, which are constrained by the observations. In long GRBs these parameters are reasonably constrained (e.g., [Panaitescu & Kumar, 2001](#); [Yost *et al.*, 2003](#)) and so is the requirement that the magnetic field is sustained long after the shock ($\sim 10^8\lambda_s$, where λ_s is the plasma skin depth; [Rossi & Rees, 2003](#)). In SHBs the current observations are not detailed enough to constrain these parameters, but the similarities to long GRB afterglows suggests that the microphysics is similar as well. This is not very surprising given that the microphysical processes are most likely affected only by local properties such as the shock velocity and the upstream magnetization and not by global properties such as the total outflow energy or large scale gradients in the external density.

Unmagnetized collisionless shocks are not well understood. [Moiseev & Sagdeev \(1963\)](#) suggested that unmagnetized Newtonian shocks are generated by the filamentation mode of the Weibel instability ([Weibel, 1959](#)), a kinetic instability that arises when the velocity distribution of plasma particles is anisotropic. The typical scale of this instability is λ_s . [Medvedev & Loeb \(1999\)](#) and [Gruzinov & Waxman \(1999\)](#) suggested that the same process may take place in relativistic GRB shocks (see however [Lyubarsky & Eichler, 2006](#)). The filamentation modes of this instability (e.g., [Fried, 1959](#); [Silva *et al.*, 2002](#); [Bret, Firpo & Deutsch, 2004, 2005](#)) result in the breakdown of the plasma into current filaments and in the generation of a magnetic field in the plane of the shock. In this picture this magnetic field, which grows to equipartition levels, provides the effective collisionality that produces the shock. [Medvedev & Loeb \(1999\)](#) suggested that this magnetic field is also responsible for the observed synchrotron emission. The generated field coherence scale is λ_s and basic considerations suggest that such a field should decay over a similar scale after the shock ([Gruzinov, 2001](#); [Milosavljević & Nakar, 2006b](#)). The field coherence scale must grow quickly enough if it is to survive along the downstream, as suggested by [Silva *et al.* \(2003\)](#) and [Medvedev *et al.* \(2005\)](#). It is currently unclear whether the coherence length of the field is growing fast enough and therefore the fate of the generated field is unknown.

An alternative idea is that the field is generated already in the upstream

by interaction between shock accelerated protons and unperturbed upstream (Gruzinov, 2001; Milosavljević & Nakar, 2006a). Interestingly, Li & Waxman (2006) used the requirement that the acceleration time of the radiating electrons (assuming Fermi acceleration) is shorter than the inverse Compton cooling time of these electrons in the upstream, in order to put a lower limit on the upstream field in front of the shock (a larger field reduces the acceleration time). They find that in several long GRBs the field must be larger than $0.2n_0^{5/8}$ mG, where n is the external density, suggesting that the upstream field is amplified. Repeating the same analysis for SHBs shows that no meaningful constraints can be derived, and a μ G field is consistent with the observations. The reason is that for typical SHB parameters inverse Compton cooling in the upstream is suppressed by the Klein-Nishina cross-section (§4.2).

Acceleration of non-thermal particles in collisionless shocks is believed to be done through diffusive shock acceleration (a.k.a. first order Fermi acceleration ; for reviews see Drury, 1983; Blandford & Eichler, 1987). Acceleration in this process takes place when a particle is scattered back and forth across the shock by interactions with plasma waves on each side. With each shock crossing the particle gains energy. GRB observations require that the acceleration process will produce electrons with a high energy power-law distribution with an index $2 \lesssim p \lesssim 3$. Theoretical predictions of relativistic diffusive shock acceleration typically suggest $p \approx 2.2$ (e.g., Achterberg *et al.*, 2001; Ellison & Double, 2002; Lemoine & Pelletier, 2003; Keshet & Waxman, 2005), which fits the observations nicely²⁹. However, there are some simplifying assumptions that go into these calculations that are not necessarily valid, and the full acceleration process is far from being understood.

During the last several years there has been a large effort to simulate relativistic collisionless shocks in three dimensions, using the particle-in-cell (PIC) method (Silva *et al.*, 2003; Fonseca *et al.*, 2003; Frederiksen *et al.*, 2004; Jaroschek, Lesch & Treumann, 2004, 2005; Nishikawa *et al.*, 2005; Spitkovsky, 2005). These simulations show, as expected, that when two unmagnetized plasma shells collide relativistically, shocks are formed by the Weibel instability, building skin depth scale equipartition magnetic field in the plane of the shock. None of the current simulations is large enough (in time and space) to achieve a steady state shock or to explore the decay of the generated magnetic field in the downstream, due to computational resource limitations. None of the simulations show a clear indication of diffusive shock acceleration. This is not very surprising, given the simulation size and the fact that the upstream field is practically zero. The reason is that in these conditions there is no upstream scattering agent that can reflect high energy particles back into the

²⁹The exact value of p depend on the details of the interaction between the accelerated particles and the magnetic turbulence (e.g., Ellison & Double, 2004; Lemoine & Revenu, 2006; Katz, Keshet & Waxman, 2006; Keshet, 2006).

shock and start the acceleration process. In reality the pre-existing upstream (e.g., ISM) magnetic field is necessary to enable reflection of particles back into the shock over scales that are much larger than the skin depth.

5 Progenitors and the central engine

In my mind, the most interesting open SHB question today is the nature of the progenitor and the processes leading to the formation of the central engine (for a recent review see [Lee & Ramirez-Ruiz , 2006](#)). This branch of research has been active for many years and some of the models were explored in great detail. Interest in this field was boosted following the recent detection of SHB afterglows, as we now have an idea about the typical environment and redshift in which SHB progenitors dwell. An immediate implication of this information is the understanding that SHB progenitors are different systems than the progenitors of long GRBs, providing the proof that long and short GRBs are two distinct physical phenomena. Nevertheless, the identity of the progenitors of SHBs is still unknown.

Coalescence of a compact binary, either a double neutron star or a neutron star (NS) and a black hole (BH) binary, is currently the leading progenitor candidate. It is also the most extensively explored model and at least NS-NS systems are observationally known to exist. Therefore, this model will be the focus of this chapter (§5.2). This progenitor candidate is of great interest since NS-NS and NS-BH coalescence events are the most promising sources of gravitational-wave (GW) signals accessible to ground-based GW observatories. The evidence supporting the merger model are indirect, and some aspects of this model seem to be ‘uncomfortable’ with the observations. Therefore, it is important at this point to keep an open mind to the possibility that SHBs may have a different origin than compact binary mergers. Other models are discussed in §5.3.

The debate about the origin of long GRBs ended only with the detection of SN spectral signatures in optical long GRB afterglow ([Stanek *et al.* , 2003](#); [Hjorth *et al.* , 2003](#)). Lacking similar direct evidence for SHBs, the next best thing is an examination of indirect environmental properties. The hope is that this information, together with the requirement that the progenitor will be, in principle, able to produce an SHB, will single out viable progenitor systems. Therefore, before discussing specific models and their predictions, I review the new constraints that the detection of SHB afterglows pose on progenitor properties.

5.1 Progenitors lifetime and intrinsic rate

SHB progenitor lifetime is constrained using two independent methods - (i) based on the observed redshift-luminosity distribution, and (ii) based on the host galaxy type distribution and the fractional association of host galaxies with galaxy clusters. The results from both methods are similar - SHB progenitor population is dominated by long-lived (\sim several Gyr) systems. Unfortunately, the current sample available for this kind of analysis is small, and it is unlikely that its size will significantly grow in the near future (see below). Therefore, the conclusions that are based on this sample should be considered with care.

5.1.1 The sample

The constraints on SHB progenitor lifetime and on the intrinsic SHB rate are statistical by nature. Therefore, the sample that is used should be chosen carefully, and selection effects should be well understood. When the first analysis exploring this topic was carried out (the end of the summer of 2005; [Nakar, Gal-Yam & Fox, 2006](#); [Guetta & Piran, 2006](#)) all four SHBs localized with arcsecond precision were associated with host galaxies (SHBs 050509, 050709, 050724) or with a galaxy structure (SHB 050813). Therefore, these four bursts constitute a complete sample in the sense that no events were left out due to possible selection effects. [Nakar, Gal-Yam & Fox \(2006\)](#) also carried out an analysis based on an extended sample of SHBs, including four IPN localized bursts (§2.3; [Gal-Yam *et al.*, 2005](#)). These constitute a complete sample of IPN bursts selected based on the size of their error boxes and locations far from the Galactic plane.

Unfortunately, the hosts and the redshifts of SHBs discovered after these first well-localized four bursts, were not identified (in some cases even an early X-ray afterglow was not detected), in part as a result of diminished observational effort. As a result, any additional SHB for which the redshift and/or host is determined (e.g., SHB 051221) cannot be currently included in an unbiased sample. The reason is that selection effects that prevent easy identification of the hosts of these bursts may strongly bias any sample that does not compensate for the undetected bursts. Hopefully, it will be possible in the future to assemble a larger unbiased sample in order to obtain more definite conclusions.

5.1.2 Constraints from SHB redshift distribution

The *observed* redshift-luminosity two-dimensional (2D) distribution is determined by the *intrinsic* redshift and luminosity distributions, modified usually

by the detector sensitivity. Thus, the goal of the analysis is to use the observed distribution to constrain the intrinsic redshift distribution (Piran, 1992; Gal-Yam & Maoz, 2004; Ando, 2004; Guetta & Piran, 2005, 2006; Nakar, Gal-Yam & Fox, 2006). Then, the lifetime of the progenitor can be constrained by making the most probable assumption that the progenitor birth rate follows the cosmic star-formation history, and that the intrinsic redshift distribution is a convolution of the cosmic birth rate with the lifetime distributions. The main disadvantage of this method is that for small observed samples the intrinsic distributions are under-constrained. It is only possible to assume several physically motivated parametric functional forms of the intrinsic distributions and constrain their parameter values.

The two-dimensional observed redshift, z , and luminosity, L , distribution is derived from the intrinsic distributions via:

$$\frac{d\dot{N}_{obs}}{dLdz} = \phi(L) \frac{R_{SHB}}{1+z} \frac{dV}{dz} S(P), \quad (36)$$

where \dot{N}_{obs} is the *observed* SHB rate and $\phi(L)$ is the *intrinsic* peak luminosity function, which is assumed to be independent of z . $0 \leq S(P) \leq 1$ is the probability for detection, including redshift determination when redshift information is needed, of a burst with a peak photon flux P , which in turn depends on L and z as well as on the spectrum of the bursts. $R_{SHB}(z)$ is the intrinsic SHB rate per unit comoving volume and comoving time. Since SHB progenitors are most likely of a stellar origin it is expected that:

$$R_{SHB}(z) \propto \int_z^\infty SFR(z') f(t(z) - t(z')) \frac{dt}{dz'} dz', \quad (37)$$

where $SFR(z)$ is the star formation rate at redshift z (per unit comoving volume and comoving time), $t(z)$ is the age of the universe at redshift z , and $f(\tau)d\tau$ is the fraction of SHB progenitors that are born with a lifetimes between τ and $\tau + d\tau$.

$S(P)$ can describe a single detector or a combination of several detectors, each weighted by its field of view and operational time. In principle if $S(P)$ is well known and if the observed sample is large enough then the intrinsic distributions can be extracted from Eq. 36. In reality we have to work with a limited sample as well as poorly understood $S(P)$. In the case of GRBs (long and short) there is a large sample of bursts, observed by *BATSE*, for which only the peak flux distribution is available while the redshift (and thus luminosity) is unknown. The *BATSE* sample can constrain the intrinsic distributions by considering the observed flux distribution which is an integration of Eq. 36:

$$\frac{d\dot{N}_{obs}}{dP} = \frac{d}{dP} \int_0^\infty dz \int_{\tilde{L}(z,P)}^\infty dL \frac{d\dot{N}_{obs}}{dLdz}, \quad (38)$$

where

$$\tilde{L}(z, P) = 4\pi d_L^2 k(z) P \quad (39)$$

is the luminosity for which a burst at a redshift z has a peak flux P . $d_L(z)$ is the luminosity distance and $k(z)$ depends on the spectrum of the bursts and includes the k-correction as well as the conversion from energy flux to photon flux. $k(z)$ is assumed to be a function of the redshift only.

If $\phi(L)$ is a single power-law, $\phi(L) = \phi_0 L^{-\beta}$, with no upper or lower cutoff (within a luminosity range that is discussed below) then the integral over z in Eq. 38 does not depend on P and thus the observed peak flux distribution does not depend on R_{SHB} and simply satisfies:

$$\frac{d\dot{N}_{obs}(P)}{dP} \propto P^{-\beta} S(P). \quad (40)$$

Note that since Eq. 40 is independent of the burst redshifts $S(P)$ here is the probability for detection alone. Similarly, the integral over L in eq. 36 results in:

$$\frac{d\dot{N}_{obs}}{dz} = (4\pi d_L^2 k(z))^{1-\beta} \phi_0 \frac{R_{SHB}}{1+z} \frac{dV}{dz} \int P^{-\beta} S(P) dP, \quad (41)$$

thereby eliminating the dependence on $S(P)$ up to a constant normalization factor. Naturally, for $\beta < 2$ an upper cutoff must exist while for $\beta > 1$ a lower limit is necessary. However, if the lower cutoff is low enough so that it affects only a negligible volume, and if the upper cutoff is high enough so it affects only the detection at high redshift, then Eqs. (40) and (41) are applicable (these cut-offs also prevent the integral over P in Eq. 41 from diverging). Therefore, if the observed peak flux distribution can be fitted by Eq. 40 then the luminosity function can be a single power-law. In this case data sets for which $S(P)$ is not well known can be readily used and Eq. 41 enables a comparison of the one-dimensional observed redshift distribution with model predictions. Unfortunately the *observed* luminosity distribution depends on $S(P)$ even when the luminosity function is a single power-law. If $S(P)$ is well known, a better constraint on the intrinsic distributions can be obtained by a comparison with the two-dimensional luminosity-redshift distribution (Eq. 36).

The observed *BATSE* peak flux distribution, $\frac{d\dot{N}_{obs}(P)}{dP}$, can be fitted successfully by a single power-law with an index $\beta = 2 \pm 0.1$ (Nakar, Gal-Yam & Fox, 2006). Therefore, it is consistent to assume a single power-law luminosity function and to use Eq. 41 on a sample of bursts from different detectors with unknown $S(P)$ - altogether 8 bursts (4 *Swift* /*HETE-2* bursts and 4 IPN bursts). Figure 11 (from Nakar, Gal-Yam & Fox, 2006) presents the observed cumulative redshift distribution comparing to the predictions of several models (Eqs. 37 & 41) taking the star formation history formula SF2 from Porciani & Madau (2001) and using different functional forms of life time distribution: (i)

lognormal, $f(\tau)d\tau = (\tau\sigma\sqrt{2\pi})^{-1}\exp[-(\ln(\tau) - \ln(\tau_*))^2/2\sigma^2]d\tau$ with various values of τ_* and narrow ($\sigma = 0.3$) or wide ($\sigma = 1$) dispersions; (ii) power-law distributions $f(\tau) \propto \tau^\eta$ with a lower cutoff at 20 Myr and an upper cutoff that is larger than the Hubble time. This figure vividly illustrates that models with a typical delay are consistent with the data only if this delay is long ($\gtrsim 4$ Gyr). Models with no typical lifetime (power-law distributions) must have a birthrate of progenitors per unit logarithmic lifetime that increases significantly as a function of lifetime (i.e., $\eta > -0.5$). The reason that models dominated by short-lived systems do not fit the data is that they under-predict the fraction of bursts at low redshift ($z \lesssim 0.3$). Since the star formation rate is higher at large redshifts ($\gtrsim 1$), while SHBs are found preferentially at low redshift (≈ 0.3), although they are bright enough to be detected at high redshift, implies that a long delay is required for the progenitors so they are born when the universe is young and produce SHBs only when it is much older. Quantitatively, [Nakar, Gal-Yam & Fox \(2006\)](#) find that for lognormal lifetime distributions (narrow and wide) $\tau_* > 4[1]$ Gyr in 95[> 99.9]% confidence and for a power-law lifetime distribution the most probable power-law index is $\eta = 0.6$ and $\eta > -0.5[-1]$ at 95[99.5]% confidence³⁰. These results are similar to those obtained by [Guetta & Piran \(2006\)](#).

The fact that the observed luminosity function fits a single power-law does not necessarily imply that the intrinsic luminosity function is a single power law as well. When an intrinsic luminosity function that is not a single power-law is considered, the threshold of the detector must be known (at least partially) and therefore the sample that can be used is reduced only to the first three *Swift* SHBs. However, in such case the full two-dimensional $L - z$ distribution can be considered. [Nakar, Gal-Yam & Fox \(2006\)](#) find that when a ‘knee shaped’ broken power law (i.e., $\phi(L)$ is steeper above the break) lifetime distribution is assumed the results are very similar to the case of a single power-law. These results suggest that the observations prefer long-lived progenitors (Gyrs) for unimodal lifetime distributions. If a bimodal luminosity function is considered then there are solutions in which the progenitor lifetime is dominant by short-lived systems. However, such luminosity functions are not expected unless SHBs are composed of two separate populations.

This analysis does not include the recent indication found by [Berger *et al.* \(2006b\)](#) that at least 1/4 of the SHBs are at $z > 0.7$ (assuming that we are

³⁰ These values are calculated assuming that SHB 050813 is at $z=0.72$ ([Gladders *et al.*, 2005](#); [Berger, 2005](#); [Prochaska *et al.*, 2005](#)). If a redshift of 1.8 is taken instead ([Berger, 2006](#)) then a narrow lognormal lifetime distribution is ruled out (cannot explain both the low and high redshift bursts). For a wide lognormal lifetime distribution $\tau_* > 2[1]$ Gyr in 95[> 99]% confidence and for a power-law lifetime distribution the most probable power-law index is $\eta = 0$ and $\eta > -0.8[-1]$ at 95[98]% confidence.

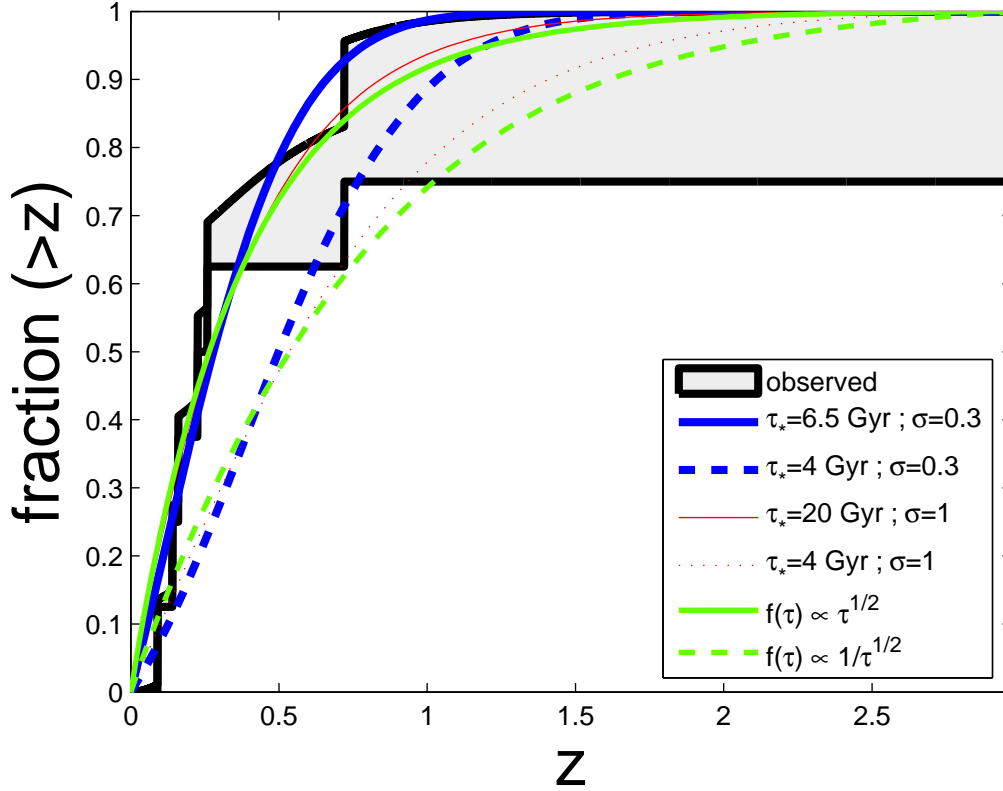


Fig. 11. The cumulative *observed* redshift distribution as predicted by various lifetime distributions when the luminosity function is $\phi(L) \propto L^{-2}$ and the star formation history is given by SF2 formula in [Porciani & Madau \(2001\)](#). The cumulative redshift distribution of the observed data (shaded area) is bracketed between the lower solid line, which is the cumulative redshift distribution of the six bursts with known redshifts, and the upper solid line, which includes also the contribution of the two bursts with upper limits (see [Nakar, Gal-Yam & Fox \(2006\)](#) for details). The figure demonstrates that only models which are dominated by long-lived progenitors provide a good fit to the data while models with short-lived progenitors under-predict the fraction of bursts at low redshift $z \lesssim 0.3$. [taken from [Nakar, Gal-Yam & Fox \(2006\)](#)]

not filled by SHBs that take place at large distances, ~ 100 kpc, from there hosts). If confirmed, this result indicates that the lifetime of a non-negligible fraction of the SHB progenitors is rather short (Gyr or less), implying that the lifetime distribution is wide (includes both old and young progenitors). It rules out a narrow lognormal ($\sigma = 0.3$) lifetime distribution or a power-law distribution with $\eta \gtrsim 0$. A wide lognormal ($\sigma = 1$) lifetime distribution with $4 < \tau_* < 8$ Gyr and a power-law distribution with $-0.5 \lesssim \eta \lesssim 0$ are consistent with all current observations.

5.1.3 Based on host galaxy types

An alternative method to estimate the progenitor lifetime is based on the spectral types of the host galaxies (Gal-Yam *et al.*, 2005). The stellar populations in early type galaxies (E & S0) is entirely dominated by old systems (several Gyr) while the population in galaxies of later types is composed of a mix of old and young systems. Therefore, the fraction of SHBs in different types of galaxies is an independent measure of the progenitor lifetime. Gal-Yam *et al.* (2005) compared the distribution of SHB host types to that of type Ia supernovae (SNe) from Mannucci *et al.* (2005), building on the extensive effort done in undertaken to constrain SNe Ia progenitor lifetime (Fig. 12). They find that a larger fraction of SHBs, compared to SNe Ia, take place in early type galaxies (at 93% confidence), implying that it is most likely that SHBs are older, on average, than SNe Ia. The typical time delay of SNe Ia, τ_{Ia} is still under debate, but all different models that assume a unimodal lifetime distribution agree that $\tau_{Ia} \gtrsim 1$ Gyr (Tonry *et al.*, 2003; Barris & Tonry, 2006; Strolger *et al.*, 2004; Gal-Yam & Maoz, 2004; Maoz & Gal-Yam, 2004; Mannucci *et al.*, 2005) and therefore SHBs, which are most likely older, have a lifetime of several Gyr. It was recently suggested that the population of SNe Ia is composed of two sub-groups - a long-lived component which is responsible for the entire SN Ia population in early type galaxies, and a short-lived component, which follows the star formation rate (Mannucci *et al.*, 2005, 2006; Scannapieco & Bildsten, 2005). If this is the case, the distribution of SHB host types is consistent with that of the long-lived SN Ia component which is several Gyr old.

Zheng & Ramirez-Ruiz (2006) constrain the lifetime of SHB progenitors directly by decomposing the total star formation history to the contribution from early- and late-type galaxies. The convolution of the split star formation history and a given lifetime distribution predicts the fraction of SHBs in each host type. Zheng & Ramirez-Ruiz (2006) find that if the lifetime distribution is a single power law, $f(\tau) \propto \tau^\eta$, then the observations suggest $\eta \gtrsim 3/2$ implying a typical lifetime of ~ 10 Gyr (note that this result is inconsistent with the recent observations of Berger *et al.* (2006b) that suggest that $\eta \lesssim 0$).

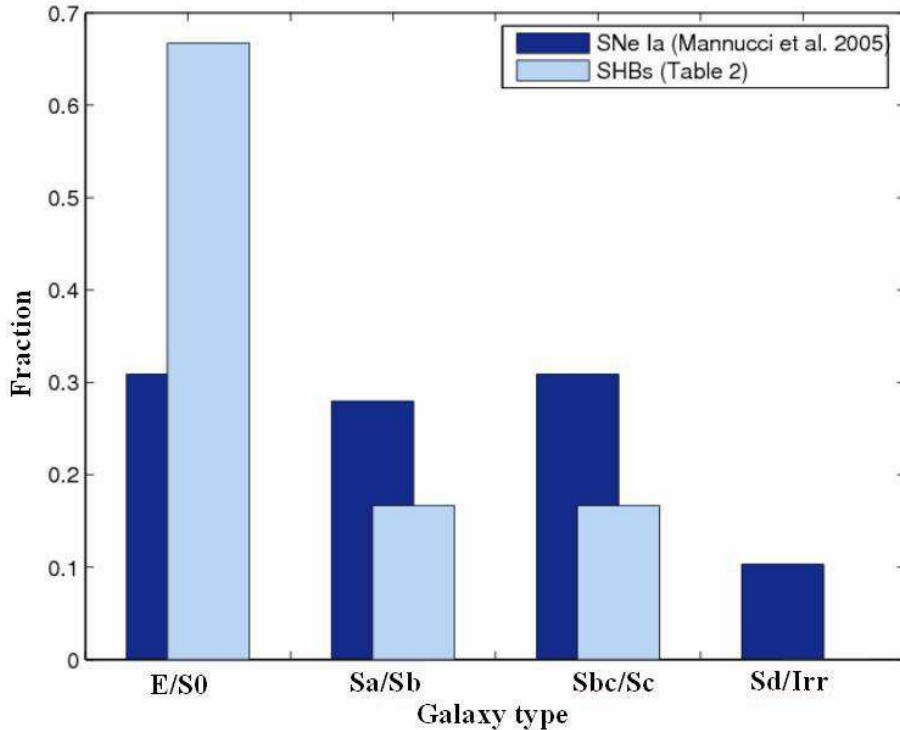


Fig. 12. A comparison between the host galaxy types (E/S0, Sa/Sb, Sbc/Sc and Sd/I) of SHBs (from Table 2) and SNe Ia (Mannucci *et al.*, 2005). The fraction of SHBs in early type galaxies is significantly larger than the fraction of SNe Ia observed in such galaxies in the nearby Universe, indicating that the progenitor systems of SHBs are probably longer-lived than those of SNe Ia. [from Gal-Yam *et al.* (2005)]

Shin & Berger (2006) follow a similar route to that of Zheng & Ramirez-Ruiz (2006), but rather than using the relative SHB rate in early- and late-type galaxies, they use the relative rates in cluster and field early-type galaxies. The advantage of this method over the early/late ratio is that the star formation histories of early-type galaxies are simpler. The disadvantage is that this method does not sample the lifetime distribution below ~ 1 Gyr since short-lived SHBs would not take place in early-type galaxies. Shin & Berger (2006) find that the current ratio of cluster to field early-type galaxies, 2, corresponds to $0 < \eta < 1$, which is consistent with earlier results from redshift distribution and early-type/late-type ratio analysis.

5.1.4 Intrinsic local rate

The observed *BATSE* local rate is $\mathcal{R}_{SHB,obs} \sim 10 \text{ Gpc}^3 \text{ yr}^{-1}$ (§2.6). This is clearly a lower limit on the true intrinsic rate. An upper limit on the SHB rate can be derived under the most probable assumption that the progenitors of SHBs are a product of at least one core-collapse supernova (e.g., a neutron

star) and that the SHB itself is a catastrophic non-repeating event. In this case the rate of SHBs is bound by the rate of core-collapse SNe. However, since the typical lifetime of SHB progenitors seems to be several Gyr, the local SHB rate corresponds to the rate of core-collapse SNe at a redshift ≈ 0.7 , which is $\sim 5 \times 10^5 \text{ Gpc}^{-3} \text{ yr}^{-1}$ (Dahlen *et al.*, 2004). Therefore, the intrinsic local rate, $\mathcal{R}_{SHB} \equiv R_{SHB}(z = 0)$, must be within the range:

$$10 \lesssim \mathcal{R}_{SHB} \lesssim 5 \times 10^5 \text{ Gpc}^{-3} \text{ yr}^{-1}. \quad (42)$$

Constraining the local rate within this range requires an estimate of the fraction of undetected bursts. These may be events that are collimated and point away from the observer, or bursts that are simply too dim to be detected. The number of bursts that are beamed away from us can be estimated by the beaming factor (i.e., the fraction of the total solid angle into which the prompt gamma-rays are emitted), f_b^{-1} . As I discuss in §4.6, the value of the beaming factor is reasonably constrained only in two bursts. In one case (SHB 051221A) it seems to be ≈ 80 (assuming a ‘top hat’ jet) and in the other (SHB 050724) it is probably much smaller. Thus it is impossible at this stage to confidently estimate the beaming factor, but current observations suggest that $1 \ll f_b \lesssim 100$. The correction for undetected dim bursts depends on the luminosity function and most strongly on its lower cutoff, L_{min} (defined so $\phi(L) = 0$ for $L < L_{min}$). Assuming the single power-law luminosity function that is found to be consistent with the data ($\phi(L) \propto L^{-2}$ $L > L_{min}$) the local rate is (Nakar, Gal-Yam & Fox, 2006):

$$\mathcal{R}_{SHB} \approx 40 f_b^{-1} \left(\frac{L_{min}}{10^{49} \text{ erg/s}} \right)^{-1} \text{ Gpc}^{-3} \text{ yr}^{-1}. \quad (43)$$

5.2 Coalescence of a compact binary

The coalescence of two neutron stars was recognized as a potential GRB progenitor already two decades ago. This possibility was briefly mentioned in Paczynski (1986), Goodman (1986) and Goodman, Dar & Nussinov (1987), and discussed in detail for the first time by Eichler *et al.* (1989) and later by Narayan, Paczynski & Piran (1992) and many others. Paczynski (1991), Narayan, Paczynski & Piran (1992) and Mochkovitch *et al.* (1993) discussed similar coalescence models of a neutron star (NS) and a stellar mass black hole (BH) as a possible progenitor. Binary mergers take place because of orbital energy and angular momentum loss to gravitational-wave radiation, as was observationally confirmed (Taylor & Weisberg, 1982). These models are natural candidates since such events must take place at a reasonable rate (see below) and the amount of gravitational energy that is liberated during the coalescence ($\sim 10^{54}$ erg) is large enough, so a small fraction of it can generate

the GRB. Additionally, in the ‘standard’ version of the merger model, the outcome of the coalescence is the same central engine as in long GRB models - a disk accreting onto a black hole. This similarity between the engines naturally explains the great similarity between the observational properties of the two phenomena. In both scenarios the duration of the burst is determined by the lifetime of the disk. The difference is that in binary mergers the disk is expected to be consumed within a fraction of a second, while in the ‘collapsar’ model for long GRBs, in-falling matter from the collapsing star feeds the disk for much longer, enabling the production of a long duration GRB.

5.2.1 The “central engine”

I. An accretion driven engine

In the most popular central engine scenario a binary merger results in the formation of a disk around a black hole (newly born in the NS-NS case). Accreting black holes are known to produce relativistic jets in other systems such as active galactic nuclei and microquasars, however the accretion rates that are required in order to power GRBs are higher by many orders of magnitude, implying different physical conditions. The models of the formation and operation of this type of SHB engine are discussed below.

I.I Forming an accretion disk in a NS-NS merger

An extensive effort was dedicated to numerical simulations of NS-NS mergers in the context of the GRB central engine. Starting from 3-dimensional Newtonian simulations with a polytropic equation of state (EOS) and no neutrino effects (Davies *et al.*, 1994), the simulations evolved to include increasingly more realistic EOS, neutrino modeling and asymmetric scenarios. These simulations were carried out mainly by two groups using different numerical schemes - Lagrangian Smooth Particle Hydrodynamics (SPH) (Rosswog *et al.*, 1999, 2000; Rosswog & Davies, 2002) and Eulerian Piecewise Parabolic Method (PPM) (Ruffert, Janka & Schaefer, 1996; Ruffert *et al.*, 1997; Ruffert & Janka, 1998, 1999, 2001). The outcomes of these simulations are rather similar. A central quasi-axisymmetric object is formed within a few orbital periods after the initial contact. This central object is surrounded by a thick disk of material at a radius of tens of km with densities of $\sim 10^{11} - 10^{12} \text{ gr cm}^{-3}$ and temperatures of $\sim 1 - 10 \text{ MeV}$. The mass of the disk depends somewhat on the initial conditions (e.g., spin, mass ratio) but is typically in the range of $0.03 - 0.3M_{\odot}$ for a system with an initial mass of $\approx 3M_{\odot}$. A narrow funnel along the axis of symmetry is relatively baryonic free and may serve as a potential site for launching a GRB jet (although it is unclear if this funnel is clean enough; Ruffert & Janka, 1998, 1999).

In recent years several groups carried out approximate (e.g., Oechslin, Rosswog & Thielemann, 2002) and fully (e.g., Shibata & Uryū, 2000) general relativistic

tic (GR) simulations of double neutron star merger. In the context of SHBs these simulations show that the general relativistic picture may be more complicated than the Newtonian one. [Oechslin & Janka \(2006\)](#) use a relativistic SPH code with conformally flat approximation of the Einstein field equations and a realistic EOS. For a range of initial conditions they find results that are rather similar to those of Newtonian simulations - a central object with a surrounding disk at a radius of tens of km with a mass $0.06-0.26M_{\odot}$. Shibata and collaborators ([Shibata, Taniguchi & Uryū, 2005](#); [Shibata & Taniguchi, 2006](#)) carried out a full general relativity simulation with a hybrid EOS that mimics a realistic stiff nuclear EOS. They find that depending on the initial mass of the system, the merger can proceed in two ways: (i) If the total mass is below some threshold ($\lesssim 2.6M_{\odot}$ depending on the EOS) a hypermassive neutron star is formed at first (a NS that is supported by differential rotation; [Baumgarte, Shapiro & Shibata, 2000](#)). If this hypermassive neutron star collapses to a black hole after a sufficient delay so it can transport angular momentum to the surrounding matter, then the mass of the remaining disk is $\gtrsim 0.01M_{\odot}$, independent of the initial NS mass ratio. Adding magnetic fields, [Shibata et al. \(2006\)](#) carry out a full GR magneto-hydrodynamic simulation of the final stages of the merger starting with a hypermassive NS as initial conditions (see also [Duez et al. , 2006](#)). They find that magnetic breaking and magnetorotational instability transfer angular momentum very efficiently and as a result a disk of $\sim 0.05M_{\odot}$ is formed by the time that the NS collapses to a BH. (ii) On the other hand, if the total mass of the system is above the threshold, the central object collapses promptly (in less than 1 ms) into a black hole, taking with it most of the mass and leaving a very small disk. A massive enough disk to be a possible SHB central engine ($\sim 0.01M_{\odot}$) is left only in cases where the mass of the two progenitor neutron stars is significantly different (mass ratio $\lesssim 0.8$), contrary to the results of [Oechslin & Janka \(2006\)](#). [Shibata & Taniguchi \(2006\)](#) suggest that the most likely reason for this difference is the approximations made by [Oechslin & Janka \(2006\)](#), that do not take into account gravitational waves radiation reaction. In the simulation by [Shibata & Taniguchi \(2006\)](#), GW radiation is one of the main channels through which the central object loses angular momentum and ultimately collapses.

I.II Forming an accretion disk in a NS-BH merger

The outcome of a NS-BH merger is less clear. The most important initial condition affecting the coalescence evolution is the mass ratio $q \equiv M_{NS}/M_{BH}$. If $q \ll 0.1$ the tidal disruption radius of the NS is within the innermost stable circular orbit, for any BH spin, and the NS plunges into the BH without leaving any residual disk (e.g., [Vallisneri, 2000](#); [Miller, 2005](#); [Rosswog, 2005](#); [Faber et al. , 2006a](#)). As I describe below, the fate of systems with $q \gtrsim 0.1$ seems more promising as SHB progenitor, but the outcome of this case is not entirely known yet.

Numerous numerical simulations of NS-BH coalescence were carried out using

Newtonian potentials. The main result of these simulations is that the formation of the disk depends strongly on the NS equation of state (EOS). In the case of soft equation of state (polytropes with $\Gamma \leq 2.5$ or Lattimer and Swesty EOS; [Lattimer & Swesty 1991](#)) the NS is tidally disrupted during its first approach, forming a massive disk ($\sim 0.3M_{\odot}$; [Janka *et al.*, 1999](#); [Lee & Kluźniak, 1999b](#); [Lee, 2000, 2001](#)). A more complex evolution is found in the case of a stiff EOS (Shen EOS [[Shen *et al.* 1998](#)] or a polytrope with $\Gamma = 3$; [Kluźniak & Lee 1998](#); [Lee & Kluźniak 1999a](#); [Lee 2000](#); [Rosswog, Speith & Wynn 2004](#)), as seems to be required by the highest measured pulsar mass $M = 2.1 \pm 0.2M_{\odot}$ ([Nice *et al.*, 2005](#)). These simulations show that a “stiff” NS is not disrupted during the first episode of mass transfer. Instead, in some cases, it bounces back into an eccentric orbit and the mass transfer resumes only after additional angular momentum is lost to gravitational wave radiation. The result is an episodic mass transfer process that lasts much longer than the duration of the simulations (massive disks are not formed before the simulations end). Based on these results, [Davies, Levan & King \(2005\)](#) developed a semi-analytic model of intermittent mass transfer, finding that the NS is disrupted after ~ 1 s, leaving a $\sim 0.1M_{\odot}$ disk.

While newtonian simulations seem to give a qualitatively correct picture of the dynamics in at least some of the NS-NS merger scenarios, it is not clear at all that they are applicable also in the case of NS-BH coalescence. An important general relativistic (GR) feature which is not treated by Newtonian simulations is the innermost stable circular orbit (ISCO). [Miller \(2005\)](#) argues that the NS tidal radius may be within the ISCO not only in the case of low q , but also in the case of comparable NS and BH masses. The reason is that for $q \gtrsim 0.25$ the mass of the NS itself begins to affect, increasing the the ISCO radius (compared to an isolated BH; e.g., [Buonanno & Damour, 1999](#)). For $q > 0.5$, even in the case of a maximally spinning BH, the tidal radius may be within the ISCO. Moreover, [Miller \(2005\)](#) suggests that even in cases where the tidal radius is slightly outside of the ISCO, GR effects can cause the NS to plunge directly into the BH without leaving a disk.

The most advanced numerical simulation of a NS-BH merger to date were presented by [Faber *et al.* \(2006a,b\)](#), that use the conformal flatness approximation for GR for a Schwarzschild³¹ BH and a polytropic EOS with $\Gamma = 2$ for the NS (no simulations were carried out for stiffer EOS). First, they carry out a simulation with $q = 0.1$ and find that indeed the NS is ‘swallowed’ by the BH without being disrupted. Then they perform a simulation in which the tidal radius is comparable to the ISCO (equivalent to $q=0.24$ for their NS modeling³²). Here they find that instead of a direct plunge, angular momen-

³¹ This approximation is exact for spherically symmetric potentials and is less appropriate for a Kerr BH.

³² As a result of the conformal flatness approximation [Faber *et al.* \(2006a\)](#) use

tum transfer during tidal disruption deposits 1/4 of the NS mass back outside the ISCO. Half of this mass becomes unbound and leaves the system, while the rest, $\approx 0.15M_\odot$, remains bound. Interestingly, only a fraction of the bound matter forms a hot and dense disk that is ready to perform as a SHB central engine. The remaining bounded mass, $\approx 0.05M_\odot$, is ejected to eccentric orbits and should fall back toward the BH after more than a second. At the end of the simulation the polar axis is not significantly polluted by baryons. These results are promising, however, BH spin is expected to play an important role in the dynamics of systems with $0.1 \lesssim q \lesssim 0.5$, so the final answer about their fate will require a full GR simulation.

I.III The accretion rate and the lifetime of the disk

Regardless of the initial progenitor (NS-NS or NS-BH binary) the SHB central engine in this model is a hot and dense torus of $0.01 - 0.3M_\odot$ that is accreted onto a stellar mass BH. The engine is active as long as efficient accretion takes place. Assuming that the burst is powered by accretion, the accretion rate can be estimated using energy requirements. The observed isotropic equivalent luminosity of SHBs is $10^{50} - 10^{52}$ erg/s. Correcting for beaming, the true luminosity is probably smaller by about one, or at most two, orders of magnitude. Taking a reasonable efficiency of accretion energy conversion into gamma-rays of $\sim 0.01 - 1\%$ (see below) implies hyper-accretion rates of $0.01 - 10M_\odot/s$. Are such accretion rates expected for a typical disk that is formed by a compact binary merger?

The accretion rate and the lifetime of the disk in this scenario was first estimated analytically and semi-analytically (Popham, Woosley & Fryer, 1999; Narayan, Piran & Kumar, 2001; Di Matteo, Perna & Narayan, 2002). The amount of energy emitted during the burst implies that the disk must be accreted efficiently (i.e, most of the disk mass must be accreted and not expelled as a wind). Efficient accretion requires efficient cooling, which at these densities can be achieved only by neutrinos. For this to occur, the temperatures and the densities in the disk should be high enough, which in turn implies that the radius of the disk should be small enough. Narayan, Piran & Kumar (2001) present an analytic approximation that is valid assuming that the disk is optically thin to neutrinos. They find that in order for efficient neutrino cooling to take place, the radius in which the disk is deposited must satisfy:

$$R_d < 44R_s \left(\frac{\alpha}{0.1}\right)^{-2/7} \left(\frac{M_{BH}}{3M_\odot}\right)^{-1} \left(\frac{M_d}{0.1M_\odot}\right)^{3/7}, \quad (44)$$

where R_s is the Schwarzschild radius of a central BH with mass M_{BH} , M_d is the disk mass and α is dimensionless viscosity parameter (Shakura & Sunyaev, 1973). As discussed above, the disk that is apparently formed in NS-NS and

q=0.1 while changing the neutron star compactness (M_{NS}/R_{NS}) in order to imitate a q=0.24 case.

NS-BH mergers satisfies this criterion³³. For a disk which is within this radius Narayan, Piran & Kumar (2001) find an accretion rate of:

$$\dot{M}_{acc} = 0.6 \left(\frac{\alpha}{0.1}\right) \left(\frac{M_{BH}}{3M_{\odot}}\right)^{-13/7} \left(\frac{M_d}{0.1M_{\odot}}\right)^{9/7} \left(\frac{R_d}{10R_s}\right)^{-3/2} M_{\odot}/s, \quad (45)$$

and a corresponding disk lifetime of

$$t_{acc} = 0.2 \left(\frac{\alpha}{0.1}\right)^{-1} \left(\frac{M_{BH}}{3M_{\odot}}\right)^{13/7} \left(\frac{M_d}{0.1M_{\odot}}\right)^{-2/7} \left(\frac{R_d}{10R_s}\right)^{3/2} s. \quad (46)$$

Note that the accretion time is set by the viscous time scale and is linear with $1/\alpha$, which is the least constrained parameter in the problem. These equations assume that the disk is optically thin to its own neutrino emission, which for the expected accretion rates is valid for $R \gtrsim 10R_s$ (Di Matteo, Perna & Narayan, 2002). A semi-analytic extension of this model to the optically thick regime was carried out by Di Matteo, Perna & Narayan (2002) and a further semi-analytic calculations of the the disk properties evolution in time is presented by Janiuk *et al.* (2004). Considerations of the strong magnetic fields that might be present in hyper-accreting disk as well as observable quantum electrodynamical effects arising from supercritical fields are discussed by Kohri & Mineshige (2002). Finally, General Relativistic effects of Kerr metric on the structure of the accretion disk are calculated by Chen & Beloborodov (2006).

A number of detailed numerical simulations in 2D (Lee & Ramirez-Ruiz, 2002; Lee, Ramirez-Ruiz & Page, 2004, 2005) and 3D (Setiawan, Ruffert & Janka, 2004) follow the evolution of the disk during its accretion. The latest simulations include detailed equation of state, approximate neutrino treatment and a viscosity described by an α -law. These simulations provide insights about the neutrino luminosity of the disk (see below) and they are in rough agreement with analytic calculations of the accretion rate and duration.

As discussed in §3.4, the burst duration is most likely comparable to, (e.g., Kobayashi, Piran & Sari, 1997), or at most larger by an order of magnitude than (Janka *et al.*, 2005; Aloy & Rezzolla, 2006), the duration of the engine activity. Hence, for a typical value of $\alpha = 0.1$ the accretion rate as well as the burst duration nicely agree with those required for SHBs. However, late engine activity, which is suggested by the observations (see §4.7 and §4.8), is not naturally explained in this model.

Several processes have been suggested to explain prolonged accretion that lasts longer than the viscous time scale. van Putten & Ostriker 2001 (see also van

³³ Mergers of a BH with less compact objects such as white dwarfs or helium stars do not satisfy this criterion and therefore are unlikely to produce long or short GRBs (Narayan, Piran & Kumar, 2001).

Putten & Levinson 2001, 2002, 2003; van Putten 2005) suggest a configuration in which the accretion is temporarily suspended due to a “magnetic wall” around a rapidly spinning black hole. This model was originally proposed for long GRBs, but it may be viable during the post-merger conditions of a compact binary, and explain long-lasting emission. In this model, the jet is energized by the spin of the BH and the accretion is suspended as long as the BH is rapidly spinning (tens of seconds for a $2.5M_{\odot}$ BH and a $0.1M_{\odot}$ disk). Proga & Zhang (2006) suggest a different scenario in which magnetic flux can be accumulated near the black hole and behave as an alternating barrier, that allows for intermittent accretion, thereby increasing the accretion time. Perna, Armitage & Zhang (2006) suggest that instabilities in the disk may cause fragmentation of the outer parts of the disk, producing separate blobs which slowly inspiral toward the black hole, producing late engine activity. Yet another possibility is that during the time that the disk is formed, some of the material is ejected into an eccentric, but bound, orbit and falls back into the BH after the disk was accreted. Such behavior is seen in the NS-BH simulation of Faber *et al.* (2006a) and may take place also during NS-NS coalescence, where some simulations show that $\sim 10^{-2}M_{\odot}$ are ejected from the system (e.g., Rosswog *et al.*, 1999; Ruffert & Janka, 2001).

I.IV Launching the jet

Two classes of processes were suggested to extract the energy of an accretion disk-black hole system and launch a relativistic jet: neutrino-anti neutrino annihilation and magnetically driven mechanisms.

I.IV.I Neutrino driven jet

In neutrino-cooled accretion disks, a significant fraction of the disk gravitational energy is converted during the accretion into neutrino flux. This energy is available to launch a jet through $\nu\bar{\nu}$ annihilation and subsequent pair production. The possible importance of neutrino annihilation as the energy source of GRB jets was recognized by many authors (e.g., Goodman, Dar & Nussinov, 1987; Eichler *et al.*, 1989; Narayan, Paczynski & Piran, 1992; Mészáros & Rees, 1992; Mochkovitch *et al.*, 1993, 1995; Witt *et al.*, 1994; Jaroszynski, 1993, 1996). While neutrinos are generated in various sites during the merger (e.g., Salmonson & Wilson, 2001), the most promising process for energy extraction is by neutrinos emitted from the cooling torus. This emission lasts long enough to power the jet and is originates far enough from the black hole so it is not strongly affected by gravitational capture or redshift of the black hole (see Asano & Fukuyama, 2000, 2001, for a discussion of gravitational effects). Moreover, the geometry of the torus implies that the most efficient annihilation sites are along the rotation axis, which also suffer the least from baryon pollution. Therefore, most numerical simulations of these systems (Ruffert *et al.*, 1997; Ruffert & Janka, 1998, 1999; Fryer *et al.*, 1999; Rosswog & Ramirez-Ruiz, 2002; Rosswog & Liebendörfer, 2003; Rosswog & Ramirez-Ruiz, 2003; Rosswog, Ramirez-Ruiz & Davies, 2003; Lee & Ramirez-

Ruiz, 2002; Lee, Ramirez-Ruiz & Page, 2004, 2005; Setiawan, Ruffert & Janka, 2004), as well as semi-analytic calculations (Popham, Woosley & Fryer, 1999; Di Matteo, Perna & Narayan, 2002; Janiuk *et al.*, 2004), were used to estimate the energy deposited by neutrinos emitted from the disk.

The energy extraction efficiency is defined as the fraction of the rest mass energy of accreted matter that is converted into pairs by $\nu\bar{\nu}$ annihilation $\epsilon_{\nu\bar{\nu}} \equiv L_{\nu\bar{\nu}}/\dot{M}c^2$ (most of the annihilation takes place along the rotation axis, where baryonic pollution is low). This efficiency is a combination of the fraction of the rest mass energy that is emitted by neutrinos, $f_{\dot{M}\rightarrow L\nu} \equiv L_{\nu}/\dot{M}c^2$, and the fraction of neutrino energy that annihilates into e^+e^- pairs, $f_{L\nu\rightarrow L\nu\bar{\nu}} \equiv L_{\nu\bar{\nu}}/L_{\nu}$. The total efficiency depends on the accretion rate. At low accretion rates ($\dot{M} < 0.1M_{\odot}/s$) the neutrino luminosity drops fast and the annihilation rate (which is proportional to the luminosity square) drops even faster. Therefore, at these accretion rates the total efficiency is very low, $\ll 10^{-4}$ (Popham, Woosley & Fryer, 1999; Setiawan, Ruffert & Janka, 2004). On the other hand, disks with accretion rates that are too high ($\dot{M} \gg 0.1M_{\odot}/s$) are optically thick, and most of the generated neutrinos are advected into the BH, thereby reducing $f_{\dot{M}\rightarrow L\nu}$ while $f_{L\nu\rightarrow L\nu\bar{\nu}}$ remains roughly constant (Di Matteo, Perna & Narayan, 2002). Maximal efficiency is obtained at $\dot{M} \sim 1M_{\odot}/s$ where $f_{\dot{M}\rightarrow L\nu} \sim 0.01 - 0.1$ and $f_{L\nu\rightarrow L\nu\bar{\nu}} \sim 10^{-3} - 10^{-2}$ (e.g., Di Matteo, Perna & Narayan, 2002). Therefore, the total efficiency of neutrino annihilation under optimal conditions is $\epsilon_{\nu\bar{\nu}} \sim 10^{-4}$. In the context of SHB central engine this optimal accretion rate is also the expected one, implying that the total energy that can be expected from this process is $\sim 10^{49}(M_d/0.1M_{\odot})$ erg where M_d is the disk mass. This energy is enough to power luminous SHBs (e.g., SHB 051221) only if their flow is narrowly collimated³⁴ and less luminous SHBs (e.g., SHB 050509B) also if they are not narrowly beamed. Current limits on the total energy of SHBs (Table 2) are still compatible with this model, but future observations may require higher energy. Ramirez-Ruiz & Socrates (2005) suggest the existence a hot corona that modifies the spectrum of the emitted neutrinos as a way to significantly increase $f_{L\nu\rightarrow L\nu\bar{\nu}}$.

I.IV.II Magnetically driven jet

An alternative method to launch relativistic jets from the BH-accretion disk system is via strong electromagnetic fields (e.g., Narayan, Paczynski & Piran, 1992; Levinson & Eichler, 1993; Thompson, 1994; Ruffert *et al.*, 1997; Mészáros & Rees, 1997b; Lee, Wijers & Brown, 2000; Brown *et al.*, 2000b; Rosswog & Ramirez-Ruiz, 2002; Rosswog, Ramirez-Ruiz & Davies, 2003; Daigne & Mochkovitch, 2002a; Lyutikov, 2006). Even if the initial magnetic field is low, it is expected to play an important role due to amplification by the magneto-rotational instability (for review of MHD accretion disks see Bal-

³⁴ Possible mechanical collimation processes are discussed and simulated by Rosswog & Ramirez-Ruiz (2002) and by Janka *et al.* (2005)

bus & Hawley, 1998). An extensive numerical effort is invested in systems of magnetized accretion onto BH, with rapid progress from simulations that use newtonian and pseudo-Newtonian potentials (e.g., Hawley, 2000; Hawley & Krolik, 2002; Hawley & Balbus, 2002; Armitage, Reynolds & Chiang, 2001; Armitage & Reynolds, 2003; Proga, 2003; Proga & Begelman, 2003; Machida & Matsumoto, 2003; Kato, Mineshige & Shibata, 2004) to GR simulations using a Kerr metric in two dimensions (McKinney & Gammie, 2004; McKinney, 2005, 2006) and in three dimensions (De Villiers, Hawley & Krolik, 2003; De Villiers *et al.*, 2005; Hirose *et al.*, 2004; Krolik, Hawley & Hirose, 2005; Hawley & Krolik, 2006). Currently, these simulations do not include neutrino physics and use simple equation of state (a constant adiabatic index of 4/3 or 5/3 is assumed) and therefore the results may not be directly applicable to the case of SHBs. Nevertheless, magnetic fields most likely play important, and maybe the major, role in jet launching. Different GRMHD simulations show a qualitatively similar picture. An accretion flow is generated within the disk by magnetic viscosity that results from amplification of the magnetic field by the magnetorotational instability (Balbus & Hawley, 1991) even if it is initially weak. The accretion results in a strong wind of magnetized plasma which is ejected from the system along the boundaries of the centrifugally evacuated funnel, and a strong Poynting flux jet is observed within the funnel. The baryonic load within the Poynting-flux-dominated funnel is low enough to allow a terminal Lorentz factor > 100 (McKinney, 2006).

Recent GRMHD simulations find that the energy of Poynting flux jets is directly related the spin of the BH and is in general agreement with the predictions of Blandford & Znajek 1977³⁵ (McKinney & Gammie, 2004; McKinney, 2005; Hawley & Krolik, 2006, see also Komissarov 2004, 2005). Energy output in Poynting flux jets increases sharply with the spin of the BH, and this process can be far more efficient than a neutrino-driven jet. Hawley & Krolik (2006) find efficiencies $\epsilon_{em} = 3 \cdot 10^{-4}, 6 \cdot 10^{-3}, 0.04$ & 0.2 for spin parameters $a/M = 0, 0.5, 0.9$ & 0.99 correspondingly ($\epsilon_{em} \equiv L_{em}/\dot{M}c^2$ where L_{em} is the luminosity of the Poynting flux jet and $a/M \equiv Jc/GM_{BH}^2$ where J is the BH angular momentum and G is the gravitational constant). McKinney (2006) simulates an accretion on a BH with a spinning parameter $a/M = 0.9375$ and finds an outflow efficiency of $\epsilon_{em} \approx 0.05$ where 10% of the jet luminosity is spread roughly uniformly within an opening angle of 0.1 rad around the polar axis. Taking an accretion disk of $0.1M_{\odot}$, this ϵ_{em} corresponds to a total emitted energy of $\approx 10^{52}$ erg out of which 10^{51} erg are within 0.1 rad of the jet axis. An observer with a viewing angle within 0.1 rad of the jet axis will infer a total isotropic equivalent energy of $\approx 10^{53}$ erg. Therefore, this process, if applicable, can easily account for the energetics and the Lorentz factors observed in SHBs.

³⁵ For a discussion of the similarities and the differences between the simulations and the BZ mechanism see Hawley & Krolik (2006).

II. Hypermagnetized neutron stars

An interesting alternative GRB engine is a compact object with an ultra-high magnetic field ($\gg 10^{15}$ G). Here, it is the energy of the magnetic field and/or the star rotation that drives a relativistic outflow, and there is no need for an accompanying accretion disk. Such a magnetized object can be a transient hypermassive NS that is formed by the coalescence of two neutron stars (Kluźniak & Lee, 1998; Rosswog & Davies, 2002; Rosswog & Ramirez-Ruiz, 2002; Rosswog, Ramirez-Ruiz & Davies, 2003; Shibata *et al.*, 2006; Duez *et al.*, 2006). Price & Rosswog (2006) carry out an MHD simulation of the merger of two neutron stars with initial magnetic fields of 10^{12} G. They find that on very short timescales (~ 1 ms) a magnetic field $> 10^{15}$ G is generated by the Kelvin-Helmholtz instability along the shear interface that forms where the two neutron stars come into contact. This field strength is clearly limited by the resolution of the simulations and therefore the actual generated field is most likely much higher. An upper limit on the field strength is the equipartition level $\sim 10^{17}$ G. If the hypermagnetized hypermassive neutron star is stable for ~ 0.1 s, as suggested by the results of Shibata & Taniguchi (2006), then the energy in the magnetic field can drive a relativistic outflow in various ways. Price & Rosswog (2006) suggest that bubbles of equipartition magnetic field can become buoyant and float up through the star surface producing a relativistic flow (Kluźniak & Lee, 1998; Lyutikov, 2003; Dai *et al.*, 2006). If a large scale field is built up then an alternative launching mechanism is the magneto-centrifugal slinging (Usov, 1992; Thompson, Chang & Quataert, 2004; Thompson, 2005). The emission time scale is the spin-down time of the star (assuming that it does not collapse first), which is ~ 0.1 s in the case of a 10^{17} G magnetic field (the initial spin of the hypermassive NS is ~ 1 ms). Since the energy source of this engine is the magnetic field and/or the rotation of the transient neutron star ($\sim 10^{53}$ erg), it can in principle produce very energetic bursts with more than 10^{51} erg. Rapidly rotating hyper-magnetized neutron star (i.e., msec magnetar) may be produced also by other progenitor systems and it is discussed in some more detail in §5.3.2

5.2.2 The lifetime of compact binaries and their merger rate

The merger rate and typical lifetime of NS-NS binaries are estimated in two ways, based on observed systems in our Galaxy and using theoretical population synthesis. In the case of NS-BH binaries only the latter method is used, as no observed systems of this kind are currently known³⁶. These aspects of compact binaries are covered in detail by other papers in this volume and therefore I will briefly review here only the main results of each method.

³⁶ The fact that no NS-BH systems are observed is not surprising given that binary detection requires a recycled pulsar, and that the birth rate of BH-recycled pulsar binaries is expected to be very low (Pfahl, Podsiadlowski & Rappaport, 2005).

I. Constraints from observed systems in the Milky Way

This method is based on counting observed NS-NS binaries in our Galaxy, and then deducing the Galactic merger rate by correcting for the completeness of the surveys and the estimated lifetime of each system (from the second supernova till the coalescence). The cosmological local rate is then derived by extrapolating the Galactic rate to a cosmological volume. The main advantage of this methods is that it is based on solid observations. As such it provides a robust lower limit on the total merger rate. The main disadvantage of this method is that it is possible that there are binary populations that cannot be detected by current surveys. For example currently detection of NS-NS binaries depends on at least one of the companions being a recycled pulsar. Therefore, it is insensitive to formation channels that do not recycle any of the pulsars, if such exist. The extrapolation from the Galactic rate to the cosmological one is also not trivial since it is not clear what is the right indicator which should be used for such an extrapolation (e.g., blue light?). Finally, the sample is small – there are only three NS-NS binaries that are used in order to estimate the Galactic rate - PSR B1913+16, PSR B1534+12, PSR J0737–3039³⁷.

The first calculations of the Galactic merger rate (Phinney, 1991; Narayan, Piran & Shemi, 1991) were of the order of $10^{-6} - 10^{-5} \text{ yr}^{-1}$, where the uncertainty was dominated by uncertain beaming correction and survey selection effects. More detailed calculations that followed obtained similar values (Curran & Lorimer, 1995; van den Heuvel & Lorimer, 1996; Arzoumanian, Cordes & Wasserman, 1999). Kalogera *et al.* (2001) carried out detailed investigation of the uncertainties in these rate estimates and found that the uncertainty in the correction for undetected faint systems can span over two orders of magnitude. With two NS-NS systems observed, PSR B1913+16 and PSR B1534+12, they estimate a rate of $\sim 10^{-6} \text{ yr}^{-1}$ when only the beaming corrections is included. Considering the correction for faint undetected pulsars, they estimate that the rate can be as high as $5 \times 10^{-4} \text{ yr}^{-1}$. Later, Kalogera, Kim & Lorimer (2003) developed a method to assign statistical significance to these estimates. They find a merger rate of $8_{-5}^{+9} \times 10^{-6} \text{ yr}^{-1}$ (68% confidence). The subsequent discovery of the relativistic binary pulsar PSR J0737–3039 (Burgay *et al.*, 2003) increased the number of systems used for rate estimation to three. The corresponding range of Galactic merger rates becomes between 1.7×10^{-5} to $2.9 \times 10^{-4} \text{ yr}^{-1}$ at 95% confidence (Kalogera *et al.*, 2004), increasing the most likely estimated rate by a factor of 6-7. This significant revision in the rate is due to the unique properties of PSR J0737–3039 (short lifetime, 2.4hr period orbit and different beam profile) that make it difficult to detect.

³⁷ Other observed NS-NS systems will not merge within the Hubble time and therefore are irrelevant for this method. The only exception, PSR B2127+11C, is excluded because of its association with a globular cluster (Anderson *et al.*, 1990; Prince *et al.*, 1991).

The extrapolation of the galactic rate to the local cosmological rate is usually done assuming that the merger rate is proportional to the blue stellar luminosity. [Phinney \(1991\)](#) obtains a conversion factor of 10^7 Gpc^{-3} . Using a similar conversion factor the most updated estimate of the local universe merger rate is $200 - 3000 \text{ Gpc}^{-3}\text{yr}^{-1}$ ([Kalogera *et al.*, 2004](#)).

The merger rate derived based on the observed Galactic sources is dominated by PSR J0737–3039, which is short-lived ($\approx 100 \text{ Myr}$). Therefore, this method predicts that the lifetime distribution of NS-NS binaries is dominated by rather short lived-systems ($\ll 1 \text{ Gyr}$). The fact that there are observed systems with lifetimes that are comparable the Hubble time or longer, implies that the observed systems lifetime distribution is broad.

II. Constraints from population syntheses

An alternative approach to evaluate the NS-NS merger rate – and the only current mean to evaluate the NS-BH merger rate – is via population synthesis (e.g., [Tutukov & Yungelson, 1994](#); [Brown, 1995](#); [Lipunov *et al.*, 1995](#); [Portegies Zwart & Spreeuw, 1996](#); [Portegies Zwart & Yungelson, 1998](#); [Bethe & Brown, 1998](#); [Fryer, Burrows & Benz, 1998](#); [Fryer, Woosley & Hartmann, 1999](#); [Bloom, Sigurdsson & Pols, 1999](#); [Belczyński & Bulik, 1999](#); [Brown *et al.*, 2000a](#); [Belczyński & Kalogera, 2001](#); [Belczynski, Bulik & Kalogera, 2002](#); [Belczynski, Bulik & Rudak, 2002](#); [Belczynski, Kalogera & Bulik, 2002](#); [Perna & Belczynski, 2002](#); [O’Shaughnessy, Kalogera & Belczynski, 2005](#); [O’Shaughnessy *et al.*, 2005](#); [de Freitas Pacheco *et al.*, 2006](#); [Dewi, Podsiadlowski & Sena, 2006](#)). The evolution of a binary is followed as a function of the initial binary properties (e.g., the zero age main sequence [ZAMS] mass of the two companions and the initial orbital separation). The advantage of this method is that it can be used to explore binary systems that cannot be observed, such as non-recycled NS-NS or NS-BH binaries. The main disadvantage of the method is that the uncertainties involved are substantial (e.g., the supernova kick distribution, common envelope evolution, etc.). As a result, the rate estimates span over two orders of magnitude, which include the range inferred from observed Galactic binaries.

An interesting outcome of this research is the suggestion by [Belczyński & Kalogera \(2001\)](#) that a formation channel of very short-lived, practically unobservable, NS-NS binaries exists. Including this channel in their most updated population synthesis code, [Belczynski *et al.* \(2005, 2006\)](#) find that the distribution of the time that the binary spends as two neutron stars, from the second supernova until coalescence, is bimodal with one peak at $\sim 10^5 \text{ yr}$ and another at $\sim 10^{10} \text{ yr}$. When the time between the formation of main sequence stars and the two supernovae is added, the lifetime distribution (from star-formation till death), $f(\tau)$, becomes flat in log space ($f(\tau) \propto \tau^{-1}$ in the notation of §5.1) with a cutoff below 10 Myr . They obtain a rather similar

lifetime distribution also for NS-BH binaries.

An alternative formation channel of NS-NS binaries is by exchange interactions in globular clusters (as in the case of PSR B2127+11C that is associated with M15). The number of NS-NS binaries that are formed by this process is expected to be significantly smaller than the number of binaries that are formed through binary evolution (e.g., [Phinney, 1991](#)). [Grindlay, Portegies Zwart & McMillan \(2006\)](#) estimate a Galactic merger rate in globular clusters of $\sim 4 \cdot 10^{-8} \text{ yr}^{-1}$ which corresponds to a cosmological local rate of $\sim 2 \text{ Gpc}^{-3} \text{ yr}^{-1}$. This rate is indeed much smaller than the estimates based on the observed systems that are not associated with globular clusters. [Hopman *et al.* \(2006\)](#) evaluate the lifetime distribution function of binaries that form in globular clusters and find that it is dominated by old systems with an average life time of $\approx 6 \text{ Gyr}$.

Estimates of the rate of NS-BH mergers vary by orders of magnitude, and so does the ratio between the NS-NS merger rate and the NS-BH merger rate. Two major open questions that determine if a NS collapses into BH during the binary evolution, and thus strongly affect the ratio between NS-NS and NS-BH binaries, is the accretion rate of a NS during common envelope phase and the maximal mass of a NS. The interesting work by [Bethe & Brown \(1998\)](#) suggests that the mergers of low-mass BH and NS should be more common than NS-NS mergers (see also [Chevalier, 1993](#); [Brown, 1995](#); [Wettig & Brown, 1996](#); [Bethe, Brown & Lee, 2005a,b](#)), since the first neutron star cannot survive a common envelope phase and it collapses into a BH following hypercritical accretion from the companion envelope. They suggest that the only way to avoid this outcome is by having two companions with similar masses (ZAMS masses no more than 4% apart) so they get into the helium burning phase at a similar time, thereby avoiding vigorous mass accretion during a common envelope phase. Using a Salpeter initial mass function ([Salpeter, 1955](#)) they find that the rate of NS-BH mergers is 20 times the rate of NS-NS mergers. This ratio is reduced to a factor of 5 when a flat initial mass function (constant dn/dM) is considered ([Lee, Brown & Park, 2006](#)). The mean lifetime of a NS-BH binary in this scenario is $\approx 5 \text{ Gyr}$ and the predicted rate (normalized to the supernova rate at a redshift of ≈ 0.7) is $\sim 10^4 \text{ Gpc}^{-3} \text{ yr}^{-1}$ ([Bethe, Brown & Lee, 2007](#), this volume).

Finally, population synthesis can be used to put an upper limit on the local rate of NS-NS and NS-BH mergers, by evaluating the fraction of binaries that survive both supernovae. This fraction depends mostly on the distribution of the supernova kick velocity, which is not well constrained. Several works show that this fraction of surviving binaries is unlikely to exceed 2% (e.g., [Pfahl *et al.*, 2002](#); [Lipunov, Postnov & Prokhorov, 1997](#)). Taking this fraction from the local rate of core-collapse SNe ([Cappellaro, Evans & Turatto, 1999](#)) implies an upper limit of $\sim 1000 \text{ Gpc}^{-3} \text{ yr}^{-1}$ on the merger rate of short-lived

binaries ($\tau \lesssim 1$ Gyr). An upper limit of $10^4 \text{ Gpc}^{-3} \text{ yr}^{-1}$ on the local merger rate of long-lived binaries ($\tau \gtrsim 4$ Gyr) is obtained by relating it to the rate of core-collapse SNe at redshift 0.7 (Dahlen *et al.*, 2004). Therefore, if SHBs are mergers of compact binaries, then from Eq. 42, the SHB-merger rate must be in the range:

$$10 \lesssim \mathcal{R}_{SHB=merger} \lesssim 10^4 \text{ Gpc}^{-3} \text{ yr}^{-1}. \quad (47)$$

5.2.3 Offsets from host galaxies and external medium densities

An important clue about the nature of the progenitors is the location of the bursts with respect to their host galaxies. The offset of the merger site of a NS-NS or NS-BH binary from its birth place was explored by several groups (Fryer, Woosley & Hartmann, 1999; Bloom, Sigurdsson & Pols, 1999; Perna & Belczynski, 2002; Belczynski *et al.*, 2006). This location depends on the natal kick of the progenitor system and the time between the kick and the merger, as well as the galactic gravitational potential. In the case of compact binaries the natal kick is expected to be between several tens to several hundreds km/s (e.g., Hobbs *et al.*, 2005) and different models of binary formation channels predict a wide duration range between the second SN and the merger (e.g., Belczynski *et al.*, 2006). A binary with an inspiral time of several Gyr born with a kick of several hundred km/s, can merge after traveling 1 Mpc, while a binary that merges within 1 Myr will always end up near its birth place. Similarly, binaries with moderate kick velocity are expected to be bound to large galaxies but not to small ones, and therefore offsets from larger galaxies are expected to be smaller. Thus, in principle, mergers can take place at any distance ($\lesssim 1$ Mpc) from their hosts, and the predicted merger distribution depends on the specific binary model considered. Belczynski *et al.* (2006) find that for their model of bimodal inspiral time distribution, the offset from highly star-forming galaxies is very small (since the merger rate is dominated by the short inspiral time population). The offset from elliptical galaxies, in which only long-lived binaries merge, is expected to be large. The typical offset from a small [giant] elliptical is about 100 [10] kpc.

The circum-burst gas density depends of course on the offset. If the merger site is outside of a field host, in the inter-galactic medium (IGM), the density is expected to be $\sim 10^{-6} \text{ cm}^{-3}$. If, on the other hand, the merger takes place within its host galaxy or in the intra-cluster medium of a galaxy cluster (ICM) the density is expected to be $> 10^{-3} \text{ cm}^{-3}$. Since the brightness of the afterglow depends on the external density (§4), afterglows of bursts with large offsets should be fainter. For example, Belczynski *et al.* (2006) present the distribution of external densities of merger sites predicted by their model for different types of hosts. They find that the lowest densities are expected for binaries that are born in small early-type galaxies, while the highest densities are found for those that are born in large star-forming galaxies.

If compact binary mergers lead to SHBs then this behavior predicts a strong selection effect that biases the observed redshift and host-type distributions. The reason is that it is very hard to detect the afterglow of a burst that takes place at a large distance from its host and even if an afterglow of such a burst is detected, it is unlikely that a host association will be secure, and therefore the SHB redshift, can be determined. As a result, a bias is expected favoring bursts with short-lived progenitors, implying higher redshifts and late-type hosts. Similarly, a bias is expected in favor early-type cluster galaxies over early-type field galaxies.

5.2.4 Comparison with the observations

The most rudimentary predictions of NS-NS and NS-BH mergers fit the SHB observations well: (i) These mergers must take place at a rate that is comparable to the SHB rate (Eq. 42). (ii) The gravitational binding energy that is liberated in these mergers is more than enough to power the observed prompt emission and afterglow. Moreover, extensive numerical and theoretical work suggests several very plausible processes to channel enough of this energy into a relativistic outflow. (iii) The duration of SHBs is explained in a rather natural way in these models, while the engine size is compact enough to allow for the observed rapid variability during the prompt emission. Following recent observations, several papers have shown that the energy and the timescales of specific events with known redshifts can be explained within the framework of the merger model (Lee, Ramirez-Ruiz & Granot, 2005; Oechslin & Janka, 2006). (iv) The most popular engine model in this scenario, hyper-accretion onto a black hole, is similar to the engine suggested for long GRBs, naturally explaining the similarity between the two phenomena. (v) SHBs do not trace the star formation, and they take place in both early- and late-type galaxies, as expected for compact binary mergers. (vi) Many SHBs are observed at low redshifts (~ 0.2) while there are indications of a population of SHBs at higher redshift (~ 1). This result indicates on a wide lifetime distribution, as some papers predict for compact binary mergers (e.g., Belczynski *et al.*, 2006). (vii) Observations suggest that some of the bursts take place in very low densities and at large offsets from their hosts, as predicted for a binary population with strong natal kicks and long lifetimes.

A more detailed comparison of this model to the observations reveals that there are also some conflicts and issues that should still be resolved between the model and the observations. The growing amount of evidence suggesting that the central engine is active for a duration that is much longer than the duration of the initial hard prompt gamma-ray emission is a major challenge to the merger model (e.g., the late flare in SHB 050709). Here, the natural engine activity time scale that the merger model predicts ($\lesssim 1$ s) is an obstacle. Nevertheless, several extensions and modifications of the model that

may explain such activity have already been suggested. An additional discrepancy between the NS-NS merger model and the observations is the inferred lifetime distribution of the merging systems. While the current observations point toward a lifetime distribution that is dominated by several Gyr old progenitors, the observed NS-NS systems in our Galaxy represent a population with a typical lifetime of ~ 100 Myr. Note that the poorly constrained lifetime distribution of NS-BH binaries is consistent with the observations of SHBs. Both the observed SHB sample and the observed NS-NS sample are very small, and therefore this discrepancy may be resolved with any of the two lifetime estimates, or both, being inaccurate. However, if supported by future SHB observations and assuming that Galactic binaries are representative of the cosmological population, lifetime considerations may rule out NS-NS coalescence and leave only NS-BH mergers as a viable SHB progenitor system.

To conclude, given the very promising rudimentary comparison of compact binary merger model predictions and observations, this remains the leading progenitor model. However, it is important to remember that all supporting arguments are indirect and none of them are even close to being as conclusive as the detection of SN spectra in the afterglows of nearby long GRBs. Therefore, it is important, especially given the fact that there are some apparent discrepancies between this model and SHB observations, to explore the possibility that SHBs are produced by entirely different systems.

5.3 *Other progenitor models*

5.3.1 *Accretion induced collapse*

An accretion induced collapse (AIC) of a rapidly rotating neutron star to a black hole was suggested by several authors as the source of GRBs (Vietri & Stella, 1998, 1999; MacFadyen, Ramirez-Ruiz & Zhang, 2005; Dermer & Atoyan, 2006). The GRB central engine in this scenario is similar to the one expected in a compact binary merger, the rapid accretion of a disk onto the newly formed BH. Here, the source of the disk is the NS material with the highest angular momentum, on the equator, while the BH is formed by material from the collapsing NS poles.

MacFadyen, Ramirez-Ruiz & Zhang (2005) propose this progenitor model to explain the ~ 100 s X-ray tail observed in some SHBs (see §2.2.2). They suggest that the collapse is initiated by accretion from a close and less compact companion and that the late X-ray emission is produced by the interaction of relativistic ejecta with the companion. Note that this scenario predicts a single smooth pulse and cannot explain variable X-ray tails (which might have

been already observed; Norris & Bonnell, 2006) or several afterglow flares, as observed following SHB 050724. Dermer & Atoyan (2006) further suggest that neutrino radiation from the NS collapse may heat and disrupt the companion, sending some of its mass toward the young BH, leading to late-time flares. They also find that the rate of such events can fit the SHB rate.

The main uncertainty in this model is the mass of the formed disk. Semi-analytic calculations and general relativistic simulations of the collapse into a black hole of a uniformly rotating star spinning at the mass-shedding limit, show that the mass of the remaining disk depends strongly on the equation of state (Cook, Shapiro & Teukolsky, 1994a,b; Shibata, Baumgarte & Shapiro, 2000; Shibata & Shapiro, 2002; Shibata, 2003; Shapiro, 2004). These calculations use a polytropic equation of state and they show that assuming a very soft EOS, $\Gamma - 4/3 \ll 1$, a massive disk may form (Shibata & Shapiro, 2002). However, a star with $\Gamma > 1.5$ collapses directly into a BH leaving practically no disk, $M_d < 10^{-3} M_\odot$ (Shibata, 2003; Shapiro, 2004). The reason is that the angular momentum of the material on the equator is not high enough in order to support it from collapsing. It is possible that if there are strong magnetic fields that help with angular momentum transfer towards the equator the outcome is different. Since neutron stars are expected to be much stiffer than a polytrope with $\Gamma = 1.5$, the current results suggest that unless strong magnetic field significantly alter the collapse outcome, AIC of a NS cannot be a GRB progenitor.

5.3.2 Magnetars

Central engine models that involve highly-magnetized neutron stars (magnetars) with magnetic fields that are similar to or larger than those observed in our Galaxy³⁸ (Duncan & Thompson, 1992; Paczynski, 1992; Kouveliotou *et al.*, 1998), come in two flavors. One is a newly born millisecond magnetar and the second is a version of SGR giant flares, in which case the magnetar already span-down significantly and is rotating slowly. A millisecond magnetar may be formed during the merger of two neutron stars as a transient, which collapses into a black hole during its spin-down, (as discussed in §5.2). A span down magnetars in old stellar population (as required by §5.1) must be therefore formed by a different progenitor system. A millisecond magnetar that span-down without collapsing may be formed for example by a merger of two white dwarfs (e.g., Saio & Nomoto, 1985; Levan *et al.*, 2006b), or an accretion-induced collapse of a white dwarf (e.g., Nomoto & Kondo, 1991).

A millisecond magnetar was first suggested as the central engine of GRBs by Usov (1992, see also Thompson, Chang & Quataert 2004; Thompson 2005).

³⁸ see Woods & Thompson (2004) for a review of Galactic magnetars

The energy source in this model is rotational energy, $\sim 5 \cdot 10^{52}$ erg, which is channeled into a relativistic outflow by magnetic luminosity. Assuming magnetic dipole emission, and that gravitational radiation can be neglected, the luminosity is (Usov, 1992):

$$L_{md} \approx 2.5 \times 10^{52} B_{16}^2 \Omega_4^4 \text{ erg/s}, \quad (48)$$

where B is the magnetic field on the neutron star surface and Ω is the magnetar angular velocity. The spin down time is:

$$T_{md} \approx 2B_{16}^{-2} \Omega_4^{-2} \text{s}. \quad (49)$$

Therefore, SHB energy considerations require $B \gtrsim 10^{15}$ G while time considerations require either $B \gtrsim 10^{16}$ G or termination of the magnetic emission before the entire rotational energy is emitted (e.g., by collapse of the magnetar into a BH).

A millisecond magnetar with a lower magnetic field ($\sim 10^{14} - 10^{15}$) is unlikely to produce the SHB itself, but it may affect the afterglow (Dai & Lu, 1998a,b; Wang & Dai, 2001; Zhang & Mészáros, 2001a; Dai, 2004). If somehow the end-product after the SHB is launched is such a magnetar then the rotational energy powers an outflow over $10^2 - 10^4$ s and this energy is injected into the external shock that produces the afterglow. This energy injection was suggested as an explanation of late flares and light curve flattening observed in SHBs 050724 and 051221A (Gao & Fan, 2005; Fan & Xu, 2006).

The second scenario is of an older magnetar that is producing the SHB in the same way as it produces SGR giant flares. Here the energy source is the magnetic field. If the field of the magnetar is similar to those inferred for Galactic objects ($\sim 10^{15}$) then it cannot produce a burst with more than $\sim 10^{47}$ erg. Dar (2005a) suggests that giant flares, such as the one observed from SGR 1806-20, are beamed in such a way that for some observers the isotropic-equivalent energy appears to be $\sim 10^{50}$ erg, thereby explaining the whole SHB population as similar extragalactic giant flares. While this model is very economic, it fails to produce the observed SHB afterglows, which are brighter by many orders of magnitude than the unbeamed afterglow of the giant flare from SGR 1806-20 (Cameron *et al.*, 2005; Gaensler *et al.*, 2005). An alternative intriguing possibility is that there are old magnetars with external magnetic fields of 10^{17} G (T. Thompson, private communication). Giant flares from such magnetars can be energetic enough to produce SHBs. Such magnetars may be the end product of a merger of two white dwarfs (Levan *et al.*, 2006b), and their birthrate and lifetime may be such that it is not surprising that none are observed in our Galaxy. Note that in this model is currently the only one where the same source may produce more than one SHB, enabling, in principle, repeated detection of SHBs from the same source.

5.3.3 Quark stars

Quark stars, if they exist, may be an entirely different energy source for both long and short GRBs. There are many models in which GRB progenitors involve a quark star (e.g., [Schramm & Olinto, 1992](#); [Ma & Xie, 1996](#); [Cheng & Dai, 1996](#); [Fryer & Woosley, 1998](#); [Dai & Lu, 1998b](#); [Dar, 1999](#); [Bombaci & Datta, 2000](#); [Ouyed & Sannino, 2002](#); [Ouyed, Dey & Dey, 2002](#); [Berezhiani *et al.*, 2003](#); [Bombaci, Parenti & Vidana, 2004](#); [Bombaci, 2005](#); [Paczyński & Haensel, 2005](#); [Ouyed, Rapp & Vogt, 2005](#); [Staff, Ouyed & Bagchi, 2006](#); [Menezes *et al.*, 2006](#); [Drago, Lavagno & Pagliara, 2006](#)). In these models the burst is initiated by a nuclear phase transition in the composition of some, or all, of the star material, usually the conversion of hadrons to quarks. This phase transition is also, usually, the main source of the burst energy. The duration of the bursts in different models is determined by different mechanisms. For example, [Menezes *et al.* \(2006\)](#) suggest that the duration in which an entire neutron star is converted into a strange quark star, triggered by the formation of seed strange quark matter, is between 1 ms and 1 s, and may lead to a SHB. [Ouyed & Sannino \(2002\)](#) suggest that both long and short GRBs are produced by hot quark stars where the difference between the two types of bursts is the progenitor mass. They find that the structure of the star is different above and below a critical mass and that the phase transition in hot quark stars below this critical mass takes ~ 1 s while for a more massive star it takes ~ 80 s. [Ouyed, Dey & Dey \(2002\)](#) suggest a model in which the engine is activated by the accretion onto a quark star. In this scenario, similar to typical GRB accretion models, the difference between long and short GRBs is in the duration of the accretion. [Dar \(2005a\)](#) suggest that SHBs, as well as soft gamma-ray repeaters and their giant flares, originate from hyper-stars, i.e. neutron stars where a considerable fraction of their neutrons have converted to hyperons. The energy source is a continuous episodic phase transition from neutron matter to hyper matter in the inner star layers.

The outcome of most quark star scenarios is the release of a large amount of energy in the form of radiation within a short time on the surface of the star. At this point these models merge with the loaded pair-radiation fireball model that leads to a relativistic outflow.

5.3.4 Type Ia SN

[Dar & de Rújula \(2003\)](#) suggested that SHBs are associated with Type Ia SNe. The prompt emission and the afterglow in this model are produced by “cannon balls” (for a review of the cannon ball model see [Dar & de Rújula, 2004](#)). The stringent limits on SN emission, which are a factor of ~ 1000 below that of a typical SN Ia, together with the fact that the variance on SN Ia peak magnitudes is small, disfavor this model.

6 Gravitational waves from SHBs

If SHBs are generated by NS-NS or NS-BH mergers then they are the electromagnetic counterparts of the most accessible gravitational-wave (GW) sources for ground-based GW observatories. As such, SHBs received a lot of attention from the GW community. The local SHB rate might have direct implications for the detection rate of GW telescopes, and more importantly searching for GW signals in association with SHBs may increase the sensitivity, and thus the detection rate, of these telescopes. Even if SHBs have a different origin they still may be powerful GW sources, although in this case the prospects for detecting their GW signals are not as promising.

6.1 NS-NS or NS-BH coalescence

Mergers of compact binaries are expected to be the first cosmological source of GW detected by ground-based observatories. The exact nature of the signal expected and the prospects for its detection are discussed in numerous papers (see [Cutler & Thorne, 2002](#), for a comprehensive review). In principle the mergers are expected to have three different phases of GW emission: the chirp inspiral signal, the coalescence signal, and the signal from the ringdown of the remaining BH. The frequency of the typical signal during the final inspiral stages of NS-NS and NS-stellar mass BH systems passes conveniently through the most sensitive frequency range of GW observatories such as LIGO³⁹ and VIRGO⁴⁰ ($\sim 100 - 500$) Hz, making it the main target for detection. At its current sensitivity LIGO-I can detect a NS-NS merger up to an average distance of about 15 Mpc, and a merger of a NS with a $10M_{\odot}$ BH up to about 30 Mpc. Beginning at the end of 2005 LIGO-I started its S5 science run, in which a full year of data is expected to be collected at this sensitivity (which is comparable to LIGO design sensitivity over almost the entire frequency range). The VIRGO design sensitivity is similar, and it is expected to be reached in the near future.

If SHBs are generated by compact binary mergers then their local rate is given by Eq. 47, implying a detection rate by current observatories of $1[10] \times 10^{-4} \lesssim \mathcal{R}_{GW} \lesssim 0.1[1] \text{ yr}^{-1}$ for NS-NS [NS- $10M_{\odot}$ BH] mergers. Therefore, in the most optimistic scenario, where SHBs are narrowly beamed and/or there are many dim undetected SHBs, LIGO-I might detect GW signals from undetected SHBs. In all other cases such a detection is unlikely. This GW detection rate is for a blind search within the data for signal from mergers. If the search

³⁹The Laser Interferometer Gravitational-Wave Observatory;
<http://www.ligo.caltech.edu/>

⁴⁰<http://wwwcascina.virgo.infn.it/>

is performed only during some short time window (say 1 min) around the time in which electromagnetic emission from SHBs is observed, the sensitivity increases (a search for a significant signal within data with longer duration requires higher signal to noise ratio). [Kochanek & Piran \(1993\)](#) estimate that a search performed only when SHBs are detected can increase the range of LIGO-I and VIRGO by a factor of ≈ 1.5 . If SHBs are preferentially beamed perpendicular to the binary orbital plane the range is increased by an additional factor of⁴¹ ≈ 1.5 . Therefore, a SHB-coincident search for GW signals may increase the detection range to $\approx 30[60]$ Mpc. The detection rate of *Swift* is about 10 SHBs per year and that of *HETE-2* and other IPN spacecraft is similar. If several percent of these bursts are within 50–100 Mpc, as suggested by [Tanvir et al. \(2005\)](#), then a coincident detection may be obtained with current facilities. Note that if SHBs are beamed so their GW-SHB coincident detection range is significantly increased then their true rate (after beaming correction) within 15 Mpc is at least comparable to the observed SHB rate within 30 Mpc. However, given that even the most optimistic scenarios predict a rate that is smaller than one merger event per year at these distances, a coincident search for SHB and a GW signal may make the difference between a detection and a non-detection by current GW observatories.

Simultaneous detection of the inspiral GW signal from a compact merger and a SHB will provide conclusive evidence that SHBs originate from compact mergers and would improve our understanding of both merger physics and SHBs significantly. GWs can provide a unique view of the formation, and possibly the operation, of the inner engine powering the burst, which are difficult to observe via any other method. A coincident detection is also most valuable in order to determine the cosmological parameters ([Dalal et al. , 2006](#)), as the GW signal of a binary merger enables an accurate determination of the luminosity distance, while the electromagnetic signal may provide an accurate measurement of the redshift. If GW signal from a merger is detected without a coincident SHB, an association may still be secured by the detection of an orphan afterglow - afterglows that are not associated with prompt emission (e.g., [Rhoads, 1997](#); [Granot et al. , 2002](#); [Nakar, Piran & Granot , 2002](#); [Totani & Panaitescu , 2002](#); [Nakar & Piran, 2003b](#); [Levinson et al. , 2002](#)). However, orphan afterglows should be searched for quickly, within days or weeks after the detection of the GW signal. The reason is, that the nearby SHBs, which might be detected by GW observatories, are most likely at the low end of the luminosity function ($\lesssim 10^{47} \text{erg}$), simply because these are the most frequent, and therefore their afterglow is not expected to be detectable many days after the burst (even though they are nearby). Moreover, the transition to Newtonian blast wave and quasi spherical emission takes place days-weeks after the burst if its energy is low.

⁴¹ The average range is obtained by averaging over all the possible orientations. The signal from a merger that is observed face-on is larger by a factor of $\sqrt{5}/2$.

Next generation observatories, which are planned to become operational in the first half of the next decade, are expected to be ten times more sensitive. For example advanced-LIGO (LIGO-II) is designed to detect NS-NS [NS - $10M_{\odot}$ BH] up to about 300[650] Mpc. As discussed above, simultaneous detections will increase LIGO-II range by a factor of 1.5-2.5 to $\approx 0.6[1.3]$ Gpc. So far, *HETE-2* observed one burst at a distance < 700 Mpc while *Swift* detected at least 2 additional SHBs at a distance $\lesssim 1$ Gpc. The GBM detector on *GLAST*⁴² is expected to have a threshold that is similar to BATSE and more than half-sky field of view, and thus it is expected to detect at least 5 SHBs within a distance of 500 Mpc every year. Therefore, if SHBs are compact binary mergers, and assuming that an efficient GRB detector will be operational simultaneously with LIGO-II, a coincident electromagnetic and GW detection is guaranteed. The benefit of the simultaneous operation of LIGO-II and an efficient GRB detector goes beyond the high likelihood to observe simultaneous SHBs and mergers if they are associated - it will also enable to disprove the association if no simultaneous detections are observed.

6.2 Other processes that radiate gravitational waves

SHBs may emit GWs also if the progenitor is not a compact binary merger. Any progenitor that involves the collapse of a rotating compact object to a black hole (e.g., the collapse of a rotating neutron star triggered by accretion; §5.3.1) will produce gravitational waves (e.g., Stark & Piran, 1985). The amplitude of these waves is highly uncertain. Moreover, the absence of an accurate signal templates will reduce their detectability. Such GW signals would most likely not be detected even by LIGO-II at distances much greater than 10 Mpc (Kokkotas & Stergioulas, 2005, , and references therein).

If the central engine is an accretion disk - BH system then disk instabilities may break the axisymmetry and lead to GW emission (e.g., van Putten & Levinson, 2001, 2002, 2003; Kobayashi & Mészáros, 2003; Araya-Góchez, 2004; van Putten, 2005; Bromberg, Levinson & van Putten, 2006). The strength of this signal is uncertain and it depends on the evolution of the disk, which is different from one model to the other. Optimistic estimates suggest that it might be detectable by LIGO-II to a distance of ~ 100 Mpc (Kobayashi & Mészáros, 2003; Bromberg, Levinson & van Putten, 2006).

An additional source of GW is the acceleration of relativistic jets (e.g., Segalis & Ori, 2001; Sago *et al.*, 2004; Piran, 2005b). Unlike electromagnetic emission, GW radiation in this case is not collimated. However, it is expected to be too weak for detection by LIGO-I and even with LIGO-II the detection range is not expected to exceed 10 Mpc by much.

⁴² <http://f64.nsstc.nasa.gov/gbm/>

Acknowledgements

I am indebt to A. Gal-Yam for numerous discussions and invaluable remarks that considerably improved this review. I am also especially grateful to E. O. Ofek and J. Granot for detailed valuable comments. It is my pleasure to thank K. Belczynski, E. Berger, G. E. Brown, D. N. Burrows, S. B. Cenko, Z. Dai, D. B. Fox, D. A. Frail, N. Gehrels, G. Ghirlanda, D. Guetta, D. Z. Holz, S. R. Kulkarni, P. Kumar, C. Kouveliotou, W. H. Lee, Z. Li, R. Perna, E. S. Phinney, T. Piran, R. D. Preece, E. Ramirez-Ruiz, R. Sari, A. M. Soderberg, E. Waxman and D. Wei for helpful discussions and comments. I thank J. Racusin and D. N. Burrows for preparing Figure 5 and to S. D. Barthelmy for providing the X-ray light curve of SHB 050724. I am grateful to R. Quimby for creating the GRBLog, which I used frequently during the preparation of this review. This work was partially supported by a senior research fellowship from the Sherman Fairchild Foundation and by NASA NNH05ZDA001N grant.

References

- Achterberg, A., Gallant, Y. A., Kirk, J. G., and Guthmann, A. W. 2001, MNRAS , 328, 393, astro-ph/0107530.
- Aloy, M. A., Janka, H.-T., and Müller, E. 2005, A&A, 436, 273, astro-ph/0408291.
- Aloy, M. A. and Rezzolla, L. 2006, ApJ, 640, L115, astro-ph/0602437.
- Amati, L. 2006, MNRAS , 941, astro-ph/0601553.
- Amati, L. *et al.* 2002, A&A , 390, 81, astro-ph/0205230.
- Anderson, S. B., Gorham, P. W., Kulkarni, S. R., Prince, T. A., and Wolszczan, A. 1990, Nature , 346, 42.
- Ando, S. 2004, Journal of Cosmology and Astro-Particle Physics, 6.
- Araya-Góchez, R. A. 2004, MNRAS , 355, 336, astro-ph/0311001.
- Armitage, P. J. and Reynolds, C. S. 2003, MNRAS , 341, 1041, astro-ph/0302271.
- Armitage, P. J., Reynolds, C. S., and Chiang, J. 2001, ApJ , 548, 868, astro-ph/0007042.
- Arzoumanian, Z., Cordes, J. M., and Wasserman, I. 1999, ApJ, 520, 696.
- Asano, K. and Fukuyama, T. 2000, ApJ , 531, 949, astro-ph/0002196.
- Asano, K. and Fukuyama, T. 2001, ApJ , 546, 1019, astro-ph/0009453.
- Bahcall, J. N. and Mészáros, P. 2000, Physical Review Letters, 85, 1362.
- Balazs, L. G., Meszaros, A., and Horvath, I. 1998, A&A, 339, 1.
- Balbus, S. A. and Hawley, J. F. 1991, ApJ , 376, 214.
- Balbus, S. A. and Hawley, J. F. 1998, Reviews of Modern Physics, 70, 1.
- Baltz, E. A. and Hui, L. 2005, ApJ , 618, 403, astro-ph/0311569.
- Band, D. *et al.* 1993, ApJ , 413, 281.
- Band, D. L. 2006, ApJ, 644, 378, astro-ph/0602267.
- Band, D. L. and Preece, R. D. 2005, ApJ , 627, 319, astro-ph/0501559.
- Barbier, L. *et al.* 2005, GCN Circular, 4194, 1.
- Barris, B. J. and Tonry, J. L. 2006, ApJ , 637, 427, astro-ph/0509655.
- Barthelmy, S. D. *et al.* 2005, Nature, 438, 994, astro-ph/0511579.
- Baumgarte, T. W., Shapiro, S. L., and Shibata, M. 2000, ApJ , 528, L29, astro-ph/9910565.
- Belczyński, K. and Bulik, T. 1999, A&A , 346, 91, astro-ph/9901193.
- Belczynski, K., Bulik, T., and Kalogera, V. 2002, ApJ, 571, L147.
- Belczynski, K., Bulik, T., and Rudak, B. 2002, ApJ , 571, 394, astro-ph/0112122.
- Belczyński, K. and Kalogera, V. 2001, ApJ, 550, L183.
- Belczynski, K., Kalogera, V., and Bulik, T. 2002, ApJ, 572, 407.
- Belczynski, K., Kalogera, V., Rasio, F. A., Taam, R. E., Zezas, A., Bulik, T., Maccarone, T. J., and Ivanova, N. 2005, ArXiv Astrophysics e-prints, astro-ph/0511811.
- Belczynski, K., Perna, R., Bulik, T., Kalogera, V., Ivanova, N., and Lamb, D. Q. 2006, ArXiv Astrophysics e-prints, astro-ph/0601458.
- Beloborodov, A. M. 2000, ApJ, 539, L25, astro-ph/0004360.

- Beloborodov, A. M. 2002, ApJ , 565, 808, astro-ph/0103321.
- Beloborodov, A. M. 2003a, ApJ, 585, L19, astro-ph/0209228.
- Beloborodov, A. M. 2003b, ApJ, 588, 931, astro-ph/0210522.
- Beloborodov, A. M. 2005, ApJ, 618, L13, astro-ph/0410050.
- Berezhiani, Z., Bombaci, I., Drago, A., Frontera, F., and Lavagno, A. 2003, ApJ , 586, 1250, astro-ph/0209257.
- Berger, E., et al. 2003, Nature , 426, 154, astro-ph/0308187.
- Berger, E. 2005, GRB Circular Network, 3801, 1.
- Berger, E. 2006, American Institute of Physics Conference Series, 836, 33, arXiv:astro-ph/0602004.
- Berger, E. *et al.* 2005, Nature, 438, 988, astro-ph/0508115.
- Berger, E., Shin, M. ., Mulchaey, J. S., and Jeltama, T. E. 2006, ArXiv Astrophysics e-prints, astro-ph/0608498.
- Berger, E., et al. 2006, ArXiv Astrophysics e-prints, arXiv:astro-ph/0611128
- Bethe, H. A. and Brown, G. E. 1998, ApJ, 506, 780.
- Bethe, H. A., Brown, G. E., and Lee, C. . 2005a, ArXiv Astrophysics e-prints, astro-ph/0510378.
- Bethe, H. A., Brown, G. E., and Lee, C. . 2005b, ArXiv Astrophysics e-prints, astro-ph/0510379.
- Blandford, R. and Eichler, D. 1987, Physics Reports , 154, 1.
- Blandford, R. D. and McKee, C. F. 1976, Physics of Fluids, 19, 1130.
- Blandford, R. D. and Znajek, R. L. 1977, MNRAS , 179, 433.
- Bloom, J. S. *et al.* 1999, Nature, 401, 453.
- Bloom, J. S. *et al.* 2006a, ArXiv Astrophysics e-prints, astro-ph/0607223.
- Bloom, J. S. *et al.* 2006b, ApJ , 638, 354, astro-ph/0505480.
- Bloom, J. S., & Prochaska, J. X. 2006, American Institute of Physics Conference Series, 836, 473, astro-ph/0602058.
- Bloom, J. S., Sigurdsson, S., and Pols, O. R. 1999, MNRAS , 305, 763.
- Bombaci, I. 2005, in AIP Conf. Proc. 797: Interacting Binaries: Accretion, Evolution, and Outcomes, ed. L. Burderi, L. A. Antonelli, F. D'Antona, T. di Salvo, G. L. Israel, L. Piersanti, A. Tornambè, and O. Straniero, 132.
- Bombaci, I. and Datta, B. 2000, ApJ , 530, L69, astro-ph/0001478.
- Bombaci, I., Parenti, I., and Vidiña, I. 2004, ApJ , 614, 314, astro-ph/0402404.
- Bret, A., Firpo, M.-C., and Deutsch, C. 2004, Phys. Rev. E , 70(4), 046401.
- Bret, A., Firpo, M.-C., and Deutsch, C. 2005, Physical Review Letters, 94(11), 115002, physics/0502097.
- Briggs, M. S. *et al.* 1996, ApJ, 459, 40.
- Bromberg, O., Levinson, A., and van Putten, M. 2006, New Astronomy, 11, 619, astro-ph/0507078.
- Brown, G. E. 1995, ApJ , 440, 270.
- Brown, G. E., Lee, C.-H., Wijers, R. A. M. J., and Bethe, H. A. 2000a, Physics Reports , 333, 471, astro-ph/9910088.
- Brown, G. E., Lee, C.-H., Wijers, R. A. M. J., Lee, H. K., Israelian, G., and Bethe, H. A. 2000b, New Astronomy, 5, 191, astro-ph/0003361.
- Buonanno, A. and Damour, T. 1999, Phys. Rev. D , 59(8), 084006, gr-

- qc/9811091.
- Burgay, M. *et al.* 2003, *Nature*, 426, 531.
- Burrows, D. N. *et al.* 2006, ArXiv Astrophysics e-prints, astro-ph/0604320.
- Cameron, P. B. *et al.* 2005, *Nature*, 434, 1112, astro-ph/0502428.
- Campana, S. *et al.* 2006, *A&A*, 454, 113, astro-ph/0603475.
- Cannizzo, J. K., Gehrels, N., and Vishniac, E. T. 2004, *ApJ*, 601, 380, astro-ph/0310113.
- Cappellaro, E., Evans, R., and Turatto, M. 1999, *A&A*, 351, 459.
- Castro-Tirado, A. J. *et al.* 2005, *GRB Circular Network*, 3673, 1.
- Chen, W.-X., & Beloborodov, A. M. 2006, ArXiv Astrophysics e-prints, arXiv:astro-ph/0607145
- Cheng, K. S., & Dai, Z. G. 1996, *Physical Review Letters*, 77, 1210, astro-ph/9510073.
- Chevalier, R. A. 1993, *ApJ*, 411, L33.
- Christensen, L., Hjorth, J., and Gorosabel, J. 2004, *A&A*, 425, 913, astro-ph/0407066.
- Cline, D. B., Czerny, B., Matthey, C., Janiuk, A., and Otwinowski, S. 2005, *ApJ*, 633, L73, astro-ph/0510309.
- Cline, D. B., Matthey, C., and Otwinowski, S. 1999, *ApJ*, 527, 827, astro-ph/9905346.
- Cline, D. B., Matthey, C., and Otwinowski, S. 2001, in *Gamma-ray Bursts in the Afterglow Era*, ed. E. Costa, F. Frontera, and J. Hjorth, 56.
- Coe, D., Benítez, N., Sánchez, S. F., Jee, M., Bouwens, R., & Ford, H. 2006, *AJ*, 132, 926
- Connaughton, V. 2002, *ApJ*, 567, 1028, astro-ph/0111564.
- Cook, G. B., Shapiro, S. L., and Teukolsky, S. A. 1994a, *ApJ*, 424, 823.
- Cook, G. B., Shapiro, S. L., and Teukolsky, S. A. 1994b, *ApJ*, 422, 227.
- Costa, E. *et al.* 1997, *Nature*, 387, 783, astro-ph/9706065.
- Covino, S. *et al.* 2006, *A&A*, 447, L5, astro-ph/0509144.
- Cowie, L. L., Barger, A. J., Hu, E. M., Capak, P., & Songaila, A. 2004, *AJ*, 127, 3137
- Cummings, J. *et al.* 2005, *GCN Circular*, 4365, 1.
- Curran, S. J. and Lorimer, D. R. 1995, *MNRAS*, 276, 347.
- Cutler, C. and Thorne, K. S. 2002, ArXiv General Relativity and Quantum Cosmology e-prints, arXiv:gr-qc/0204090.
- Dahlen, T. *et al.* 2004, *ApJ*, 613, 189.
- Dai, Z. G. 2004, *ApJ*, 606, 1000, astro-ph/0308468.
- Dai, Z. G., & Cheng, K. S. 2001, *ApJ*, 558, L109, astro-ph/0105055.
- Dai, Z. G. and Lu, T. 1998a, *A&A*, 333, L87, astro-ph/9810402.
- Dai, Z. G., & Lu, T. 1998b, *Physical Review Letters*, 81, 4301
- Dai, Z. G. and Lu, T. 2002, *ApJ*, 565, L87, astro-ph/0111454.
- Dai, Z. G., Wang, X. Y., Wu, X. F., and Zhang, B. 2006, *Science*, 311, 1127, astro-ph/0602525.
- Daigne, F. and Mochkovitch, R. 1998, *MNRAS*, 296, 275, astro-ph/9801245.
- Daigne, F., and Mochkovitch, R. 2002a, *A&A*, 388, 189, astro-ph/0203298.

- Daigne, F. and Mochkovitch, R. 2002b, MNRAS, 336, 1271, astro-ph/0207456.
- Dalal, N., Holz, D. E., Hughes, S. A., & Jain, B. 2006, Phys. Rev. D , 74, 063006
- Dar, A. 1999, A&AS , 138, 505.
- Dar, A. 2005a, ArXiv Astrophysics e-prints, arXiv:astro-ph/0509257.
- Dar, A. 2005b, GRB Circular Network, 2942, 1.
- Dar, A. and de Rujula, A. 2003, GCN Circular, 2174, 1.
- Dar, A. and de Rujula, A. 2004, Physics Reports , 405, 203, astro-ph/0308248.
- Davies, M. B., Benz, W., Piran, T., and Thielemann, F. K. 1994, ApJ , 431, 742, astro-ph/9401032.
- Davies, M. B., Levan, A. J., and King, A. R. 2005, MNRAS, 356, 54, astro-ph/0409681.
- de Freitas Pacheco, J. A., Regimbau, T., Vincent, S., and Spallicci, A. 2006, International Journal of Modern Physics D, 15, 235, astro-ph/0510727.
- de Ugarte Postigo, A. *et al.* 2006, ApJ , 648, L83.
- De Villiers, J.-P., Hawley, J. F., and Krolik, J. H. 2003, ApJ , 599, 1238, astro-ph/0307260.
- De Villiers, J.-P., Hawley, J. F., Krolik, J. H., and Hirose, S. 2005, ApJ , 620, 878, astro-ph/0407092.
- Della Valle, M. *et al.* 2006, ArXiv Astrophysics e-prints, astro-ph/0608322.
- Derishev, E. V., Kocharovsky, V. V., and Kocharovsky, V. V. 1999a, A&A, 345, L51.
- Derishev, E. V., Kocharovsky, V. V., and Kocharovsky, V. V. 1999b, ApJ, 521, 640.
- Dermer, C. D. 2002, ApJ , 574, 65, astro-ph/0005440.
- Dermer, C. D. 2004, ApJ, 614, 284, astro-ph/0403508.
- Dermer, C. D. 2006, ArXiv Astrophysics e-prints, arXiv:astro-ph/0611194
- Dermer, C. D. and Atoyan, A. 2003, Physical Review Letters, 91(7), 071102.
- Dermer, C. D. and Atoyan, A. 2006, ApJ , 643, L13, astro-ph/0601142.
- Dermer, C. D., & Atoyan, A. 2006, New Journal of Physics, 8, 122
- Dermer, C. D., Chiang, J., and Mitman, K. E. 2000, ApJ, 537, 785.
- Dermer, C. D. and Mitman, K. E. 1999, ApJ, 513, L5, astro-ph/9809411.
- Dermer, C. D., & Humi, M. 2001, ApJ , 556, 479
- Dermer, C. D. and Mitman, K. E. 2004, in Astronomical Society of the Pacific Conference Series, ed. M. Feroci, F. Frontera, N. Masetti, and L. Piro, 301.
- Dewi, J. D. M., Podsiadlowski, P., and Sena, A. 2006, MNRAS , 368, 1742, astro-ph/0602510.
- Di Matteo, T., Perna, R., and Narayan, R. 2002, ApJ , 579, 706, astro-ph/0207319.
- Donaghy, T. Q. *et al.* 2006, ArXiv Astrophysics e-prints, astro-ph/0605570.
- Drago, A., Lavagno, A., and Pagliara, G. 2006, Nuclear Physics A, 774, 823, astro-ph/0510018.
- Drenkhahn, G. and Spruit, H. C. 2002, A&A, 391, 1141, astro-ph/0202387.
- Drury, L. O. 1983, Reports of Progress in Physics, 46, 973.
- Duez, M. D., Liu, Y. T., Shapiro, S. L., Shibata, M., and Stephens, B. C.

- 2006, Physical Review Letters, 96(3), 031101, astro-ph/0510653.
- Duncan, R. C. 2001, in AIP Conf. Proc. 586: 20th Texas Symposium on relativistic astrophysics, 495.
- Duncan, R. C. and Thompson, C. 1992, ApJ , 392, L9.
- Eichler, D. 2002, MNRAS, 335, 883, astro-ph/0204512.
- Eichler, D., Livio, M., Piran, T., and Schramm, D. N. 1989, Nature, 340, 126.
- Eldridge, J. J., Genet, F., Daigne, F., and Mochkovitch, R. 2006, MNRAS, 367, 186, astro-ph/0509749.
- Ellison, D. C. and Double, G. P. 2002, Astroparticle Physics, 18, 213, astro-ph/0202106.
- Ellison, D. C. and Double, G. P. 2004, Astroparticle Physics, 22, 323, astro-ph/0408527.
- Faber, J. A., Baumgarte, T. W., Shapiro, S. L., and Taniguchi, K. 2006a, ApJ, 641, L93, astro-ph/0603277.
- Faber, J. A., Baumgarte, T. W., Shapiro, S. L., Taniguchi, K., and Rasio, F. A. 2006b, Phys. Rev. D, 73(2), 024012, astro-ph/0511366.
- Fan, Y. and Piran, T. 2006, MNRAS, 369, 197, astro-ph/0601054.
- Fan, Y.-Z., Dai, Z.-G., Huang, Y.-F., and Lu, T. 2002, Chinese Journal of Astronomy and Astrophysics, 2, 449, astro-ph/0306024.
- Fan, Y.-Z. and Xu, D. 2006, MNRAS , L79+, astro-ph/0605445.
- Fan, Y. Z., Zhang, B., and Proga, D. 2005, ApJ , 635, L129, astro-ph/0509019.
- Fenimore, E. E., Madras, C. D., and Nayakshin, S. 1996, APJ, 473, 998, astro-ph/9607163.
- Finn, L. S., Mohanty, S. D., and Romano, J. D. 1999, Phys. Rev. D , 60(12), 121101, gr-qc/9903101.
- Fishman, G. J. and Meegan, C. A. 1995, Annual Review of Astronomy and Astrophysics, 33, 415.
- Fonseca, R. A., Silva, L. O., Tonge, J. W., Mori, W. B., and Dawson, J. M. 2003, Physics of Plasmas, 10, 1979.
- Fox, D. B. *et al.* 2005, Nature, 437, 845.
- Fox, D. W. *et al.* 2003, Nature, 422, 284.
- Frail, D. A., Kulkarni, S. R., Nicastro, S. R., Feroci, M., and Taylor, G. B. 1997, Nature , 389, 261.
- Frail, D. A., Waxman, E., and Kulkarni, S. R. 2000, ApJ, 537, 191, astro-ph/9910319.
- Frederiks, D. D., Aptekar, R. L., Golenetskii, S. V., Il'Inskii, V. N., Mazets, E. P., Palshin, V. D., and Cline, T. L. 2004, in Astronomical Society of the Pacific Conference Series, ed. M. Feroci, F. Frontera, N. Masetti, and L. Piro, 197.
- Frederiks, D. D., Pal'shin, V. D., Aptekar', R. L., Golenetskii, S. V., Cline, T. L., and Mazets, E. P. 2006, ArXiv Astrophysics e-prints, astro-ph/0609544.
- Frederiksen, J. T., Hededal, C. B., Haugbølle, T., and Nordlund, Å. 2004, ApJ , 608, L13, astro-ph/0308104.
- Freedman, D. L. and Waxman, E. 2001, ApJ, 547, 922, astro-ph/9912214.

- Fried, B. D. 1959, *Phys. Fluids*, 2, 337.
- Fruchter, A. S. *et al.* 2006, *Nature*, 441, 463, astro-ph/0603537.
- Fryer, C., Burrows, A., and Benz, W. 1998, *ApJ*, 496, 333, astro-ph/9710333.
- Fryer, C. L. and Woosley, S. E. 1998, *ApJ*, 501, 780, astro-ph/9802112.
- Fryer, C. L., Woosley, S. E., and Hartmann, D. H. 1999, *ApJ*, 526, 152.
- Fryer, C. L., Woosley, S. E., Herant, M., and Davies, M. B. 1999, *ApJ*, 520, 650, astro-ph/9808094.
- Fukugita, M., Hogan, C. J., and Peebles, P. J. E. 1998, *ApJ*, 503, 518.
- Fynbo, J. P. U. *et al.* 2006, *ArXiv Astrophysics e-prints*, astro-ph/0608313.
- Gaensler, B. M. *et al.* 2005, *Nature*, 434, 1104, astro-ph/0502393.
- Gaensler, B. M., Slane, P. O., Gotthelf, E. V., and Vasisht, G. 2001, *ApJ*, 559, 963.
- Gal-Yam, A. *et al.* 2006, *ArXiv Astrophysics e-prints*, astro-ph/0608257.
- Gal-Yam, A. and Maoz, D. 2004, *MNRAS*, 347, 942.
- Gal-Yam, A. *et al.* 2005, *ArXiv Astrophysics e-prints*, astro-ph/0509891.
- Gallant, Y. A., & Achterberg, A. 1999, *MNRAS*, 305, L6, astro-ph/9812316
- Galama, T. J. *et al.* 1998, *Nature*, 395, 670.
- Gao, W. H. and Fan, Y. Z. 2005, *ArXiv Astrophysics e-prints*, astro-ph/0512646.
- Garnavich, P. M., Loeb, A., and Stanek, K. Z. 2000, *ApJ*, 544, L11, astro-ph/0008049.
- Gaudi, B. S., Granot, J., and Loeb, A. 2001, *ApJ*, 561, 178, astro-ph/0105240.
- Gehrels, N. *et al.* 2005, *Nature*, 437, 851.
- Gehrels, N., *et al.* 2006, *Nature in press*, astro-ph/0610635.
- Ghirlanda, G., Celotti, A., and Ghisellini, G. 2002, *A&A*, 393, 409, astro-ph/0206377.
- Ghirlanda, G., Ghisellini, G., and Celotti, A. 2004, *A&A*, 422, L55.
- Ghirlanda, G., Magliocchetti, M., Ghisellini, G., and Guzzo, L. 2006, *MNRAS*, 368, L20.
- Gladders, M., Berger, E., Morrell, N., and Roth, M. 2005, *GRB Circular Network*, 3798, 1.
- Golenetskii, S., Aptekar, R., Mazets, E., Pal'shin, V., Frederiks, D., and Cline, T. 2005a, *GCN Circular*, 4394, 1.
- Golenetskii, S. *et al.* 2005b, *GCN Circular*, 4197, 1.
- Goodman, J. 1986, *ApJ*, 308, L47.
- Goodman, J., Dar, A., and Nussinov, S. 1987, *ApJ*, 314, L7.
- Gorosabel, J. *et al.* 2006, *A&A*, 450, 87, astro-ph/0510141.
- Granot, J. 2005, *ApJ*, 631, 1022, astro-ph/0504254.
- Granot, J. 2006, To appear in *Rev. Mex. Astron. Astrof.*, astro-ph/0610379
- Granot, J. and Königl, A. 2003, *ApJ*, 594, L83, astro-ph/0304286.
- Granot, J., Königl, A., and Piran, T. 2006, *MNRAS*, 370, 1946, astro-ph/0601056.
- Granot, J. and Kumar, P. 2006, *MNRAS*, 366, L13, astro-ph/0511049.
- Granot, J. and Loeb, A. 2001, *ApJ*, 551, L63, astro-ph/0101234.
- Granot, J., Miller, M., Piran, T., Suen, W. M., and Hughes, P. A. 2001, in

- Gamma-ray Bursts in the Afterglow Era, ed. E. Costa, F. Frontera, and J. Hjorth, 312.
- Granot, J., Nakar, E., and Piran, T. 2003, *Nature* , 426, 138, astro-ph/0304563.
- Granot, J., Piran, T., and Sari, R. 1999a, *ApJ* , 513, 679, astro-ph/9806192.
- Granot, J., Piran, T., and Sari, R. 1999b, *ApJ*, 527, 236, astro-ph/9808007.
- Granot, J., Piran, T., & Sari, R. 2000, *ApJ* , 534, L163
- Granot, J. and Sari, R. 2002, *ApJ*, 568, 820, astro-ph/0108027.
- Granot, J., Panaitescu, A., Kumar, P., & Woosley, S. E. 2002, *ApJ* , 570, L61
- Grimsrud, O. M. and Wasserman, I. 1998, *MNRAS*, 300, 1158.
- Grindlay, J., Portegies Zwart, S., and McMillan, S. 2006, *Nature Physics*, 2, 116, astro-ph/0512654.
- Grupe, D., Burrows, D. N., Patel, S. K., Kouveliotou, C., Zhang, B., Meszaros, P., Wijers, R. A. M., and Gehrels, N. 2006, *ArXiv Astrophysics e-prints*, astro-ph/0603773.
- Gruzinov, A. 2001, *ApJ* , 563, L15, astro-ph/0107106.
- Gruzinov, A. and Waxman, E. 1999, *ApJ* , 511, 852, astro-ph/9807111.
- Guetta, D. and Piran, T. 2005, *A&A*, 435, 421.
- Guetta, D. and Piran, T. 2006, *A&A* , 453, 823, astro-ph/0511239.
- Guetta, D., Piran, T., and Waxman, E. 2005, *ApJ*, 619, 412.
- Guetta, D., Spada, M., and Waxman, E. 2001, *ApJ*, 557, 399, astro-ph/0011170.
- Guilbert, P. W., Fabian, A. C., and Rees, M. J. 1983, *MNRAS* , 205, 593.
- Hawley, J. F. 2000, *ApJ* , 528, 462, astro-ph/9907385.
- Hawley, J. F. and Balbus, S. A. 2002, *ApJ* , 573, 738, astro-ph/0203309.
- Hawley, J. F. and Krolik, J. H. 2002, *ApJ* , 566, 164, astro-ph/0110118.
- Hawley, J. F. and Krolik, J. H. 2006, *ApJ* , 641, 103, astro-ph/0512227.
- Hirose, S., Krolik, J. H., De Villiers, J.-P., and Hawley, J. F. 2004, *ApJ* , 606, 1083, astro-ph/0311500.
- Hjorth, J. *et al.* 2003, *Nature*, 423, 847.
- Hjorth, J. *et al.* 2005a, *ApJ*, 630, L117.
- Hjorth, J. *et al.* 2005c, *Nature*, 437, 859.
- Hobbs, G., Lorimer, D. R., Lyne, A. G., and Kramer, M. 2005, *MNRAS* , 360, 974, astro-ph/0504584.
- Hopman, C., Guetta, D., Waxman, E., and Portegies Zwart, S. 2006, *ApJ* , 643, L91, astro-ph/0603440.
- Horváth, I. 2002, *A&A*, 392, 791, astro-ph/0205004.
- Hullinger, D. *et al.* 2005, *GCN Circular*, 4400, 1.
- Hurley, K. *et al.* 2005, *Nature*, 434, 1098.
- Hurley, K. *et al.* 1994, *Nature* , 372, 652.
- Ioka, K., Kobayashi, S., and Zhang, B. 2005, *ApJ*, 631, 429, astro-ph/0409376.
- Ioka, K. and Nakamura, T. 2001, *ApJ* , 561, 703, astro-ph/0102028.
- Janiuk, A., Perna, R., Di Matteo, T., and Czerny, B. 2004, *MNRAS*, 355, 950, astro-ph/0406362.
- Janka, H. ., Aloy, M. ., Mazzali, P. A., and Pian, E. 2005, *ArXiv Astrophysics e-prints*, astro-ph/0509722.

- Janka, H.-T., Eberl, T., Ruffert, M., and Fryer, C. L. 1999, *ApJ* , 527, L39, astro-ph/9908290.
- Jaroschek, C. H., Lesch, H., and Treumann, R. A. 2004, *ApJ* , 616, 1065.
- Jaroschek, C. H., Lesch, H., and Treumann, R. A. 2005, *ApJ* , 618, 822.
- Jaroszynski, M. 1993, *Acta Astronomica*, 43, 183.
- Jaroszynski, M. 1996, *A&A* , 305, 839, astro-ph/9506062.
- Jin, Z.-P., Yan, T., Fan, Y.-Z., & Wei, D.-M. 2006, *ArXiv Astrophysics e-prints*, arXiv:astro-ph/0610010
- Kalogera, V., Kim, C., and Lorimer, D. R. 2003, in *Gravitational-Wave Detection*. Edited by Cruise, Mike; Saulson, Peter. *Proceedings of the SPIE*, Volume 4856, pp. 134-145 (2003)., 134.
- Kalogera, V. *et al.* 2004, *ApJ*, 601, L179.
- Kalogera, V., Narayan, R., Spergel, D. N., and Taylor, J. H. 2001, *ApJ*, 556, 340.
- Kaneko, Y., Preece, R. D., Briggs, M. S., Paciesas, W. S., Meegan, C. A., & Band, D. L. 2006, *ApJ* , 166, 298
- Kato, Y., Mineshige, S., and Shibata, K. 2004, *ApJ* , 605, 307, astro-ph/0307306.
- Katz, B., Keshet, U., and Waxman, E. 2006, *ArXiv Astrophysics e-prints*, astro-ph/0607345.
- Katz, J. I. 1994, *ApJ*, 422, 248.
- Katz, J. I. 1997, *ApJ*, 490, 633, astro-ph/9701176.
- Katz, J. I. and Canel, L. M. 1996, *ApJ*, 471, 915.
- Kawai, N. *et al.* 2005, *GCN Circular*, 4359, 1.
- Keshet, U. 2006, *ArXiv Astrophysics e-prints*, astro-ph/0608182.
- Keshet, U. and Waxman, E. 2005, *Physical Review Letters*, 94(11), 111102, astro-ph/0408489.
- King, A. R., Pringle, J. E., and Wickramasinghe, D. T. 2001, *MNRAS* , 320, L45, astro-ph/0011150.
- Kluźniak, W. and Lee, W. H. 1998, *ApJ* , 494, L53+, astro-ph/9712019.
- Kluźniak, W. and Ruderman, M. 1998, *ApJ*, 505, L113, astro-ph/9712320.
- Kobayashi, S. and Mészáros, P. 2003, *ApJ* , 589, 861, astro-ph/0210211.
- Kobayashi, S., Piran, T., and Sari, R. 1997, *ApJ*, 490, 92, astro-ph/9705013.
- Kobayashi, S. and Sari, R. 2000, *ApJ*, 542, 819, astro-ph/9910241.
- Kobayashi, S. and Sari, R. 2001, *ApJ*, 551, 934, astro-ph/0101006.
- Kochanek, C. S. and Piran, T. 1993, *ApJ*, 417, L17+.
- Kohri, K., & Mineshige, S. 2002, *ApJ* , 577, 311
- Kokkotas, K. D. and Stergioulas, N. 2005, *ArXiv General Relativity and Quantum Cosmology e-prints*, arXiv:gr-qc/0506083.
- Komissarov, S. S. 2004, *MNRAS* , 350, 1431, astro-ph/0402430.
- Komissarov, S. S. 2005, *MNRAS* , 359, 801, astro-ph/0501599.
- Königl, A. 2004, *AIP Conf. Proc. 727: Gamma-Ray Bursts: 30 Years of Discovery*, 727, 257, astro-ph/0312224.
- Koopmans, L. V. E. and Wambsganss, J. 2001, *MNRAS* , 325, 1317, astro-ph/0011029.

- Kouveliotou, C. *et al.* 1998, *Nature* , 393, 235.
- Kouveliotou, C., Meegan, C. A., Fishman, G. J., Bhat, N. P., Briggs, M. S., Koshut, T. M., Paciesas, W. S., and Pendleton, G. N. 1993, *ApJ*, 413, L101.
- Krimm, H. *et al.* 2005, *GCN Circular*, 3667, 1.
- Krimm, H., *et al.* 2006, *GCN* 5704
- Krolik, J. H., Hawley, J. F., and Hirose, S. 2005, *ApJ* , 622, 1008, astro-ph/0409231.
- Kulkarni, S. R. 2005, *ArXiv Astrophysics e-prints*, astro-ph/0510256.
- Kulkarni, S. R., *et al.* 1998, *Nature* , 393, 35
- Kulkarni, S. R. *et al.* 1999, *ApJ* , 522, L97, astro-ph/9903441.
- Kumar, P. 1999, *ApJ* , 523, L113
- Kumar, P. and Granot, J. 2003, *ApJ*, 591, 1075, astro-ph/0303174.
- Kumar, P. and Panaitescu, A. 2000, *ApJ*, 541, L51, astro-ph/0006317.
- Kumar, P. and Panaitescu, A. 2004, *MNRAS* , 354, 252, astro-ph/0309161.
- Kumar, P. and Piran, T. 2000a, *ApJ*, 532, 286, astro-ph//9906002.
- Kumar, P. and Piran, T. 2000b, *ApJ*, 535, 152, astro-ph/9909014.
- La Parola, V. *et al.* 2006, *ArXiv Astrophysics e-prints*, astro-ph/0602541.
- Lamb, D. Q., Donaghy, T. Q., and Graziani, C. 2004, *New Astronomy Review*, 48, 459, astro-ph/0309456.
- Lattimer, J. M. and Swesty, F. D. 1991, *Nuclear Physics A*, 535, 331.
- Lattimer, J. M. and Schramm, D. N. 1974, *ApJ* , 192, L145.
- Lattimer, J. M. and Schramm, D. N. 1976, *ApJ* , 210, 549.
- Lazzati, D., Ghirlanda, G., and Ghisellini, G. 2005, *MNRAS*, 362, L8.
- Lazzati, D., Ramirez-Ruiz, E., and Ghisellini, G. 2001, *A&A*, 379, L39, astro-ph/0110215.
- Lazzati, D., Rossi, E., Covino, S., Ghisellini, G., and Malesani, D. 2002, *A&A*, 396, L5, astro-ph/0210333.
- Lee, C. ., Brown, G. E., and Park, E. 2006, *ArXiv Astrophysics e-prints*, astro-ph/0607442.
- Lee, H. K., Wijers, R. A. M. J., and Brown, G. E. 2000, *Physics Reports* , 325, 83, astro-ph/9906213.
- Lee, W. H. 2000, *MNRAS* , 318, 606, astro-ph/0007206.
- Lee, W. H. 2001, *MNRAS* , 328, 583, astro-ph/0108236.
- Lee, W. H. and Kluźniak, W. L. 1999a, *MNRAS* , 308, 780, astro-ph/9904328.
- Lee, W. H. and Kluźniak, W. L. 1999b, *ApJ* , 526, 178, astro-ph/9808185.
- Lee, W. H. and Ramirez-Ruiz, E. 2002, *ApJ* , 577, 893, astro-ph/0206011.
- Lee, W. H., Ramirez-Ruiz, E., and Granot, J. 2005, *ApJ*, 630, L165, astro-ph/0506104.
- Lee, W. H., Ramirez-Ruiz, E., and Page, D. 2004, *ApJ* , 608, L5, astro-ph/0404566.
- Lee, W. H., Ramirez-Ruiz, E., and Page, D. 2005, *ApJ* , 632, 421, astro-ph/0506121.
- LeeRuiz06
- Lee, W. H. and Ramirez-Ruiz, E., To appear in GRB Focus Issue of *New Journal of Physics*.

- Lemoine, M. and Pelletier, G. 2003, *ApJ* , 589, L73, astro-ph/0304058.
- Lemoine, M. and Revenu, B. 2006, *MNRAS* , 366, 635, astro-ph/0510522.
- Levan, A. J. *et al.* 2006a, *ApJ* , 648, L9, astro-ph/0603282.
- Levan, A. J., Wynn, G. A., Chapman, R., Davies, M. B., King, A. R., Priddey, R. S., and Tanvir, N. R. 2006b, *MNRAS* , 368, L1, astro-ph/0601332.
- Levinson, A. and Eichler, D. 1993, *ApJ* , 418, 386.
- Levinson, A., Ofek, E. O., Waxman, E., and Gal-Yam, A. 2002, *ApJ*, 576, 923.
- Li, C. and Sari, R. 2006, In preparation.
- Li, L.-X. and Paczyński, B. 1998, *ApJ* , 507, L59, astro-ph/9807272.
- Li, Z., Dai, Z. G., & Lu, T. 2002, *A&A* , 396, 303, astro-ph/0208435
- Li, Z. and Waxman, E. 2006, *ArXiv Astrophysics e-prints*, astro-ph/0603427.
- Lipkin, Y. M. *et al.* 2004, *ApJ*, 606, 381.
- Lipunov, V. M., Postnov, K. A., and Prokhorov, M. E. 1997, *MNRAS*, 288, 245.
- Lipunov, V. M., Postnov, K. A., and Prokhorov, M. E. 2001, *Astronomy Reports*, 45, 236, astro-ph/9908136.
- Lipunov, V. M., Postnov, K. A., Prokhorov, M. E., Panchenko, I. E., and Jorgensen, H. E. 1995, *ApJ* , 454, 593, astro-ph/9504045.
- Lithwick, Y. and Sari, R. 2001, *ApJ*, 555, 540, astro-ph/0011508.
- Lloyd, N. M. and Petrosian, V. 2000, *ApJ*, 543, 722, astro-ph/0007061.
- Lloyd, N. M., Petrosian, V., and Mallozzi, R. S. 2000, *ApJ* , 534, 227, astro-ph/9908191.
- Lloyd-Ronning, N. M. and Ramirez-Ruiz, E. 2002, *ApJ* , 576, 101, astro-ph/0205127.
- Lloyd-Ronning, N. M. and Zhang, B. 2004, *ApJ*, 613, 477, astro-ph/0404107.
- Loeb, A. and Perna, R. 1998, *ApJ* , 495, 597, astro-ph/9708159.
- Lyubarsky, Y. 2006, *ApJ* , 652, 1297, astro-ph/0611015
- Lyubarsky, Y. and Eichler, D. 2006, *ApJ* , 647, 1250, astro-ph/0512579.
- Lyutikov, M. 2003, *MNRAS* , 346, 540, astro-ph/0303384.
- Lyutikov, M. 2004, in 35th COSPAR Scientific Assembly, 237.
- Lyutikov, M. 2006, *New Journal of Physics*, 8, 119, astro-ph/0512342
- Lyutikov, M. and Blandford, R. 2002, in *Beaming and Jets in Gamma Ray Bursts*, ed. R. Ouyed, 146.
- Lyutikov, M. and Blandford, R. 2003, *ArXiv Astrophysics e-prints*, astro-ph/0312347.
- Lyutikov, M. and Blandford, R. 2004, in *Astronomical Society of the Pacific Conference Series*, ed. M. Feroci, F. Frontera, N. Masetti, and L. Piro, 449.
- Ma, F. and Xie, B. 1996, *ApJ* , 462, L63+, astro-ph/9603134.
- MacFadyen, A. I. 2003, in *From Twilight to Highlight: The Physics of Supernovae*, ed. W. Hillebrandt and B. Leibundgut, 97.
- MacFadyen, A. I., Ramirez-Ruiz, E., and Zhang, W. 2005, *ArXiv Astrophysics e-prints*, arXiv:astro-ph/0510192.
- MacFadyen, A. I. and Woosley, S. E. 1999, *ApJ* , 524, 262, astro-ph/9810274.
- Machida, M. and Matsumoto, R. 2003, *ApJ* , 585, 429, astro-ph/0211240.
- Magliocchetti, M., Ghirlanda, G., and Celotti, A. 2003, *MNRAS*, 343, 255.

- Mannucci, F., della Valle, M., Panagia, N., Cappellaro, E., Cresci, G., Maiolino, R., Petrosian, A., and Turatto, M. 2005, *A&A*, 433, 807.
- Mannucci, F., Della Valle, M., & Panagia, N. 2006, *MNRAS*, 370, 773
- Mao, S. and Loeb, A. 2001, *ApJ*, 547, L97, astro-ph/0010029.
- Maoz, D. and Gal-Yam, A. 2004, *MNRAS*, 347, 951.
- Markwardt, C. *et al.* 2005, *GCN Circular*, 4037, 1.
- Markwardt, C., et al. 2006, *GCN* 5882
- Mazets, E. P., Aptekar, R. L., Frederiks, D. D., Golenetskii, S. V., Il'Inskii, V. N., Palshin, V. D., Cline, T. L., and Butterworth, P. S. 2004, in *Astronomical Society of the Pacific Conference Series*, ed. M. Feroci, F. Frontera, N. Masetti, and L. Piro, 102.
- Mazets, E. P. *et al.* 1981, *Astrophysics and Space Science*, 80, 3.
- McBreen, S., Quilligan, F., McBreen, B., Hanlon, L., & Watson, D. 2001, *A&A*, 380, L31
- McKinney, J. C. 2005, *ApJ*, 630, L5, astro-ph/0506367.
- McKinney, J. C. 2006, *MNRAS*, 368, 1561, astro-ph/0603045.
- McKinney, J. C. and Gammie, C. F. 2004, *ApJ*, 611, 977, astro-ph/0404512.
- McMahon, E., Kumar, P., and Piran, T. 2006, *MNRAS*, 366, 575, astro-ph/0508087.
- Medvedev, M. V. 2000, *ApJ*, 540, 704, astro-ph/0001314.
- Medvedev, M. V., Fiore, M., Fonseca, R. A., Silva, L. O., and Mori, W. B. 2005, *ApJ*, 618, L75, astro-ph/0409382.
- Medvedev, M. V. and Loeb, A. 1999, *ApJ*, 526, 697, astro-ph/9904363.
- Meegan, C., Hurley, K., Connors, A., Dingus, B., and Matz, S. 1997, in *AIP Conf. Proc. 410: Proceedings of the Fourth Compton Symposium*, 407.
- Menezes, D. P., Melrose, D. B., Providência, C., and Wu, K. 2006, *Phys. Rev. C*, 73(2), 025806.
- Mészáros, P. 2006, *Reports of Progress in Physics*, 69, 2259, astro-ph/0605208.
- Mészáros, P., Laguna, P., and Rees, M. J. 1993, *ApJ*, 415, 181.
- Mészáros, P., Ramirez-Ruiz, E., and Rees, M. J. 2001, *ApJ*, 554, 660, astro-ph/0011284.
- Meszáros, P. and Razzaque, S. 2006, *ArXiv Astrophysics e-prints*, astro-ph/0605166.
- Mészáros, P. and Rees, M. J. 1992, *ApJ*, 397, 570.
- Mészáros, P. and Rees, M. J. 1997a, *ApJ*, 476, 232, astro-ph/9606043.
- Mészáros, P. and Rees, M. J. 1997b, *ApJ*, 482, L29+, astro-ph/9609065.
- Mészáros, P. and Rees, M. J. 2000, *ApJ*, 530, 292, astro-ph/9908126.
- Mészáros, P., Rees, M. J., and Papathanassiou, H. 1994, *ApJ*, 432, 181.
- Mészáros, P. and Waxman, E. 2001, *Physical Review Letters*, 87(17), 171102.
- Metzger, M. R., Djorgovski, S. G., Kulkarni, S. R., Steidel, C. C., Adelberger, K. L., Frail, D. A., Costa, E., and Frontera, F. 1997, *Nature*, 387, 878.
- Milgrom, M. and Usov, V. 1995, *ApJ*, 449, L37+.
- Miller, M. C. 2005, *ApJ*, 626, L41, astro-ph/0505094.
- Milosavljević, M. and Nakar, E. 2006a, *ApJ* in press, astro-ph/0512548.
- Milosavljević, M. and Nakar, E. 2006b, *ApJ*, 641, 978, astro-ph/0508464.

- Milosavljević, M., Nakar, E., and Spitkovsky, A. 2006, *ApJ* , 637, 765, astro-ph/0507553.
- Mochkovitch, R., Hernanz, M., Isern, J., and Loiseau, S. 1995, *A&A* , 293, 803.
- Mochkovitch, R., Hernanz, M., Isern, J., and Martin, X. 1993, *Nature* , 361, 236.
- Modestino, G. and Moleti, A. 2002, *Phys. Rev. D* , 65(2), 022005, astro-ph/0110620.
- Modestino, G. and Pizzella, G. 2000, *A&A* , 364, 419.
- Moiseev, S. S. and Sagdeev, R. Z. 1963, *Journal of Nuclear Energy*, 5, 43.
- Nakar, E., Gal-Yam, A., and Fox, D. B. 2006, *ApJ* , 650, 281, astro-ph/0511254.
- Nakar, E., Gal-Yam, A., Piran, T., and Fox, D. B. 2006, *ApJ*, 640, 849, astro-ph/0502148.
- Nakar, E. and Granot, J. 2006, *ArXiv Astrophysics e-prints*, astro-ph/0606011.
- Nakar, E. and Oren, Y. 2004, *ApJ* , 602, L97, astro-ph/0310236.
- Nakar, E. and Piran, T. 2002a, *ApJ*, 572, L139, astro-ph/0202404.
- Nakar, E. and Piran, T. 2002b, *MNRAS*, 330, 920, astro-ph/0103192.
- Nakar, E. and Piran, T. 2002c, *MNRAS*, 331, 40, astro-ph/0103210.
- Nakar, E., Piran, T., & Granot, J. 2002, *ApJ* , 579, 699
- Nakar, E. and Piran, T. 2003a, *ApJ*, 598, 400, astro-ph/0303156.
- Nakar, E. and Piran, T. 2003b, *New Astronomy*, 8, 141, astro-ph/0207400.
- Nakar, E. and Piran, T. 2004, *MNRAS*, 353, 647, astro-ph/0403461.
- Nakar, E. and Piran, T. 2005, *MNRAS* , 360, L73, astro-ph/0412232.
- Nakar, E., Piran, T., and Granot, J. 2003, *New Astronomy*, 8, 495, astro-ph/0210631.
- Nakar, E., Piran, T., and Sari, R. 2005, *ApJ*, 635, 516, astro-ph/0502052.
- Narayan, R., Paczynski, B., and Piran, T. 1992, *ApJ*, 395, L83.
- Narayan, R., Piran, T., and Kumar, P. 2001, *ApJ*, 557, 949, astro-ph/0103360.
- Narayan, R., Piran, T., and Shemi, A. 1991, *ApJ*, 379, L17.
- Nice, D. J., Splaver, E. M., Stairs, I. H., Löhmer, O., Jessner, A., Kramer, M., and Cordes, J. M. 2005, *ApJ* , 634, 1242, astro-ph/0508050.
- Nishikawa, K.-I., Hardee, P., Richardson, G., Preece, R., Sol, H., and Fishman, G. J. 2005, *ApJ* , 622, 927, astro-ph/0409702.
- Nomoto, K. and Kondo, Y. 1991, *ApJ*, 367, L19.
- Norris, J. P. and Bonnell, J. T. 2006, *ApJ*, 643, 266, astro-ph/0601190.
- Norris, J. P., Cline, T. L., Desai, U. D., and Teegarden, B. J. 1984, *Nature* , 308, 434.
- Norris, J. P., Marani, G. F., and Bonnell, J. T. 2000, *ApJ*, 534, 248, astro-ph/9903233.
- Norris, J. P., Nemiroff, R. J., Bonnell, J. T., Scargle, J. D., Kouveliotou, C., Paciesas, W. S., Meegan, C. A., and Fishman, G. J. 1996, *ApJ*, 459, 393.
- Norris, J. P., Scargle, J. D., and Bonnell, J. T. 2001, in *Gamma-ray Bursts in the Afterglow Era*, ed. E. Costa, F. Frontera, and J. Hjorth, 40.
- Nousek, J. A. *et al.* 2006, *ApJ* , 642, 389, astro-ph/0508332.

- Oechslin, R. and Janka, H.-T. 2006, MNRAS, 368, 1489, astro-ph/0507099.
- Oechslin, R., Rosswog, S., and Thielemann, F.-K. 2002, Phys. Rev. D , 65(10), 103005, gr-qc/0111005.
- Ofek, E. O. 2006, Submitted to ApJ.
- Ofek, E. O., Cenko, S. B., Gal-Yam, A., and Fox, D. B. 2006a, Submitted to ApJ.
- Ofek, E. O. *et al.* 2006b, ApJ in press, astro-ph/0609582.
- O'Shaughnessy, R., Kalogera, V., and Belczynski, K. 2005, ApJ , 620, 385, astro-ph/0408387.
- O'Shaughnessy, R., Kim, C., Fragos, T., Kalogera, V., and Belczynski, K. 2005, ApJ , 633, 1076, astro-ph/0504479.
- Ouyed, R., Dey, J., and Dey, M. 2002, A&A , 390, L39, astro-ph/0105109.
- Ouyed, R., Rapp, R., and Vogt, C. 2005, ApJ , 632, 1001, astro-ph/0503357.
- Ouyed, R. and Sannino, F. 2002, A&A , 387, 725, astro-ph/0103022.
- Paczynski, B. 1986, ApJ, 308, L43.
- Paczynski, B. 1991, Acta Astronomica, 41, 257.
- Paczynski, B. 1992, Acta Astronomica, 42, 145.
- Paczynski, B. 1998, ApJ , 494, L45+, astro-ph/9710086.
- Paczyński, B. and Haensel, P. 2005, MNRAS , 362, L4, astro-ph/0502297.
- Paczynski, B. and Xu, G. 1994, ApJ, 427, 708.
- Page, K. L. *et al.* 2006, ApJ, 637, L13, astro-ph/0512358.
- Palmer, D. M. *et al.* 2005, Nature, 434, 1107.
- Palmer, D., et al. 2006, GCN 5905
- Panaiteanu, A. 2006, MNRAS, 367, L42, astro-ph/0511588.
- Panaiteanu, A. and Kumar, P. 2000, ApJ, 543, 66, astro-ph/0003246.
- Panaiteanu, A. and Kumar, P. 2001, ApJ, 560, L49, astro-ph/0108045.
- Panaiteanu, A., Kumar, P., and Narayan, R. 2001, ApJ, 561, L171, astro-ph/0108132.
- Panaiteanu, A. and Mészáros, P. 2000, ApJ, 544, L17, astro-ph/0009309.
- Parsons, A. *et al.* 2005, GCN Circular, 3935, 1.
- Parsons, A., et al. 2006, GCN 5930
- Pe'er, A. and Wijers, R. A. M. J. 2006, ApJ, 643, 1036, astro-ph/0511508.
- Peng, F., Königl, A., and Granot, J. 2005, ApJ , 626, 966.
- Perna, R., Armitage, P. J., and Zhang, B. 2006, ApJ , 636, L29, astro-ph/0511506.
- Perna, R. and Belczynski, K. 2002, ApJ, 570, 252.
- Pfahl, E., Podsiadlowski, P., and Rappaport, S. 2005, ApJ , 628, 343, astro-ph/0502122.
- Pfahl, E., Rappaport, S., Podsiadlowski, P., and Spruit, H. 2002, ApJ, 574, 364.
- Phinney, E. S. 1991, ApJl, 380, L17.
- Piran, T. 1992, ApJ, 389, L45.
- Piran, T. 1999, Phys. Rep., 314, 575, astro-ph/9810256.
- Piran, T. 2000, Physics Reports , 333, 529, astro-ph/9907392.
- Piran, T. 2005a, in AIP Conf. Proc. 784: Magnetic Fields in the Universe:

- From Laboratory and Stars to Primordial Structures., ed. E. M. de Gouveia dal Pino, G. Lugones, and A. Lazarian, 164.
- Piran, T. 2005b, *Reviews of Modern Physics*, 76, 1143, astro-ph/0405503.
- Piran, T. and Shemi, A. 1993, *ApJ* , 403, L67, astro-ph/9211009.
- Piran, T., Shemi, A., and Narayan, R. 1993, *MNRAS*, 263, 861.
- Popham, R., Woosley, S. E., and Fryer, C. 1999, *ApJ* , 518, 356, astro-ph/9807028.
- Popov, S. B. and Stern, B. E. 2006, *MNRAS* , 365, 885, astro-ph/0503532.
- Porciani, C. and Madau, P. 2001, *ApJ*, 548, 522.
- Portegies Zwart, S. F. and Spreeuw, H. N. 1996, *A&A* , 312, 670.
- Portegies Zwart, S. F. and Yungelson, L. R. 1998, *A&A*, 332, 173.
- Preece, R. D., Briggs, M. S., Mallozzi, R. S., Pendleton, G. N., Paciesas, W. S., and Band, D. L. 1998, *ApJ*, 506, L23, astro-ph/9808184.
- Preece, R. D., Briggs, M. S., Mallozzi, R. S., Pendleton, G. N., Paciesas, W. S., and Band, D. L. 2000, *ApJS*, 126, 19, astro-ph/9908119.
- Price, D. J. and Rosswog, S. 2006, *Science*, 312, 719, astro-ph/0603845.
- Prince, T. A., Anderson, S. B., Kulkarni, S. R., and Wolszczan, A. 1991, *ApJ* , 374, L41.
- Prochaska, J. X., Bloom, J. S., Chen, H.-W., Hansen, B., Kalirai, J., Rich, M., and Richer, H. 2005, *GRB Circular Network*, 3700, 1.
- Proga, D. 2003, *ApJ* , 585, 406, astro-ph/0210642.
- Proga, D. and Begelman, M. C. 2003, *ApJ* , 592, 767, astro-ph/0303093.
- Proga, D. and Zhang, B. 2006, *MNRAS* , 370, L61, astro-ph/0601272.
- Pruet, J. and Dalal, N. 2002, *ApJ* , 573, 770, astro-ph/0106300.
- Rachen, J. P. and Mészáros, P. 1998, *Phys. Rev. D*, 58(12), 123005.
- Ramirez-Ruiz, E., Dray, L. M., Madau, P., and Tout, C. A. 2001, *MNRAS*, 327, 829, astro-ph/0012396.
- Ramirez-Ruiz, E., García-Segura, G., Salmonson, J. D., and Pérez-Rendón, B. 2005, *ApJ*, 631, 435, astro-ph/0412446.
- Ramirez-Ruiz, E., & Socrates, A. 2005, *ArXiv Astrophysics e-prints*, arXiv:astro-ph/0504257
- Rees, M. J. and Mészáros, P. 1992, *MNRAS*, 258, 41P.
- Rees, M. J. and Mészáros, P. 1994, *ApJ*, 430, L93, astro-ph/9404038.
- Rees, M. J. and Mészáros, P. 1998, *ApJ*, 496, L1+, astro-ph/9712252.
- Rhoads, J. E. 1997, *ApJ*, 487, L1+, astro-ph/9705163.
- Rhoads, J. E. 1999, *ApJ*, 525, 737, astro-ph/9903399.
- Roming, P. W. A. *et al.* 2006, *ArXiv Astrophysics e-prints*, astro-ph/0605005.
- Rossi, E., Lazzati, D., and Rees, M. J. 2002, *MNRAS*, 332, 945, astro-ph/0112083.
- Rossi, E. and Rees, M. J. 2003, *MNRAS* , 339, 881, astro-ph/0204406.
- Rossi, E. M., Beloborodov, A. M., and Rees, M. J. 2006, *MNRAS*, 369, 1797, astro-ph/0512495.
- Rosswog, S. 2005, *ApJ*, 634, 1202.
- Rosswog, S. and Davies, M. B. 2002, *MNRAS* , 334, 481.
- Rosswog, S., Davies, M. B., Thielemann, F.-K., and Piran, T. 2000, *A&A* ,

- 360, 171, astro-ph/0005550.
- Rosswog, S. and Liebendörfer, M. 2003, MNRAS , 342, 673, astro-ph/0302301.
- Rosswog, S., Liebendörfer, M., Thielemann, F.-K., Davies, M. B., Benz, W., and Piran, T. 1999, A&A , 341, 499, astro-ph/9811367.
- Rosswog, S. and Ramirez-Ruiz, E. 2002, MNRAS , 336, L7, astro-ph/0207576.
- Rosswog, S. and Ramirez-Ruiz, E. 2003, MNRAS , 343, L36, astro-ph/0306172.
- Rosswog, S., Ramirez-Ruiz, E., and Davies, M. B. 2003, MNRAS, 345, 1077, astro-ph/0110180.
- Rosswog, S., Speith, R., and Wynn, G. A. 2004, MNRAS , 351, 1121, astro-ph/0403500.
- Ruffert, M. and Janka, H.-T. 1998, A&A , 338, 535, astro-ph/9804132.
- Ruffert, M. and Janka, H.-T. 1999, A&A , 344, 573, astro-ph/9809280.
- Ruffert, M. and Janka, H.-T. 2001, A&A , 380, 544, astro-ph/0106229.
- Ruffert, M., Janka, H.-T., and Schaefer, G. 1996, A&A , 311, 532, astro-ph/9509006.
- Ruffert, M., Janka, H.-T., Takahashi, K., and Schaefer, G. 1997, A&A , 319, 122, astro-ph/9606181.
- Rybicki, G. B. and Lightman, A. P. 1979, Radiative processes in astrophysics, : New York, Wiley-Interscience, 1979. 393 p.).
- Sago, N., Ioka, K., Nakamura, T., and Yamazaki, R. 2004, Phys. Rev. D , 70(10), 104012, gr-qc/0405067.
- Saio, H. and Nomoto, K. 1985, A&A, 150, L21.
- Sakamoto, T. *et al.* 2005, GCN Circular, 4275, 1.
- Sakamoto, T. *et al.* 2006, ApJ, 636, L73, astro-ph/0512149.
- Salmonson, J. D. and Wilson, J. R. 2001, ApJ , 561, 950, astro-ph/0108196.
- Salpeter, E. E. 1955, ApJ , 121, 161.
- Sari, R. 1997, ApJ , 489, L37+.
- Sari, R. and Esin, A. A. 2001, ApJ, 548, 787.
- Sari, R. and Mészáros, P. 2000, ApJ, 535, L33, astro-ph/0003406.
- Sari, R. and Piran, T. 1995, ApJ, 455, L143+, astro-ph/9512125.
- Sari, R. and Piran, T. 1997, ApJ, 485, 270, astro-ph/9701002.
- Sari, R. and Piran, T. 1999, ApJ, 520, 641, astro-ph/9901338.
- Sari, R., Piran, T., and Halpern, J. P. 1999, ApJ, 519, L17, astro-ph/9903339.
- Sari, R., Piran, T., and Narayan, R. 1998, ApJ, 497, L17+, astro-ph/9712005.
- Sato, G. *et al.* 2005, GCN Circular, 3793, 1.
- Sato, G. *et al.* 2006a, GCN Circular, 5064, 1.
- Sato, G. *et al.* 2006b, GCN Circular, 5381, 1.
- Scannapieco, E. and Bildsten, L. 2005, ApJ, 629, L85.
- Scargle, J. D., Norris, J. P., and Bonnell, J. T. 1998, in American Institute of Physics Conference Series, ed. C. A. Meegan, R. D. Preece, and T. M. Koshut, 181.
- Schaefer, B. E. 2006, ApJ, 642, L25.
- Schaefer, B. E., Cline, T. L., Hurley, K. C., and Laros, J. G. 1998, ApJs, 118, 353.

- Schmidt, M. 2001, ApJ, 559, L79.
- Schmidt, W. K. H. 1978, Nature, 271, 525.
- Schneid, E. J. *et al.* 1992, A&A , 255, L13.
- Schramm, D. N. and Olinto, A. V. 1992. Nuclear physics and astrophysics. Technical report.
- Sedov, L. I. 1946, Prikl. Mat. i Mekh., 10, 241.
- Segalis, E. B. and Ori, A. 2001, Phys. Rev. D , 64(6), 064018, gr-qc/0101117.
- Setiawan, S., Ruffert, M., and Janka, H.-T. 2004, MNRAS , 352, 753, astro-ph/0402481.
- Shakura, N. I., & Sunyaev, R. A. 1973, A&A , 24, 337
- Shapiro, S. L. 2004, ApJ , 610, 913, astro-ph/0404338.
- Shemi, A. and Piran, T. 1990, ApJ, 365, L55.
- Shen, H., Toki, H., Oyamatsu, K., and Sumiyoshi, K. 1998, Nuclear Physics A, 637, 435, nucl-th/9805035.
- Shibata, M. 2003, ApJ , 595, 992, astro-ph/0310020.
- Shibata, M., Baumgarte, T. W., and Shapiro, S. L. 2000, Phys. Rev. D , 61(4), 044012, astro-ph/9911308.
- Shibata, M., Duez, M. D., Liu, Y. T., Shapiro, S. L., and Stephens, B. C. 2006, Physical Review Letters, 96(3), 031102, astro-ph/0511142.
- Shibata, M. and Shapiro, S. L. 2002, ApJ , 572, L39, astro-ph/0205091.
- Shibata, M. and Taniguchi, K. 2006, Phys. Rev. D, 73(6), 064027, astro-ph/0603145.
- Shibata, M., Taniguchi, K., and Uryū, K. 2005, Phys. Rev. D, 71(8), 084021, gr-qc/0503119.
- Shibata, M. and Uryū, K. 2000, Phys. Rev. D , 61(6), 064001, gr-qc/9911058.
- Shin, M.-S. and Berger, E. 2006, ArXiv Astrophysics e-prints, astro-ph/0609336.
- Silva, L. O., Fonseca, R. A., Tonge, J. W., Dawson, J. M., Mori, W. B., and Medvedev, M. V. 2003, ApJ , 596, L121, astro-ph/0307500.
- Silva, L. O., Fonseca, R. A., Tonge, J. W., Mori, W. B., and Dawson, J. M. 2002, Physics of Plasmas, 9, 2458.
- Soderberg, A. M. *et al.* 2006a, ApJ , 650, 261, astro-ph/0601455.
- Soderberg, A. M. *et al.* 2006b, ArXiv Astrophysics e-prints, astro-ph/0607511.
- Soderberg, A. M. and Ramirez-Ruiz, E. 2002, MNRAS, 330, L24, astro-ph/0110519.
- Sommer, M. *et al.* 1994, ApJ , 422, L63.
- Spitkovsky, A. 2005, in AIP Conf. Proc. 801: Astrophysical Sources of High Energy Particles and Radiation, ed. T. Bulik, B. Rudak, and G. Madejski, 345.
- Staff, J., Ouyed, R., and Bagchi, M. 2006, ArXiv Astrophysics e-prints, astro-ph/0608470.
- Stanek, K. Z. *et al.* 2003, ApJ, 591, L17.
- Stark, R. F. and Piran, T. 1985, Physical Review Letters, 55, 891.
- Strolger, L.-G. *et al.* 2004, ApJ, 613, 200.
- Symbalisty, E. and Schramm, D. N. 1982, Astrophysical Letters , 22, 143.

- Tanvir, N. R., Chapman, R., Levan, A. J., and Priddey, R. S. 2005, *Nature* , 438, 991, astro-ph/0509167.
- Taylor, G. 1950, *Royal Society of London Proceedings Series A*, 201, 175.
- Taylor, G. B., Frail, D. A., Berger, E., and Kulkarni, S. R. 2004, *ApJ*, 609, L1, astro-ph/0405300.
- Taylor, G. B., Momjian, E., Pihlström, Y., Ghosh, T., & Salter, C. 2005, *ApJ* , 622, 986
- Taylor, G. B., & Granot, J. 2006, *Modern Physics Letters A*, 21, 2171
- Taylor, J. H. and Weisberg, J. M. 1982, *ApJ* , 253, 908.
- Thompson, C. 1994, *MNRAS*, 270, 480.
- Thompson, C. 2006, *ApJ* , 651, 333 , astro-ph/0507387.
- Thompson, C. and Duncan, R. C. 1995, in *ASP Conf. Ser. 72: Millisecond Pulsars. A Decade of Surprise*, ed. A. S. Fruchter, M. Tavani, and D. C. Backer, 301.
- Thompson, C. and Madau, P. 2000, *ApJ* , 538, 105, astro-ph/9909111.
- Thompson, C., Mészáros, P., and Rees, M. J. 2006, *ArXiv Astrophysics e-prints*, astro-ph/0608282.
- Thompson, T. A. 2005, *Nuovo Cimento C Geophysics Space Physics C*, 28, 583, astro-ph/0504620.
- Thompson, T. A., Chang, P., and Quataert, E. 2004, *ApJ* , 611, 380, astro-ph/0401555.
- Tonry, J. L. *et al.* 2003, *ApJ*, 594, 1.
- Totani, T., & Panaitescu, A. 2002, *ApJ* , 576, 120
- Tueller, J. *et al.* 2005, *GCN Circular*, 3964, 1.
- Tutukov, A. V. and Yungelson, L. R. 1994, *MNRAS* , 268, 871.
- Usov, V. V. 1992, *Nature* , 357, 472.
- Usov, V. V. 1994, *MNRAS*, 267, 1035, astro-ph/9312024.
- Vallisneri, M. 2000, *Physical Review Letters*, 84, 3519, gr-qc/9912026.
- van den Heuvel, E. P. J. and Lorimer, D. R. 1996, *MNRAS*, 283, L37.
- van Paradijs, J. *et al.* 1997, *Nature* , 386, 686.
- van Putten, M. H. P. M. 2005, *ArXiv Astrophysics e-prints*, astro-ph/0510348.
- van Putten, M. H. P. M. and Levinson, A. 2001, *ApJ* , 555, L41, astro-ph/0105429.
- van Putten, M. H. P. M. and Levinson, A. 2002, *Science*, 295, 1874.
- van Putten, M. H. P. M. and Levinson, A. 2003, *ApJ* , 584, 937, astro-ph/0212297.
- van Putten, M. H. P. M. and Ostriker, E. C. 2001, *ApJ* , 552, L31, astro-ph/0010440.
- Vietri, M. 1995, *ApJ*, 453, 883.
- Vietri, M. and Stella, L. 1998, *ApJ* , 507, L45, astro-ph/9808355.
- Vietri, M. and Stella, L. 1999, *ApJ* , 527, L43, astro-ph/9910008.
- Villasenor, J. S. *et al.* 2005, *Nature*, 437, 855.
- Vlahakis, N. and Königl, A. 2003a, *ApJ*, 596, 1080, astro-ph/0303482.
- Vlahakis, N. and Königl, A. 2003b, *ApJ*, 596, 1104, astro-ph/0303483.
- Vlahakis, N., Peng, F., and Königl, A. 2003a, *ApJ* , 594, L23, astro-

- ph/0306029.
- von Neumann, J. 1947, Los Alamos Sci. Lab. Tech. Series, 7.
- Wang, X. Y., Cheng, K. S., & Tam, P. H. 2005, *ApJ* , 621, 894
- Wang, W. and Dai, Z.-G. 2001, *Chinese Physics Letter*, 18, 1153, astro-ph/0103284.
- Wang, X. and Loeb, A. 2000, *ApJ*, 535, 788, astro-ph/9910477.
- Watson, D., Hjorth, J., Jakobsson, P., Xu, D., Fynbo, J. P. U., Sollerman, J., Thöne, C. C., and Pedersen, K. 2006, *ArXiv Astrophysics e-prints*, astro-ph/0604153.
- Waxman, E. 1995, *Physical Review Letters*, 75, 386.
- Waxman, E. 1997a, *ApJ* , 491, L19+, astro-ph/9709190.
- Waxman, E. 1997b, *ApJ*, 489, L33+, astro-ph/9705229.
- Waxman, E. 1997c, *ApJ*, 485, L5+, astro-ph/9704116.
- Waxman, E. 2000, *Physica Scripta Volume T*, 85, 117, astro-ph/9911395.
- Waxman, E. 2004, *ArXiv Astrophysics e-prints*, astro-ph/0412554.
- Waxman, E. 2006, *ArXiv Astrophysics e-prints*, astro-ph/0607353.
- Waxman, E. and Bahcall, J. 1997, *Physical Review Letters*, 78, 2292.
- Waxman, E. and Bahcall, J. 1999, *Phys. Rev. D*, 59(2), 023002.
- Waxman, E. and Bahcall, J. N. 2000, *ApJ* , 541, 707, hep-ph/9909286.
- Waxman, E., Kulkarni, S. R., and Frail, D. A. 1998, *ApJ*, 497, 288, astro-ph/9709199.
- Wei, D. M., & Lu, T. 2000, *A&A* , 360, L13
- Wei, D. M., & Lu, T. 1998, *ApJ* , 505, 252
- Weibel, E. S. 1959, *Physical Review Letters*, 2, 83.
- Wettig, T. and Brown, G. E. 1996, *New Astronomy*, 1, 17.
- Wick, S. D., Dermer, C. D., and Atoyan, A. 2004, *Astroparticle Physics*, 21, 125.
- Witt, H. J., Jaroszynski, M., Haensel, P., Paczynski, B., and Wambsganss, J. 1994, *ApJ* , 422, 219.
- Wirth, G. D., et al. 2004, *AJ* , 127, 3121
- Woods, P. M. and Thompson, C. 2004, *ArXiv Astrophysics e-prints*, astro-ph/0406133.
- Wosley, S. E. 1993, *ApJ* , 405, 273.
- Wu, X. F., Dai, Z. G., Huang, Y. F., & Lu, T. 2005, *MNRAS* , 357, 1197, astro-ph/0412011.
- Yost, S. A., Harrison, F. A., Sari, R., and Frail, D. A. 2003, *ApJ*, 597, 459, astro-ph/0307056.
- Zhang, B., Fan, Y. Z., Dyks, J., Kobayashi, S., Mészáros, P., Burrows, D. N., Nousek, J. A., and Gehrels, N. 2006, *ApJ*, 642, 354, astro-ph/0508321.
- Zhang, B. and Kobayashi, S. 2005, *ApJ*, 628, 315, astro-ph/0404140.
- Zhang, B., Kobayashi, S., and Mészáros, P. 2003, *ApJ*, 595, 950, astro-ph/0302525.
- Zhang, B. and Mészáros, P. 2001a, *ApJ* , 552, L35, astro-ph/0011133.
- Zhang, B. and Mészáros, P. 2001b, *ApJ*, 559, 110.
- Zhang, B. and Mészáros, P. 2002, *ApJ*, 571, 876, astro-ph/0112118.

- Zhang, B. and Mészáros, P. 2004, International Journal of Modern Physics A, 19, 2385, astro-ph/0311321.
- Zheng, Z. and Ramirez-Ruiz, E. 2006, ArXiv Astrophysics e-prints, astro-ph/0601622.